UNIVERSITY OF HAWAII
LIBRARY
Nov 14 '57

The PHILOSOPHICAL MAGAZINE

FIRST PUBLISHED IN 1798

---

l. 2 Eighth Series No. 22 October 1957

A Journal of Theoretical Experimental and Applied Physics

EDITOR
PROFESSOR N. F. MOTT, M.A., D.Sc., F.R.S.

EDITORIAL BOARD
SIR LAWRENCE BRAGG, O.B.E., M.C., M.A., D.Sc., F.R.S.
SIR GEORGE THOMSON, M.A., D.Sc., F.R.S.
PROFESSOR A. M. TYNDALL, C.B.E., D.Sc., F.R.S.

PRICE £1 5s. 0d.
Annual Subscription £13 10s. 0d. payable in advance

ALERE FLAMMAM.
Printed and Published by
TAYLOR & FRANCIS LTD.
RED LION COURT, FLEET STREET, LONDON, E.C.4

Announcing a new International Quarterly Journal to appear in January 1958

Molecular Physics

Editor: H. C. LONGUET-HIGGINS
Assistant Editor: J. H. VAN DER WAALS

Editorial Board:

J. Bjerrum, *Copenhagen*; C. A. Coulson, *Oxford*; F. H. C. Crick, *Cambridge*; P. J. W. Debye, *Cornell*; O. Hassel, *Oslo*; W. Heitler, *Zürich*; J. O. Hirschfelder, *Wisconsin*; D. F. Hornig, *Princeton*; J. A. A. Ketelaar, *Amsterdam*; J. G. Kirkwood, *Yale*; R. Kronig, *Delft*; J. W. Linnett, *Oxford*; A. Liquori, *Rome*; Dame Kathleen Lonsdale, *London*; P-O. Löwdin, *Uppsala*; M. Magat, *Paris*; W. S. Moffitt, *Harvard*; R. S. Mulliken, *Chicago*; A. Münster, *Frankfurt*: L. J. Oosterhoff, *Leiden*; L. E. Orgel, *Cambridge*; J. A. Pople, *Cambridge*; I. Prigogine, *Brussels*; R. E. Richards, *Oxford*; J. S. Rowlinson, *Manchester*; G. S. Rushbrooke, *Newcastle upon Tyne*; L. E. Sutton, *Oxford*; H. W. Thompson, *Oxford*; B. Vodar, *Bellevue, Paris.*

Physicists, chemists and their biological colleagues have a fundamental common interest in the properties of molecules and molecular assemblies and the need has been growing for a journal which would bring together experimental and theoretical contributions to this field.

The physical aspects of molecules will be dealt with, in particular:

1. The structure of molecules as determined by physical methods and interpreted by quantum mechanics;
2. The electromagnetic properties of molecules and the processes of molecular excitation, ionization and dissociation;
3. The interaction between molecules and the equilibrium and transport properties of molecular assemblies.

The following contributions have been received for the first volume:

1. Nuclear Magnetic Resonance and Rotational Isomerism in Substituted Ethanes. By J. A. Pople
2. Dielectric Properties of Iodine in Aromatic Solvents at 9000 Mc./sec. By G. W. Nederbragt and J. Pelle
3. On the Dipole Moments of Azines. By H. F. Hameka and A. M. Liquori
4. Electron–Electron Separation in Molecular Hydrogen. By M. P. Barnett, F. W. Birss and C. A. Coulson
5. On Irreversible Processes in Quantum Mechanics. By I. Prigogine and M. Toda
6. The Transport of Energy and Momentum in a Dense Fluid of Rough Spheres. By J. P. Valleau
7. Constant Pressure in Statistical Mechanics. By W. Byers Brown
8. One-dimensional Multicomponent Mixtures. By H. C. Longuet-Higgins

Price per part £1 5s. 0d.
Subscription per volume (4 issues) £4 15s. 0d. post free, payable in advance

Printed and Published by

TAYLOR & FRANCIS LTD
RED LION COURT, FLEET STREET, LONDON, E.C.4

Orders originating in U.S.A. and Canada should be sent to the
Academic Press Inc., 111 Fifth Avenue, New York, 3, N.Y., U.S.A.

Liquid⇌Solid Equilibrium in Copper and Silver Alloys; with an Appendix on the Equilibrium Diagram of the System Copper–Arsenic†

By William Hume-Rothery and Jennifer Burns
Department of Metallurgy, Oxford

[Received June 17, 1957]

Summary

The liquidus and solidus curves for the α-solid solutions, of Cd, In, Sn, and Sb in Ag, and of Zn, Ga, Ge, and As, in Cu are discussed. In the Ag-series a given depression of the solidus is produced by atomic percentages of Cd, In, Sn, and Sb proportional to $1/2^2 : 1/3^2 : 1/4^2 : 1/6^2$, and in the Cu-series by amounts of Zn and Ga proportional to $1/3^2 : 1/4^2$. The increases in mean lattice spacing produced by a given atomic percentage of Cd, In, Sn, and Sb dissolved in Ag are as 2 : 3 : 4 : 6, and by a given atomic percentage of Zn and Ga dissolved in Cu are as 3 : 4. The solidus curves and lattice distortions thus involve the same whole number sequences, but this correspondence breaks down in the system Cu–As where the electrochemical factor is high, and the same effect to a lesser degree is apparent in the system Cu–Ge. In the systems Ag–Cd, Ag–In, Ag–Sn, Cu–Zn, Cu–Ga, and Cu–Ge the liquidus and solidus curves in dilute solutions are connected by a relation of the type $x_l = k\sqrt{x_s}$ where x_l and x_s are the atomic percentages of solute in the liquid and solid phases. In this class of alloy the liquidus and solidus curves depend primarily upon electron concentration, modified by lattice distortion, and diagrams are given showing these effects. Increasing electrochemical factor (e.g. Cu–As, Ag–Mg) produces an additional steeper fall in the liquidus and solidus. The equations of H. Jones are used to calculate the effects of solute elements on the latent heat of fusion of Ag and Cu, and the way in which these are affected by electron concentration and lattice distortion is discussed.

§ 1. Introduction

The solid solutions‡ of Cd, In, Sn, and Sb in silver, and of Zn, Ga, Ge, and As in copper show many properties for which the changes produced by a given atomic percentage of solute increase with the valency (v) of the latter. The increases in the mean lattice spacing produced by a given atomic percentage of Cd, In, Sn, and Sb dissolved in silver are as

---

† Communicated by the Author.

‡ Chemical symbols are used for abbreviation, and for clarity in describing the relative effects of different elements.

2 : 3 : 4 : 6 (Hume-Rothery and Reynolds 1937, Owen and Roberts 1939), whilst for Zn, Ga, Ge, and As dissolved in copper the increases are as 3 : 4 : 5 : 7. In the liquid$\rightleftharpoons$solid equilibria for the α-solid solutions in silver, a given depression of the liquidus is produced by amounts of Cd, In, Sn, and Sb proportional to $1/2\,a : 1/3\,a : 1/4\,b : 1/5\,b$, where a and b are very nearly equal (Hume-Rothery, Mabbott, and Channel-Evans 1934† Hume-Rothery and Reynolds 1937 a), and H-R, M, and C-E showed that to a first approximation a similar relation existed for the α-solid solutions of Zn, Ga, and Ge in copper. These authors also claimed that the corresponding depressions of the solidus curves were roughly proportional to $1/v^2$, but this relation was not exact.

The curious whole number relations for the lattice distortions and depressions of liquidus curves are not understood, and the experimental accuracy is not sufficiently great to preclude a departure of 0·1 from the exact whole numbers. Since the liquidus and solidus curves give the compositions of the two phases in equilibrium with each other, any really fundamental relation will probably involve the compositions of both phases, and although a definite valency effect is clear, the apparent agreement with whole number sequences may be of no significance.

The general theory of alloys suggests that the structures of this type of alloy are determined by the interplay of three factors (1) electron concentration, (2) size-factor, and (3) electrochemical factor, the last-named being important only when the solvent and solute differ appreciably in electrochemical characteristics. In the present paper we discuss the liquidus and solidus curves in greater detail, and give new results for the system copper–arsenic in which the electrochemical factor is considerable. The discussion is confined to alloys of copper and silver with solute elements whose valencies are higher, and whose ionic radii are smaller than those of the solvent. Under such conditions the lattice distortion is due mainly to the valency electrons of the solute.

§ 2. THE EQUILIBRIUM DIAGRAMS

Figure 1 shows the equilibrium diagrams in such a way as to distinguish between the temperature–composition limits in which the alloys are totally solid or totally liquid. In the systems Ag–Cd and Cu–Zn, the liquidus curves show only slight deviations from a smooth curve between the melting points of the two metals, and except at the extreme Cd-rich and Zn-rich ends of the diagram the horizontal portions of the solidus curves are short. In the systems Ag–In and Cu–Ga, the liquidus curves are again nearly smooth curves across the diagram, but the solidus curves show marked falls after about 35 atm% solute.

The system Ag–Sn shows the same characteristics except that the marked widening in the freezing range occurs at about 25 atm% Sn. In contrast to this, the system Cu–Ge shows a slight maximum at

---

† This paper will be referred to as H-R, M, and C-E.

26 atm% Ge, and the generally falling liquidus and solidus curves end in a eutectic at 37 atm% Ge.

On passing to the elements of Group V, this difference is accentuated. In the system Ag–Sb there is a general fall in the liquidus and solidus until a eutectic is reached in the middle of the diagram. In contrast to this, the system Cu–As shows a pronounced maximum at 26 atm% As.

Fig. 1

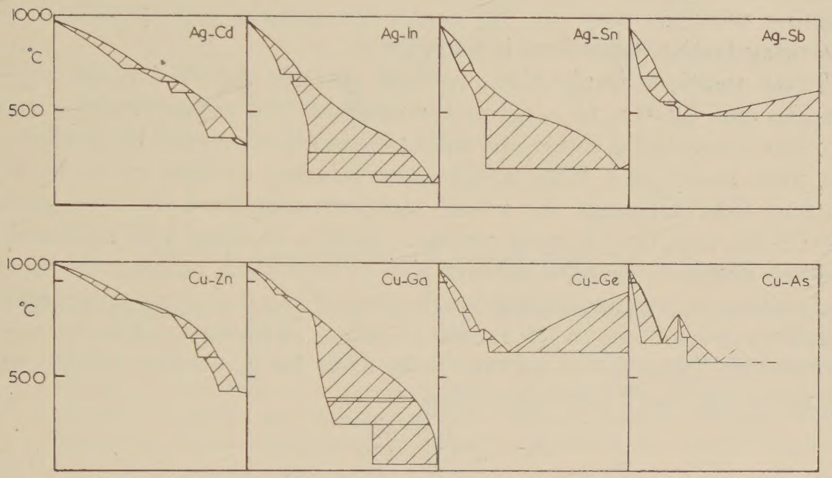

In these diagrams the upper lines are the liquidus curves of the systems concerned. The shaded areas are the (liquid+solid) 2-phase fields, and the areas below these are those in which the alloys are totally solid.

We may interpet these differences as showing that, in the systems Ag–Cd, Ag–In, Ag–Sn, Cu–Zn, and Cu–Ga, the electrochemical factor is comparatively small, so that the equilibrium diagrams are determined mainly by the electron concentration and size-factor (i.e. lattice distortion) effects. In the system Cu–Ge, the electrochemical factor is already beginning to affect the form of the diagram, and is playing a far more important part in the system Cu–As. This interpretation is confirmed by the fact that the equilibrium diagram of the system Cu–Si is very like that of the system Cu–Ge, but with a much more pronounced maximum in the liquidus curve, as would be expected from the more electronegative nature of silicon.

§ 3. THE LIQUIDUS AND SOLIDUS CURVES: EMPIRICAL RELATIONS

In view of recent data (see p. 1195) H-R, M, and C-E's claim that the depression of the solidus curves is proportional to $1/v^2$ is incorrect. Instead of this we find that for dilute solutions in the silver series, a given depression of the solidus curves is produced by atomic percentages of Cd, In, Sn, and Sb proportional to $1/2^2 : 1/3^2 : 1/4^2 : 1/6^2$, whilst in the copper series a given depression of the solidus curves is produced by amounts of Zn, and Ga proportional to $1/3^2 : 1/4^2$. These whole numbers are the same as those involved for the lattice distortions†.

We also find that although H-R, M, and C-E's claim that a given depression of the liquidus curves was produced by atomic percentages of Zn, Ga, and Ge proportional to $1/2 : 1/3 : 1/4$ was a rough general approximation, the relative depressions for Zn and Ga are in much better agreement with the factors $1/3 : 1/4$, where the whole numbers are again those involved for the lattice distortions. Even though the whole number relations may not be exact, the general correspondence with the mean lattice distortions is undoubted.

These relations imply that, for the systems Ag–Cd, Ag–In, Ag–Sn, Cu–Zn, and Cu–Ga, at a given temperature the concentrations x_l and x_s of the solute in the liquid and solid phases are connected by a relation of the type $x_l = k\sqrt{x_s}$. This is the same relation as that given by H-R, M, and C-E, although the whole numbers suggested by these authors for Cu–Zn and Cu–Ga were wrong. Such a relation will not hold for systems in which the solid solution is very restricted, because the liquidus and solidus are connected thermodynamically so that x_l retains a definite value when $x_s=0$, i e. when no solid solution is formed. For the case of monatomic dilute solutions the value of x_l for $x_s=0$ can be calculated by means of Van't Hoff's equation

$$x_l - x_s = \frac{\lambda}{RT}\left(\frac{1}{T} - \frac{1}{T_0}\right).$$

In fig. 2, x_l for the silver alloys at 900°c is plotted against $\sqrt{x_s}$, together with the value for $x_s=0$ calculated from the above equation. The points for Ag–Cd, Ag–In, and Ag–Sn lie on a straight line through the origin. The points for Ag–Zn and Ag–Hg, where the divalent solutes are from adjacent Periods also lie on this straight line, although at 900°c the solidus curve in the system Ag–Hg involves such a long extrapolation from the observed points that the test is not a critical one. The points for Ag–Sb, Ag–Ga, Ag–Ge, and Ag–Pb‡ where x_s is small show a gradual tailing off towards the calculated value for $x_s=0$. The point for Ag–Al is in fair agreement with the straight line, and the only wide deviation is for the system Ag–Mg, where the electrochemical factor is large, and the equilibrium diagram shows a pronounced maximum in the equiatomic region of the β phase, and the point lies above the line in fig. 2.

The general conclusion to be drawn from fig. 2 is that for this class of alloy the curve connecting x_l and x_s approaches asymptotically to the calculated value for $x_s=0$ in cases where x_s is small, and to a straight line through the origin (i.e. a direct proportionality) when x_s is large, provided that the electrochemical factors are small.

---

† As explained before, the experimental accuracy does not entitle us to claim an exact whole number effect, but we use the whole numbers for abbreviation in discussion.

‡ In this system Ag–Pb the ionic radius of the Pb^{4+} ion is smaller than that of Ag^{+}, although if Pb dissolves in the incompletely ionized form the ionic radius of the Pb^{2+} ion would be greater.

Fig. 2

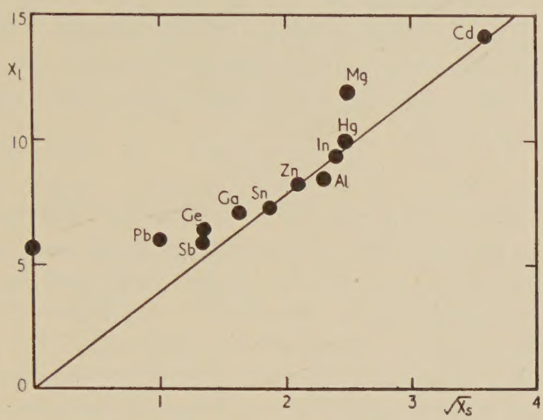

In this diagram x_l is plotted against $\sqrt{x_s}$, where x_l and x_s are the atomic percentages of solute in the liquid and solid (α) phases in equilibrium with one another at 900°c in the alloys of silver with the elements shown. The value for $x_s=0$ is calculated by Van't Hoff's equation. Similar diagrams are obtained at any constant temperature above 900°c whilst at lower temperatures the relation gradually becomes less exact.

Fig. 3

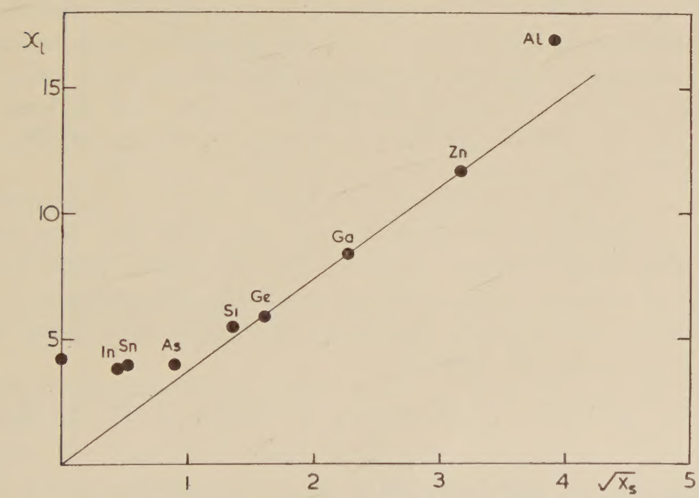

x_l plotted against $\sqrt{x_s}$ for copper alloys at 1035°c. See fig. 2.

In fig. 3, x_l is plotted against $\sqrt{x_s}$ for the copper alloys at 1035°c; this temperature is chosen because it is just above that of the ($\alpha+\beta\rightleftharpoons$Liquid) eutectic in the system Cu–Al and is thus the lowest temperature for which a point from this system can be included. The points for Cu–Zn, Cu–Ga, and Cu–Ge lie on a straight line through the origin, whilst that for Cu–As lies above this line, as for Ag–Sb in fig. 2. In the system Cu–Al, the depression of liquidus and solidus is abnormally small, for reasons which are not understood, and the Cu–Al point is above the line in fig. 3, as is the case for the Ag–Mg point in fig. 2, and Al and Mg are the two most electropositive of the solutes. The points for Cu–In and Cu–Sn where the solid solubility is small approach the value calculated for $x_s=0$, but for these the ionic radii of the solutes are of the same order as that of Cu^+.

§ 4. Electron Concentration and Lattice Distortion

We may accept the view that, when the electrochemical factor is small, the liquidus and solidus curves are determined first by the electron concentration, modified by the size factor or lattice distortion. The mean lattice distortion as measured by ordinary X-ray diffraction is (apart from lattice vacancies) directly related to the change in atomic volume, but it is not a very satisfactory quantity because it fails to take into account the local distortions around the solute atoms. Attempts to measure the local distortions have been made for other alloys by Warren, Averbach and Roberts (1951) but the results are not yet sufficiently precise for the present purpose. In a qualitative way some of this difficulty can be overcome by comparing mean lattice distortions in alloys containing the same concentration of solute atoms, since in this case the distortion results from the same number of centres. This policy is adopted on p. 1188 whilst in other cases we can only use the mean values at different concentrations. In the absence of high-temperature data we can only use lattice-spacings determined at room temperature. This seems justified in view of the fact that Owen and Roberts (1939) showed that the relative effects of different elements on the lattice-spacings of these alloys were the same at 300°C. as at 18°C.

In the alloys under consideration a given electron concentration is produced by atomic proportions of (Zn, Cd), (Ga, In), (Ge, Sn), and (As, Sb) proportional to 12 : 6 : 4 : 3. In the silver series where the mean lattice distortion produced by equiatomic percentages of Cd, In, Sn and Sb are as 2 : 3 : 4 : 6, the lattice distortions at a given electron concentration are in the ratios :

$$(12\times 2)\ \text{Ag Cd} : (6\times 3)\ \text{Ag In} : (4\times 4)\ \text{Ag Sn} : (3\times 6)\ \text{Ag Sb},\ \text{i.e.}\ 24 : 18 : 16 : 18.$$

In the copper series where the lattice distortion factors are 3, 4, 5 and 7, the lattice distortions at a given electron concentration are in the ratios :

$$(12\times 3)\ \text{Cu Zn} : (6\times 4)\ \text{Cu Ga} : (4\times 5)\ \text{Cu Ge} : (3\times 7)\ \text{Cu As},\ \text{i.e.}\ 36 : 24 : 20 : 21.$$

In each series, therefore, the mean lattice distortion for a given electron concentration decreases markedly on passing from the divalent to the trivalent solute, with a further decrease on passing to the tetravalent solute, after which there is a slight increase on passing to the solute of Group V.

§ 5. THE α-LIQUIDUS AND SOLIDUS CURVES

Figure 4 shows the liquidus and solidus curves for the above series of alloys plotted in terms of electron concentration, and the following points may be noted—for abbreviation we shall refer to the 2-phase (Liquid+Solid) region as the (L+S) field.

For the silver series, the width of the (L+S) fields increases with the valency of the solute. The (L+S) field for Ag–In is not placed symmetrically about that for (Ag–Cd but is shifted clearly in the direction of higher temperature. On passing to Ag–Sn the (L+S) field widens further, and is not quite symmetrical about the Ag–In (L+S) field, and although slight, the shift is again in the direction of higher temperature. On passing to Ag–Sb this tendency is reversed and the greatly widened (L+S) region is moving in the direction of lower temperature. These changes run parallel to the factors for mean lattice distortions at constant electron concentrations which are (p. 1182) as 24 : 18 : 16 : 18.

Fig. 4

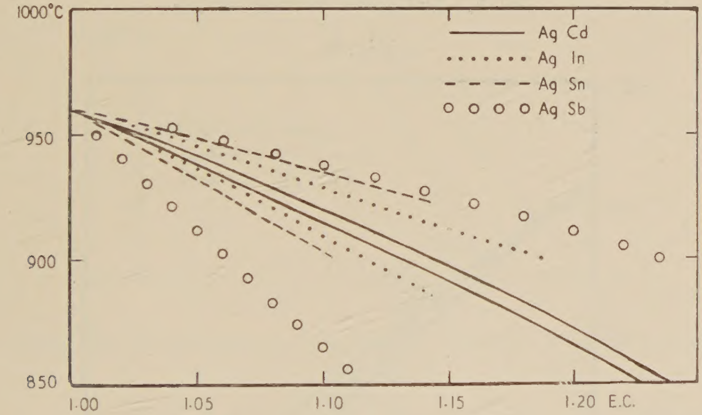

α-liquidus and solidus curves plotted against electron concentration for Ag–Cd, Ag–In, Ag–Sn and Ag–Sb alloys.

For the copper series (fig. 5) the relative widths and positions of the (L+S) fields for the systems Cu–Zn and Cu–Ga resemble those for Ag–Cd and Ag–In, but for Cu–Ge and Cu–As this correspondence breaks down. In terms of electron concentration, the liquidus curves for Cu–Ga, Cu–Ge, and Cu–As are roughly similar, but the solidus curves for Cu–Ge and Cu–As are distinctly lower. The effect is very marked for Cu–As, and this suggests that increasing electrochemical factor acts so as to lower the general direction of the (L+S) field.

It was shown by Andrews and Hume-Rothery (1941) that in the α/β brass kind of equilibrium a simple relation existed between the lattice distortions and the electron concentrations of the lines half way between the compositions of the two phases in equilibrium. We may, therefore, define a quantity $\bar{x}$ by the relation $\bar{x}=\frac{1}{2}(x_s+x_l)$ where x_s and x_l are the atomic fractions of the solute in the solid and liquid phases at a given temperature.

Fig. 5

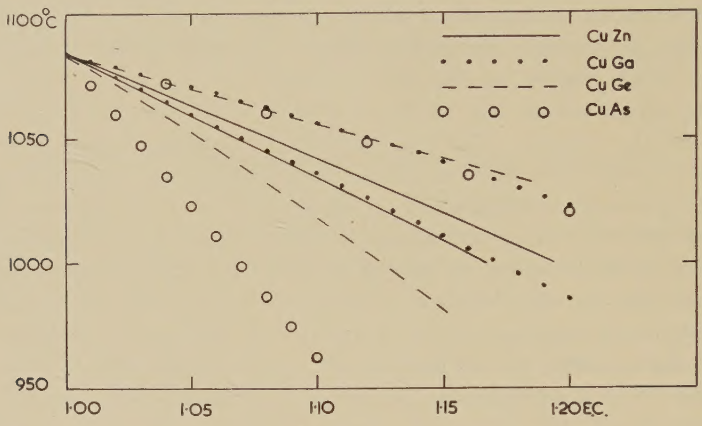

α-liquidus and solidus curves plotted against electron concentration for Cu–Zn, Cu–Ga, Cu–Ge and Cu–As alloys.

Fig. 6

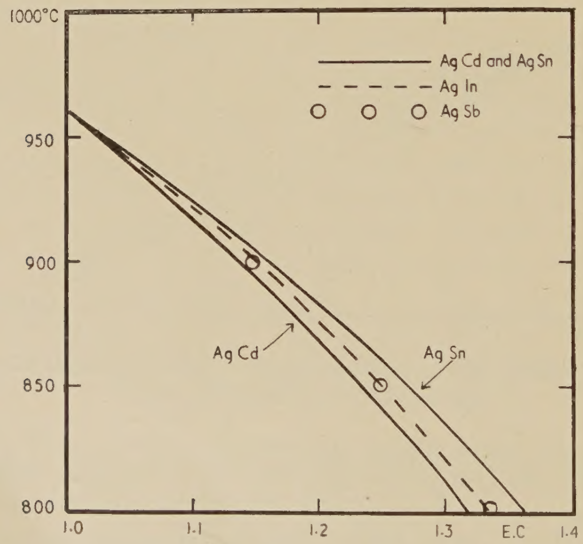

$\bar{x}$ *versus* electron concentration for Ag–Cd, Ag–In, Ag–Sn, and Ag–Sb alloys. $\bar{x}$ is equal to $\frac{1}{2}(x_l+x_s)$ and is, thus, the line half-way between the liquidus and solidus curves.

Figure 6 shows the relation between $\bar{x}$ (in electron concentration) and temperature for the silver alloys. On passing from Ag–Cd → Ag–In → Ag–Sn the $\bar{x}$ curves rise, and then on passing to Ag–Sb the $\bar{x}$ curve falls and is almost the same as that for Ag–In. These effects are in the same order as the mean lattice distortions at a given electron concentration, and the coincidence of the $\bar{x}/T$ curves for Ag–In and Ag–Sb is remarkable in view of the equality of the mean lattice distortions for a given electron concentration for these two solutes.

Figure 7 shows the $\bar{x}/T$ relations for the copper alloys. For Cu–Zn and Cu–Ga the relative positions of the two curves resemble those for Ag–Cd and Ag–In in fig. 6, but on passing to Group IV the $\bar{x}/T$ curve is lowered for Cu–Ge, in contrast to the behaviour of the Ag–Sn curve in fig. 6, whilst the curve for Cu–As shows a striking fall, in agreement with the increasing electrochemical factor.

Fig. 7

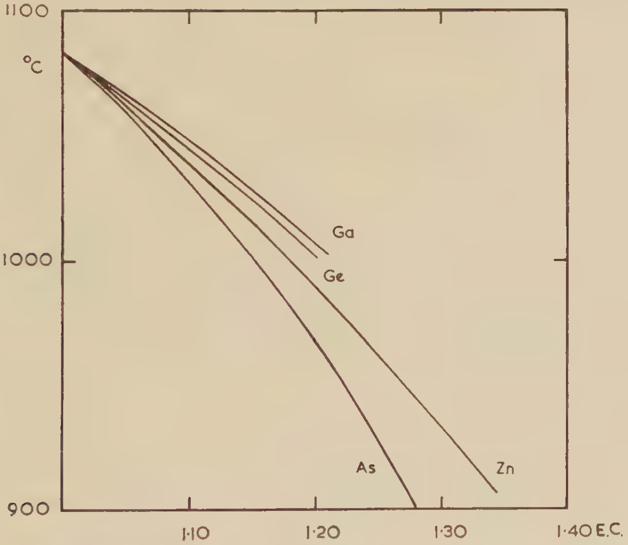

$\bar{x}$ *versus* electron concentration for Cu–Zn, Cu–Ga, Cu–Ge, and Cu–As alloys. See fig. 6.

We may, therefore, conclude that the $\bar{x}/T$ curves are determined primarily by electron concentration, and are depressed by increasing lattice distortion and by increasing electrochemical factor. We can thus understand why the $\bar{x}/T$ curve for the system Cu–Si nearly coincides with that for Cu–Ge. For in the Cu–Si α-solid solution, the lattice distortion is very small, and would favour a high $\bar{x}/T$ curve, whilst the more electronegative nature of silicon would favour a low $\bar{x}/T$ curve, and we can understand how the two effects tend to neutralize each other.

§ 6. THE ΔU VALUES

The liquidus and solidus curves discussed above are not independent, but are connected thermodynamically. Following Jones (1937) we may write F_{l} and F_{s} for the free energies per atom for the liquid and solid phases in equilibrium with one another at a given temperature, and let x_l and x_s be the compositions, i.e. the atomic fractions of the solute in the two phases. The conditions for equilibrium are expressed by the two equations:

$$\frac{\partial F_l}{\partial x_l}=\frac{\partial F_s}{\partial x_s}=\frac{F(x_l)-F(x_s)}{x_l-x_s}. \qquad \text{(1)}$$

The free energy of each phase may be written in the form

$$F_x=U(x)+C+D. \qquad \text{(2)}$$

$U(x)$ is the internal energy of the alloy at the absolute zero of temperature as a function of its composition, measured with respect to the energies of the individual atoms. C is the free energy associated with the rise of temperature from the absolute zero to temperature T, and is thus equal to:

$$\int_0^T C_v dT-T\int_0^T\frac{C_v}{T}dT.$$

D is the disorder term arising from the entropy of mixing and is equal to

$$kT\{x\ln x+(1-x)\ln(1-x)\}.$$

Jones assumed that the change in vibrational energy with composition at a fixed temperature was the same for both liquid and solid phases, so that the C term of eqn. (2) could be ignored in considering differences between the free energies in liquid and solid states. In this way, Jones obtained an expression for the quantity ΔU defined by:

$$\Delta U=(U_s-U_l)_{\bar{x}}-(U_s-U_l)_0$$

where $(U_s-U_l)_{\bar{x}}$ is the difference between the internal energies of the solid and (supercooled) liquid phases of composition $\bar{x}$ at the absolute zero, and $(U_s-U_l)_0$ has the same meaning for the pure solvent. This equation is †:

$$\Delta U=\left(\frac{T_0-T}{T_0}\right)\lambda-kT\left\{\ln\frac{1-x_s}{1-x_l}+\bar{x}\ln\frac{x_s(1-x_l)}{x_l(1-x_s}\right\} \qquad \text{(3)}$$

where λ and T_0 are the latent heat of fusion, and melting point of the pure solvent. x_s and x_l are the compositions of solid and liquid phases in equilibrium at temperature T, and $\bar{x}=\frac{1}{2}(x_s+x_l)$ is the same quantity referred to on p. 1187.

The second term in (3) arises from the disorder term in eqn. (1), and is small (5-10%) compared with the first term in (3). The increase in ΔU is thus determined mainly by the depression of the $\bar{x}/T$ curve.

ΔU may be regarded as the decrease in the latent heat of fusion resulting from the addition of a fraction $\bar{x}$ of solute—more strictly it is the decrease in the latent heat of fusion of the solid to (hypothetical) supercooled liquid at the absolute zero. Positive values of ΔU mean that the liquidus and solidus are depressed by the addition of solute, whilst negative values of ΔU correspond to a rise in melting point.

---

† This equation is printed wrongly in Jones' paper, but the calculated values are correct. We have to thank Professor Jones for discussion of this point.

The Jones equation, thus, enables the ΔU values to be calculated from the liquidus and solidus curves. Since the $\bar{x}/T$ curves fall progressively more steeply with increasing valency of the solute, the curves

Fig. 8

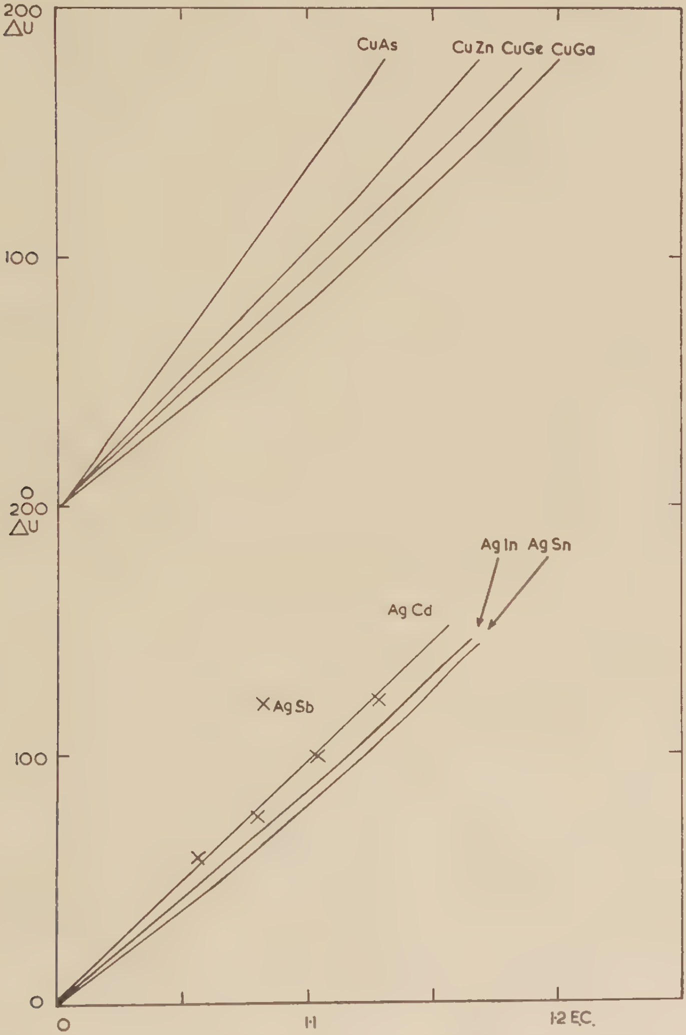

ΔU *versus* electron concentration for silver and copper alloys. For the definition of ΔU, see p. 1186.

connecting ΔU with $\bar{x}$ (in atomic concentrations) show, for a given value of $\bar{x}$ a progressive increase in ΔU on passing along the series Cu–Zn, Ga, Ge and Ag–Cd, In, Sn, Sb, and Jones claimed that ΔU was very nearly proportional to the electron concentration.

Since the work of Jones more accurate data have become available, the details of which are given in Appendix B. Figure 8 shows the electron concentration plotted against the ΔU values calculated from the new data, and the following points may be noted.

(1) When plotted against electron concentration, the ΔU curves are not superposed, and consequently ΔU does not depend on electron concentration alone.

(2) In the copper series the ΔU/e.c. curves† for Cu–Zn and Cu–Ga are displaced so that ΔU increases with the lattice distortion factors for a given electron concentration (p. 1185). For Cu–As, the ΔU/e.c. curve is much higher than would be expected from the lattice distortion factors which as shown on p. 1182 are as 36 : 24 : 20 : 21 for a given electron concentration in the solutions of Zn, Ga, Ge, and As in copper. We may reasonably ascribe this to the electrochemical factor, and the fact that the curve for Cu Ge is above that for Cu Ga may be the result of the electrochemical factor beginning to exert its effect in the system Cu Ge (see p. 1179).

(3) In the silver series where the lattice distortions at constant electron concentration are as 24 : 18 : 16 : 18 for Ag–Cd, In, Sn, and Sb, the ΔU curves for the system Ag–Cd, Ag–In, and Ag–Sn follow the lattice distortion sequence, but the Ag–Sb curve is higher than would be expected in contrast to the behaviour of the empirical $\bar{x}$ curves of fig. 6. This might suggest that in the system Ag–Sb, the electrochemical factor was beginning to exert its effect, but the approximations in Jones' treatment do not justify further discussion.

§ 7. THE RELATION BETWEEN ΔU AND THE MEAN LATTICE DISTORTION

As explained previously (p. 1182) the mean lattice distortion is directly related to the change in atomic volume, but fails to take into account the different local distortions which may occur round different solute elements. If we consider alloys containing a given atomic percentage of solute, the mean lattice distortions proceed from the same number of disturbing centres, and the conditions may be more directly comparable than if the atomic percentage of solute is a variable.

Figure 9 shows ΔU plotted against the mean lattice distortions, Δa, for the Ag–Cd, In, Sn, Sb alloys containing 2, 6, and 12 atm% of solute. The points lie on straight lines, the extrapolations of which indicate negative values of ΔU for $\Delta a=0$. In all of these alloys the formation of the solid solution results in an increase in the electron concentration which is responsible for most of the lattice expansion. We may perhaps interpret the negative value of ΔU as indicating that, if in this series of alloys Δa were zero, there would have to be some strong attractive force in order to neutralize the expansion resulting from the increased electron concentration, and this attraction would stabilize the solid phases and raise the melting point (i.e.—ΔU). In the system Ag–Sb, $\bar{x}=12$ corresponds to a point slightly above the peritectic horizontal of the α-phase (fig. 1) and since the α-solid solution extends only to 7 atm% Sb, we have assumed that the lattice distortion follows the 2 : 3 : 4 : 6 sequence referred to on p. 1178.

---

† For abbreviation we refer to the ΔU *versus* electron concentration curves as the ΔU/e.c. curves.

Fig. 9

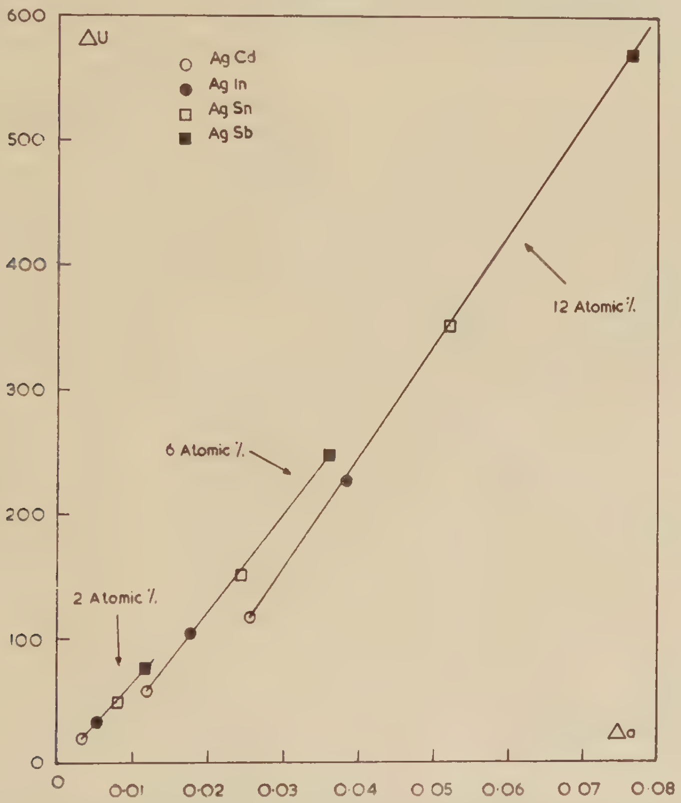

ΔU is plotted against Δa for constant atomic percentages of Cd, In, Sn, and Sb dissolved in Ag. Δa is the mean lattice distortion of the solid solution.

Figure 10 shows points for ΔU in the series Ag–Zn, Ag–Ga, and Ag–Ge, all at 6 atm% of solute. For these, there is lattice contraction in the systems Ag–Zn and Ag–Ga, and a very small lattice expansion for Ag–Ge. The points lie on a straight line parallel to that for the Ag–Cd, In, Sn, Sb series but with a positive value of ΔU for $\Delta a=0$. These values suggest that, if we take a given atomic percentage of solute, there is in each series a similar linear relation between ΔU and Δa, but that the lines are displaced on passing from one series to the other, so that ΔU increases with the difference between solvent and solute in the Periodic Table. This relation is not, however, shown in the sequence Ag–Mg and Ag–Al where the former system has a large electrochemical factor as revealed by a maximum in the melting point of the Ag Mg β phase.

As explained on p. 1186 the ΔU terms are determined mainly by the depression of the $\bar{x}$ *versus* T curves in the systems concerned, and the above relations between ΔU and Δa are thus accompanied by similar relations between Δa and ΔT, the depression of the $\bar{x}/T$ curve below the melting point of the solvent.

Fig. 10

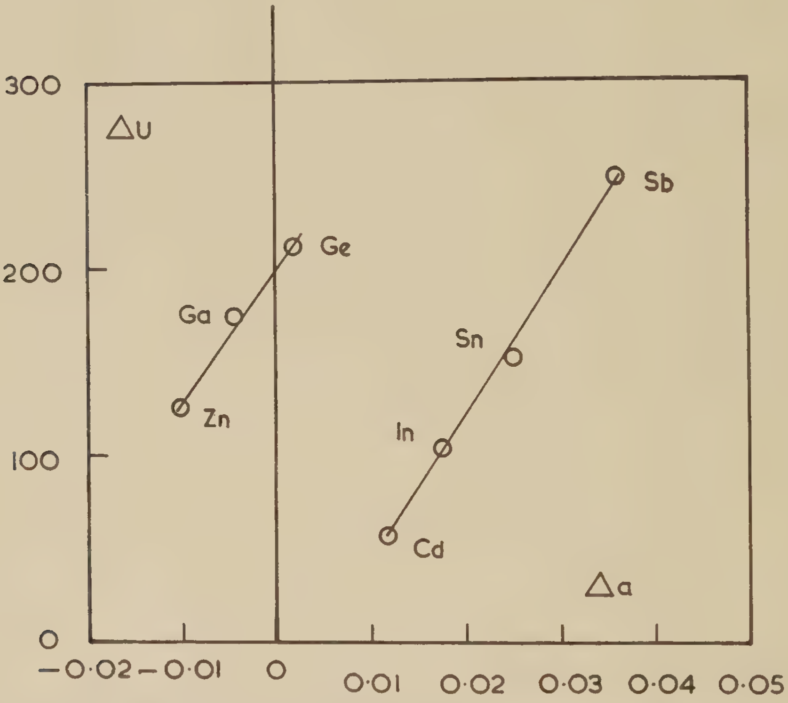

ΔU is plotted against Δa for solid solutions containing 6 atomic% of Zn, Ga, Ge, and of Cd, In, Sn, and Sb.

The relations described in the preceding sections confirm the view that in a series such as Ag(Cd, In, Sn, Sb) and Cu(Zn, Ga, Ge, As) the liquidus and solidus relations are determined primarily by electron concentration, but that this simple dependence is modified both by lattice distortion and electrochemical factor. The relative effects in the systems Ag(Cd, In, Sn) and Ag(Zn, Ga, Ge) suggest that, for a given atomic percentage of solute, the ΔU values are a linear function of the lattice distortion Δa, but that each sequence involves its own characteristic type of distortion. In the systems Ag(Cd, In, Sn, Sb) and Cu(Zn, Ga) where the electrochemical factors are small, the correspondence between the factors for the lattice distortions and depressions of the solidus curves is remarkable, and the apparently whole number relations require explanation. In a later paper it is hoped to deal with the relations in systems such as Cu–In where the ionic radius of the solute is large.

ACKNOWLEDGMENTS

Thanks are due to Professor Sir Cyril Hinshelwood, F.R.S., and to Dr. F. M. Brewer for laboratory accommodation and other facilities which have greatly encouraged the present work. Dr. A. Hellawell must also be thanked for determining the Ag–Ge liquidus and solidus points used in fig. 10.

APPENDIX A

THE SYSTEM COPPER–ARSENIC†

1. *Introduction and Previous Work*

The liquidus curve of the system Cu–As was investigated by Bengough and Hill (1910), according to whom the α-liquidus falls steeply to a eutectic at 683°c, and then rises to a maximum in the region 25–28 atm% As, corresponding to the formation of the phase usually known as Cu_3As. The α-solid solubility curve below 686°c was established accurately by the x-ray work of Mertz and Mathewson (1937) and of Owen and Morris (1949). In the present work the liquidus has been determined accurately almost as far as the second eutectic at 46 atm% As and 600°c. The α-solidus has been established by microscopical methods, and by x-ray methods some information has been gained of the solid phases in the region 25–32 atm% arsenic.

2. *Experimental Methods*

(*a*) *Metals used*

The British Non-Ferrous Metals Research Association kindly presented three master alloys containing approximately 18, 36, and 46 atm% As. These were made from pure copper and high purity arsenic, and contained a trace of phosphorus in order to ensure freedom from oxygen. In view of the close resemblance between the chemical characteristics of phosphorus and arsenic, it was felt that the presence of a trace of phosphorus was less serious than that of oxygen. The Association also kindly prepared a series of cast and hot rolled copper-rich alloys which were used for the preparation of alloys of intermediate composition, and also for the solidus determination.

(*b*) *Cooling curve methods*

For alloys containing up to 30 atm% arsenic cooling curves were taken by conventional methods, using an atmosphere of purified argon in a closed tube furnace designed by Hellawell and Hume-Rothery (1957).

---

† The experimental work described was carried out by one of us (J.B.) for Part II of the Honours Course in Chemistry at the University of Oxford.

The cooling curve ingots weighed about 40 g, and all the standard precautions† were taken to ensure the accuracy of the temperature measurements and the absence of temperature gradients in the melt. The ingots were weighed after the experiments, and up to 21 atm% arsenic the loss of weight was negligible. Beyond this point the experiment was stopped as soon as the liquidus point had been established, and the ingot was rapidly cooled so that no appreciable loss of arsenic occurred after the arrest. Separate experiments were made in order to determine the temperatures of the eutectic and peritectic horizontals. All ingots were analysed after the experiment.

The above methods were satisfactory for alloys containing up to about 30 atm% arsenic, but beyond this point the loss of arsenic by volatilization was too great. Further progress was made by melting the alloys in closed silica tubes into which the thermocouple sheath was inserted by means of a fused joint. The whole was packed in sand in an iron tube, and heated in an electric furnace which was rocked during the taking of the cooling curve.

(*c*) *The determination of the α-solidus*

The cast and hot-rolled specimens prepared by the British Non-Ferrous Metals Research Association were homogenized in sealed tubes containing sufficient argon to give a pressure of approximately one atmosphere at the highest temperature used. After homogenization, specimens were annealed at successively higher temperatures and, after quenching were examined microscopically for the presence of chilled liquid.

(*d*) *Identification of phases by X-ray methods*

For this work use was made of the methods described by Owen and Morris (1949). Suitable proportions of the powdered master alloys were heated together in sealed silica tubes at constant temperature, after which the tube was quenched, and a Debye-Scherrer powder x-ray diffraction photograph was taken. Owing to the volatility of the arsenic a product of uniform composition was readily obtained after six hours at 575°c, and 24 hours at 450°c, and the phases present were identified by their diffraction patterns. This work was not carried out in detail, but it established the approximate positions of the phase-boundaries.

(*e*) *Analyses of the alloys*

The chemical analyses were carried out by Messrs. Johnson Matthey and Co. Ltd., and thanks are due to Dr. J. C. Chaston for his care and attention. In the cooling curve work, the whole ingot was dissolved except for the small portions lost in preparing the microsections. For the solidus determinations the actual specimens used for microscopical examination were analysed. In the x-ray work the powders of the critical alloys were analysed after the annealing treatment at 575°c, and these compositions were assumed for the powders annealed at 450°c.

---

† See W. Hume-Rothery and P. W. Reynolds (1937 a), and *Metallurgical Equilibrium Diagrams* by W. Hume-Rothery, J. W. Christian and W. B. Pearson.

3. *Experimental Results*

The results of the cooling curve experiments are given in the table, and are plotted in fig. 11. The temperature of the first eutectic horizontal was determined as lying between 684° and 685°c from three cooling curve experiments, and as between 685° and 686°c from arrests on heating curves. The true value may be taken as 685°±1°c, corresponding to the reaction Liquid$\rightleftharpoons\alpha+\beta$. The liquidus rises to a maximum at 26–27 atm% As and 827°c at which temperature the β-phase is in equilibrium with the liquid. The liquidus then falls to a peritectic horizontal at 709°c corresponding with the reaction Liquid$+\beta\rightleftharpoons\gamma$, where the γ-phase has the composition 30–31 atm% As. From this point the liquidus falls to the second eutectic horizontal at 46 atm% As and 600°c where the liquid is in equilibrium with solid γ and solid arsenic.

Atm% As	Liquidus point (°c)	Notes	Atm% As	Liquidus point (°c)	Notes
0·91	1072	A	22·70	795	A
1·74	1064	A	24·10	815	A
2·59	1053	A	25·42	826	A
5·21	1017	A	26·25	827	A
8·14	969	A	28·69	798	A
9·94	928	A	30·16	772	A
12·66	860	A	30·52	763	A
14·75	794	A	36·7	684	B
16·91	735	A	40·1	653	B
18·23	687	A	43·4	626	B
20·85	757	A			

Notes. The first and second, and fourth and fifth columns give respectively the compositions of the ingots by analysis, and the temperatures of the first arrests on the cooling curves.

The experiments marked A were carried out by conventional methods and those marked B were made with sealed tubes (p. 1192).

The α-solidus curve is shown in fig. 11, and was confirmed by two points from unpublished work by Miss Sutherland. The α-solid solubility curve in fig. 11 is that of Owen and Morris (1949) and shows an inflection at 380°c which suggests that a transformation on decomposition of the β-phase occurs at this temperature. No thermal arrests were detected in this region, suggesting that the transformation occurs too slowly or with too small an evolution of heat to be detected on an ordinary cooling curve. In agreement with the earlier workers an arrest was found at about 300°c for an alloy containing about 27 atm% As, but it was not possible to examine this in detail.

Fig. 11

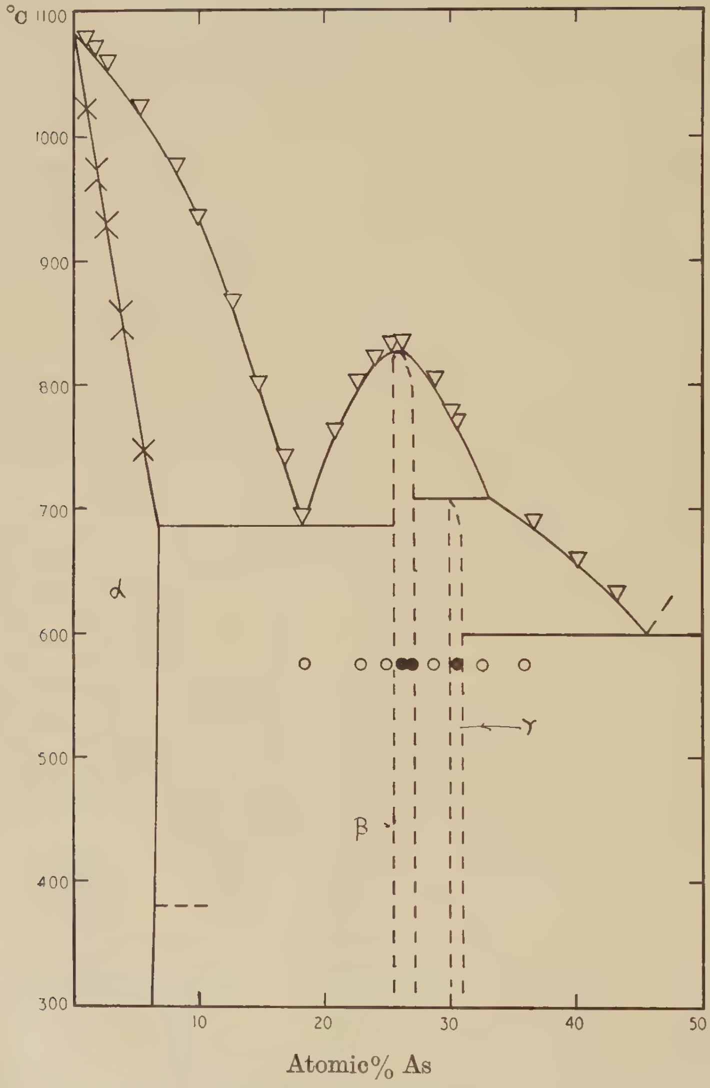

The x-ray diffraction films from the annealed and quenched powders gave clear and sharp lines for the 575°c specimens, and these suggested that the β-phase has a range of composition extending over at least 1 atm%. At 450°c the films for alloys in the region of the β-phase were satisfactory and showed no significant difference from those at 575°c, but for higher arsenic contents the films were less distinct, and it is hoped to investigate this problem later.

APPENDIX B

Sources of Data

For the liquidus and solidus curves, the tables of Hume-Rothery, Mabbott and Channel-Evans (1934) have been used, together with data from the following later sources.

Ag–Cd, Ag–In, Ag–Sn, Ag–Sb. Liquidus Curves. Hume-Rothery and Reynolds (1937 a).

Ag–Sb. Solidus. Hume-Rothery and Reynolds (1937 b) and (Miss) A. Sutherland (unpublished).

Cu–Ge. Liquidus points by J. Reynolds (1955) agree with those of H-R, M, and C-E.

Ag–Zn. Andrews, Davies, Hume-Rothery and Oswin (1941).

Ag–Ga.* Hume-Rothery and Andrews (1942).

Ag–Ge. A. Hellawell. (Unpublished.)

Ag–Mg.* Andrews and Hume-Rothery (1943).

Ag–Hg. Smithells (1955).

Cu–As. Liquidus and Solidus. Appendix A of present paper.

Cu–In. Liquidus and Solidus. J. Reynolds (1955). The Liquidus is in good agreement with that of Weibke and Eggers (1934), but the depression of the solidus is much greater.

The lattice distortion values have been taken from the data of Hume-Rothery, Lewin and P. W. Reynolds (1936), Owen and Roberts (1939), Owen and Edmunds (1938), and Owen and Rowlands (1940), and also from the sources marked * above.

References

Andrews, K. W., Davies, H. E., Hume-Rothery, W., and Oswin, C. R., 1941, *Proc. roy. Soc.* A, **177,** 149.

Andrews, K. W., and Hume-Rothery, W., 1941, *Proc. roy. Soc.* A, **178,** 464; 1943, *J. Inst. Metals*, **69,** 485.

Bengough, G. D., and Hill, B. P., 1910, *J. Inst. Metals*, **3,** 53.

Hellawell, A., and Hume-Rothery, W., 1957, *Phil. Trans. roy. Soc.* A, **249,** 417.

Hume-Rothery, W., and Andrews, K. W., 1942, *J. Inst. Metals*, **68,** 133.

Hume-Rothery, W., Lewin, G. F., and Reynolds, P. W., 1936, *Proc. roy. Soc.* A, **157,** 167.

Hume-Rothery, W., Mabbott, G. W., and Channel-Evans, K. M., 1934, *Phil. Trans. roy. Soc.* A, **233,** 1.

Hume-Rothery, W., and Reynolds, P. W., 1937 a, *Proc. roy. Soc.* A, **160,** 282; 1937 b, *J. Inst. Metals*, **60,** 365.

Jones, H., 1937, *Proc. phys. Soc. Lond.*, **49,** 243.

Mertz, J. C., and Matthewson, C. H., 1937, *Trans. Amer. Inst. Min. Met. Engrs.*, **124,** 59.

Owen, E. A., and Edmunds, I. G., 1938, *J. Inst. Metals*, **63,** 265.
Owen, E. A., and Morris, D. P., 1949–50, *J. Inst. Metals*, **76,** 145.
Owen, E. A., and Roberts, E. W., 1939, *Phil. Mag.*, **27,** 294.
Owen, E. A., and Rowlands, V. W., 1940, *J. Inst. Metals*, **66,** 371.
Reynolds, J., 1955, *Thesis*, Oxford.
Smithells, C. J., 1955, *Metals Reference Book.*
Warren, B. E., Averbach, B. L., and Roberts, B. W., 1951, *J. appl. Phys.*, **22,** 1493.
Weibke, F., and Eggers, H., 1934, *Z. anorg. Chem.*, **220,** 273.

The Centre of a Dislocation : I

By Elizabeth H. Yoffe
Cavendish Laboratory, University of Cambridge

[Received July 11, 1957]

Summary

An attempt is made to describe mathematically the state of stress at the centre of an edge dislocation. The discontinuity in stress across the slip plane suggests the use of the more general type of dislocation previously investigated by the author. As shown in the earlier paper the more general dislocation may be built up from an array of simple edge dislocations. Here the converse is applied; the simple edge dislocation is presented as the difference of two or more dislocations of the more general type. By this means it is possible to eliminate the central singularity hitherto obtained in the elastic dislocation, to calculate the stresses at all points, and to plot the law of force acting across the slip plane. The method is believed to be new, and is found capable of wider application.

---

§ 1. Introduction

The stress field of an edge dislocation as originally calculated by the theory of elasticity is not valid at the centre of the dislocation for two reasons, firstly because certain of the strain components are too large for elasticity theory to be applied, and secondly because the stresses and displacements as given by the theory become infinite at the centre. The problem is to find an alternative description for the state of stress at the centre consistent with the known elastic solution throughout the rest of the elastic body.

Originally the singularity at the centre was avoided by cutting out a small circular cylinder around the dislocation line and applying elasticity theory only to the region outside this. But Orowan pointed out that the actual physical strains need be large only near the slip plane, so that the half space to either side of it might reasonably be treated as an elastic continuum. The result of this was the well-known calculation by Peierls (1940) later extended by Nabarro (1947) and by Foreman *et al.* (1951) in which two elastic regions were joined across the slip plane by certain non elastic forces. These were related to the surface displacements of the two regions by a Law of Force, originally taken as sinusoidal in form but later modified by the insertion of parameters.

By this method valuable results were obtained concerning the variation of width of a dislocation with the Law of Force, and the applied stress necessary to set a dislocation in motion. But there are several fundamental objections to the theory which cannot entirely be ignored.

Firstly the solution does not agree with that of elastic theory even at large distances, although the strains are very small there and the theory might be expected to apply. Instead, Peierls' displacements approach those which would be obtained from the elastic solution by removing a strip of width $a/(1-\sigma)$ (where σ is Poissons ratio, a the interatomic distance normal to the slip plane) along the slip plane, and rejoining the remaining regions at a distance a while ignoring the differences in normal stress on the two surfaces. Thus even at great distances from the centre the two half planes do not rejoin to form an elastic continuum, since even there the equations of elasticity are not satisfied across the slip plane.

Secondly it is not always valid to assume, as Peierls has done, that the Law of Force must reduce to the form

$$\widehat{xy}=\mu\,\frac{\nabla u}{a}$$

for small strains. Here $\widehat{xy}$ is the shear stress or shearing force per unit area, μ the shear modulus and ∇u is the difference in the tangential components of displacement:

$$\nabla u=[u]_{y=a/2}-[u]_{y=-a/2}.$$

For in the elastic region the usual stress-strain relations must hold, i.e.

$$\widehat{xy}=\mu\left(\frac{\partial u}{\partial y}+\frac{\partial v}{\partial x}\right).$$

The term $\mu\partial u/\partial y$ corresponds to $\mu\nabla u/a$ in the Law of Force, but $\partial v/dx$ has been ignored. This term is by no means negligible for an edge dislocation, but is of the same order as $\partial u/\partial y$ along the slip plane. It is readily verified from the elastic solution (cf. Read 1953) that in fact, for x much greater than y, the relation between $\widehat{xy}$ and u is

$$\widehat{xy}\doteqdot\frac{2\mu}{(3-2\mu)}\cdot\frac{\nabla u}{a}$$

instead of the 'Law of Force' as assumed by Peierls and Nabarro.

The Law of Force was originally defined (Frenkel 1926) as the relation between applied stress and relative displacement when two half planes are sheared uniformly over one another. Then no contradiction arises since there is no variation with x. The Law should not, however, be applied without modification to a non-uniform stress field.

To avoid these difficulties a different approach is made in the present paper. The body is treated as elastic throughout but with discontinuities of stress or displacement across a limited band of the slip plane. By assuming certain simple distributions of the relative displacement it is possible to represent the centre in terms of higher order dislocations. The method of combining these dislocations to represent a Burgers edge dislocation at large distances is described in § 2. The method is applied to first order dislocations in § 3 and to second order dislocations in § 4. The resulting Law of Force is calculated and discussed in § 5.

§ 2. The General Method

As shown previously by the author (Mann, 1949) it is possible to find simple functions describing the state of stress in an elastic body having given discontinuities of displacement or transverse stress across a certain plane. A state of plane strain is assumed, and axes x, y are chosen along and normal to the slip plane respectively as in figure 1.

Fig. 1

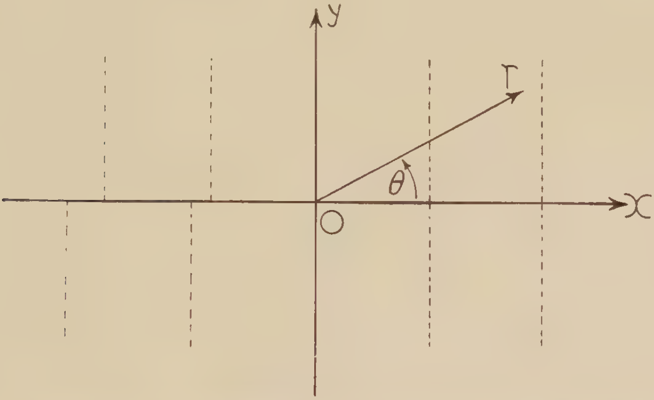

Diagram of an edge dislocation of arbitrary order showing coordinate axes.

Let r, θ be polar coordinates, measured from the positive x axis, and let u, v be the x-, y-components of displacement. Then an edge dislocation of order n is defined as one for which the relative displacement u' is proportional to the nth power of the distance from the origin :

$$u' \equiv [u]_{\theta=\pi} - [u]_{\theta=-\pi}$$

$$= \alpha_n r^n \qquad \qquad (1)$$

where α_n is a constant.

The Volterra or Burgers edge dislocation is described as one of zero order, since the relative displacement is constant over half the slip plane :

$$u' = \alpha_0 = b \text{ say.} \qquad \qquad (2)$$

The stress system corresponding to an edge dislocation of any order n was derived in the previous paper. It may be expressed briefly in terms of a stress function U_n, from which the components of stress and displacement are readily derived.

The method to be used in this paper is based on the following argument. Since all the equations of elasticity are linear, a stress or displacement derived from the sum of two stress functions is equal to the sum of the corresponding stresses or displacements derived from the stress functions separately. Moreover if all the functions are continuous and differentiable, it is possible to differentiate a stress function with respect to x, and, treating the derivative as a new stress function, derive from it new stresses and displacements. Each such component is equal to the derivative of the corresponding component derived from the original stress function.

The stress functions of the edge dislocations afford particular examples of this property. The stress function U_2 of a second order edge dislocation is given by :

$$U_2=By\left[2(x^2-y^2)\log r-4xy\theta-3x^2+\frac{5y^2}{3}\right] \quad . \; . \; . \; . \quad (3)$$

where B is a real arbitrary constant, and from it are derived stresses and displacements :

$$\widehat{xy}_2=-4B(x\log r-x-2y\theta)$$

$$2\mu u_2=4B[(2-\sigma)xy-(3-2\sigma)xy\log r+\theta((2-\sigma)y^2-(1-\sigma)x^2)].$$

The relative displacement at $\theta=\pm\pi$ is given by :

$$2\mu u'=-8\pi B(1-\sigma)x^2$$

$$u'=-\frac{4\pi B(1-\sigma)x^2}{\mu}$$

$$=\alpha_2 r^2 \text{ say.} \quad . \; . \; . \; . \; . \; . \; . \; . \quad (4)$$

The function U_2 may be differentiated with respect to x to give a new stress function U_1,

$$U_1=\frac{\partial U_2}{\partial x}$$

$$=4By(x\log r-x-y\theta) \quad . \; . \; . \; . \; . \; . \; . \quad (5)$$

which gives stresses and displacements :

$$\widehat{xy}_1=-4B\left(\log r+\frac{y^2}{r^2}\right)$$

$$=\frac{\partial\widehat{xy}_2}{\partial x}. \quad . \; . \; . \; . \; . \; . \; . \; . \; . \; . \; . \quad (6)$$

$$2\mu u_1=-4B[(3-2\sigma)y\log r+2(1-\sigma)x$$

$$=2\mu\frac{\partial u_2}{\partial x}$$

$$u'_1=\frac{\partial u'_2}{\partial x}$$

$$=-\frac{8\pi B(1-\sigma)x}{\mu}$$

$$=-2\alpha_2 r.$$

U_1 is therefore the stress function of a first order edge dislocation. It may be differentiated to give a third stress function U_0:

$$U_0 = \frac{\partial^2 U_2}{\partial x^2}$$

$$= 4By \log r \quad . \quad . \quad . \quad . \quad . \quad . \quad . \quad . \quad . \quad (7)$$

$$\widehat{xy}_0 = \frac{\partial xy_1}{\partial x}$$

$$= -\frac{4Bx \cos 2\theta}{r^2} \quad . \quad . \quad . \quad . \quad . \quad . \quad . \quad . \quad (8)$$

$$2\mu u_0 = 2\mu \frac{\partial u_1}{\partial x}$$

$$= -2B[\sin 2\theta + 4(1-\sigma)\theta].$$

The relative displacement is u'_0 where :

$$u'_0 = \frac{\partial u'_1}{\partial x}$$

$$= -\frac{8\pi B(1-\sigma)}{\mu}$$

$$= 2\alpha_2.$$

U_0 is therefore the stress function of a zero order or Volterra edge dislocation. Moreover comparison of eqns. (4), (6) and (8) shows that, with increasing order of the dislocation, the stresses and displacements become progressively more regular at the origin and less so at infinity.

For this reason a more regular centre for the zero order dislocation may be formed by combining higher order dislocations at suitable positions. These must be so chosen that each component of the combined system approximates at large distances to the corresponding component of the zero order dislocation, that is, to its own first derivative if first order dislocations are used, or to its own second derivative if second order dislocations are used.

Let some component of a first order dislocation take the value $f(x, y)$ at any point P and values f_1, f_2 at adjacent points P_1, P_2 respectively arranged as in fig. 2. Then for sufficiently small h, and differentiable f, the finite difference relation holds :

$$\frac{\partial f}{\partial x} \doteqdot \frac{f_1 - f_2}{2h} \quad . \quad . \quad . \quad . \quad . \quad . \quad . \quad . \quad (9)$$

and, since f increases rapidly with r, (9) is also true for fixed h and sufficiently large r, with proportional error of the order h^2/r^2.

But
$$f_1 = f(x+h, y)$$
$$= f(x_2, y_2)$$

where x_2, y_2 are the coordinates of P referred to D_2 as origin. Similarly

$$f_2 = f(x_1, y_1)$$

giving the approximate relation

$$f(x_2, y_2) - f(x_1, y_1) \doteqdot 2h \frac{\partial f(x, y)}{\partial x} \quad . \quad . \quad . \quad . \quad (10)$$

for large r. This states that if a first order dislocation is situated at D_2 and a similar one of opposite sign at D_1, then at any sufficiently distant point P a component of the combined stress systems is approximately equal to $2h$ times the derivative of that component, that is, to the corresponding component of the zero order dislocation. Such a system is investigated more fully in § 3.

Fig. 2

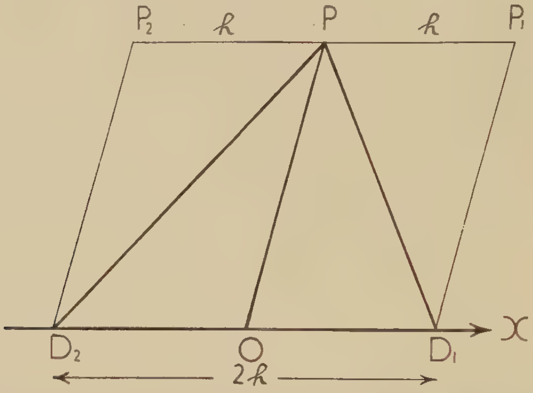

Diagram illustrating the equivalence between the difference at one point of similar components of two separated dislocations and the difference in the values at two separate points of a component of one dislocation.

Similarly a representation in terms of second order dislocations may be obtained from the finite difference approximation to the second derivative. Second order dislocations are placed at D_1 and D_2, and a double negative one at O. On dividing by h^2 the result at large distances is the second derivative of the component considered, that is, the corresponding component of the zero order dislocation (see § 4).

The method may clearly be extended to third or higher order derivatives if desired. Second order dislocations are sufficient for the present purpose since their components of stress and displacement are all finite at the centre.

§ 3. FIRST ORDER DISLOCATIONS

The zero order edge dislocation with relative displacement (Burger's vector) b may be represented by first order dislocations (5) by suitable choice of the arbitrary constant. Let one such dislocation be situated at D_2 and an equal negative one (B replaced by $-B$) at D_1 as in fig. 3. On dividing by $2h$ the stress function of the combined system is given by

$$U=\frac{2By}{h}[(x+h)\log r_2-(x-h)\log r_1-2h+y(\theta_1-\theta_2)] \quad . \quad . \quad (11)$$

where r_1, θ_1 are measured from D_1, and r_2, θ_2 from D_2 as in fig. 3:

$$r_2{}^2=(x+h)^2+y^2$$

$$\tan\theta_2=\frac{y}{x+h}\text{ etc.}$$

From eqn. (6) the relative displacement takes the following values along the slip plane :

$$\begin{aligned} u' &= 0 \quad \text{for } x \geqslant h \\ &= -\frac{4\pi B(1-\sigma)(h-x)}{\mu h} \quad \text{for } -h \leqslant x \leqslant h \\ &= -\frac{8\pi B(1-\sigma)}{\mu} \quad \text{for } x \leqslant -h. \end{aligned} \qquad (12)$$

Fig. 3

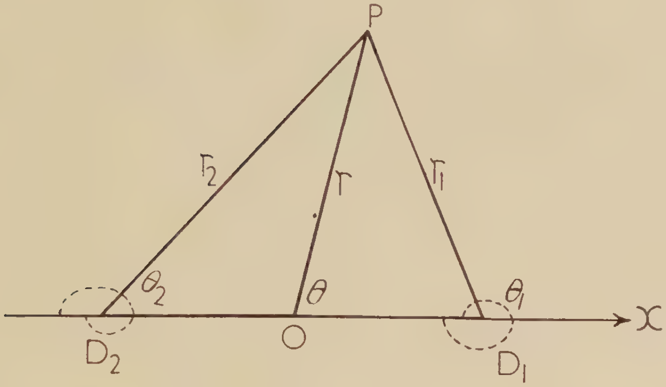

Diagram showing the origins of the various coordinates.

So $u'=b$ on the negative axis if B is chosen suitably :

$$B = \frac{-\mu b}{8\pi(1-\sigma)}.$$

The stress components of this dislocation are readily derived from the stress function :

$$\left.\begin{aligned} \widehat{xx} &= \frac{-\mu b}{2\pi(1-\sigma)}\left[\frac{(x-h)y}{r_1^2} - \frac{(x+h)y}{r_2^2} + 2(\theta_1-\theta_2)\right], \\ \widehat{yy} &= \frac{-\mu b y}{2\pi(1-\sigma)}\left[\frac{x+h}{r_2^2} - \frac{x-h}{r_1^2}\right], \\ \widehat{xy} &= \frac{-\mu b}{2\pi(1-\sigma)}\left[\log\left(\frac{r_1}{r_2}\right) + y^2\left(\frac{1}{r_1^2} - \frac{1}{r_2^2}\right)\right]. \end{aligned}\right\} \qquad (13)$$

The stress components $\widehat{xx}$ and $\widehat{yy}$ are finite everywhere, but $\widehat{xy}$ becomes infinite at D_1 and D_2. The stress $\widehat{xx}$ is discontinuous across the slip plane between D_1 and D_2 as indicated in fig. 4. Both displacements remain finite in the finite plane.

At points a large distance from O the stress field approaches that of a zero order dislocation by (10). This may be verified directly. From fig. 3

$$\begin{aligned} r_1 \sin\theta_1 &= r \sin\theta = r_2 \sin\theta_2 \\ r_1 \cos\theta_1 + h &= r \cos\theta = r_2 \cos\theta_2 - h \end{aligned} \qquad (14)$$

and, for r large compared with h,

$$\theta_1-\theta_2 \doteqdot \frac{2h\sin\theta}{r}$$

$$\log\left(\frac{r_2}{r_1}\right) \doteqdot \frac{2h\cos\theta}{r}$$

with an error of the order h^2/r^2. On substituting from (14) in eqn. (11) it is readily verified that U approaches U_0 for r large :

$$\begin{aligned} U &\doteqdot \frac{2By}{h}\left[x.\frac{2h\cos\theta}{r}+2h\log r-2h+y.\frac{2h\sin\theta}{r}\right] \\ &=4By\log r \\ &=U_0. \end{aligned}$$

Similarly it may be verified that each stress component approaches that of the zero order dislocation at large distances.

Fig. 4

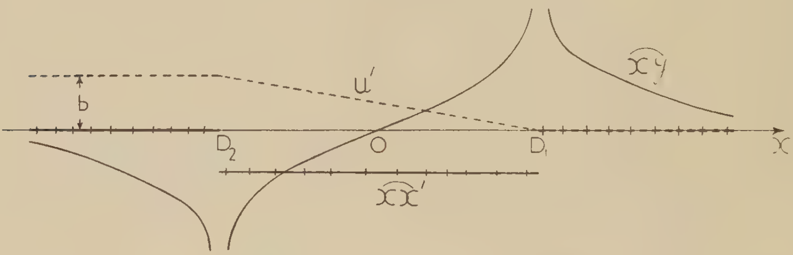

Curves drawn to an arbitrary scale indicating certain components of the edge dislocation expressed as the difference of two first order dislocations.

The zero order dislocation is often represented by the symbol ⊥, the horizontal line representing the slip plane and the vertical line the extra row of atoms above it. If the symbol ╷┘ is introduced to represent a first order dislocation as in fig. 1, the result of this section may be summarized diagrammatically as :

$$┐ + ╷┘ = ⊥ . \qquad (15)$$

The final dislocation involves slip by the distance b if the first order ones have relative displacements $\pm br/2h$ and are distant $2h$ apart. The symmetrical relation

$$⊥ = └╷ + ┌╵$$

is also valid.

§ 4. Second Order Dislocations

It was shown in § 2 that the stress function of the first order dislocation may be obtained by differentiating the stress function of the second order dislocation with respect to x. Therefore, repeating the argument of § 3, a first order dislocation may be represented at large distances by the difference of two second order dislocations.

This may be stated symbolically :

$$╵╵┐ + ╷╷┘ = ╷┘ \qquad (16)$$

where the symbol 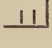 represents a second order dislocation of the form shown in fig. 1.

On comparing (16) and (15) a relation is obtained for the zero order dislocation in terms of four second order dislocations :

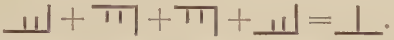

. . . . . (17)

Positive dislocations of the type (3) are placed at D_1 and D_2, and two similar negative dislocations at points nearer the origin, say at $x=\pm k$. The relative displacement of the final dislocation is $u'=b$ if the second order dislocations are such that

$$u'=\pm\frac{br^2}{2(h^2-k^2)}.$$

The simplest case, which will be considered in detail, is that of $k=0$, the two negative dislocations being situated at the origin. It will be shown in § 5 that varying k gives different Laws of Force.

The result (17) may also be written in terms of stress functions :

$$U=U_2(x+h,y)-U_2(x+k,y)-U_2(x-k,y)+U_2(x-h,y)$$
$$\rightarrow(h^2-k^2)U_0(x,y)$$

or, for $k=0$

$$U=U_2(x+h,y)-2U_2(x,y)+U_2(x-h,y)$$
$$\rightarrow h^2U_0(x,y). \quad . \quad . \quad . \quad . \quad . \quad . \quad . \quad . \quad . \quad . \quad . \quad . \quad (18)$$

In eqn. (3) for U_2 the constant B must now be chosen as

$$-\mu b/8\pi(1-\sigma)h^2$$

$$U=\frac{-\mu by}{8\pi(1-\sigma)h^2}\Big[((x-h)^2-y^2)\log((x+h)^2+y^2)-2(x^2-y^2)\log(x^2+y^2)$$
$$+((x-h)^2-y^2)\log((x-h)^2+y^2)-6h^2$$
$$-4y^{-1}\left((x+h)\tan^{-1}\frac{y}{x+h}-2x\tan^{-1}\frac{y}{x}+(x-h)\tan^{-1}\frac{y}{x-h}\right)\Big]$$
$$=\frac{-\mu by}{4\pi(1-\sigma)h^2}\left[\sum_i(x_i{}^2-y^2)\log r_i-2y\sum_i x_i\theta_i-3h^2\right]. \quad . \quad . \quad . \quad . \quad (19)$$

The suffix i and summation sign have been introduced for brevity :

$$\sum_i f_i\equiv f(x+h)-2f(x)+f(x-h)$$

for any function f of x.

The stress components are derived from eqn. (19) :

$$\left.\begin{aligned}\widehat{xx}&=\frac{\mu b}{2\pi(1-\sigma)h^2}\left[3y\log\left(\frac{r_1r_2}{r_2}\right)+2\sum_i x_i\theta_i\right],\\ \widehat{yy}&=\frac{-\mu b}{2\pi(1-\sigma)h^2}y\log\left(\frac{r_1r_2}{r^2}\right),\\ \widehat{xy}&=\frac{\mu b}{2\pi(1-\sigma)h^2}\left[\sum_i x_i\log r_i-2y\sum_i\theta_i\right].\end{aligned}\right\} \quad . \quad . \quad (20)$$

At large distances these approach the stress components of the zero order dislocation (cf. Read 1953) :

$$\widehat{xx} \to \frac{-\mu b}{2\pi(1-\sigma)r}\sin\theta(2+\cos 2\theta),$$

$$\widehat{yy} \to \frac{\mu b}{2\pi(1-\sigma)r}\sin\theta\cos 2\theta,$$

$$\widehat{xy} \to \frac{\mu b}{2\pi(1-\sigma)r}\cos\theta\cos 2\theta.$$

The components of displacement are given by :

$$u=\frac{b}{4\pi(1-\sigma)h^2}\left[(3-2\sigma)y\sum_i x_i\log r_i+(1-\sigma)\sum_i x_i^2\theta_i-(2-\sigma)y^2\sum_i\theta_i\right]$$

$$v=\frac{-b}{8\pi(1-\sigma)h^2}\left[(1+2\sigma)y^2\log\frac{(r_1r_2)}{r^2}+(1+2\sigma)h^2+(1-2\sigma)\sum_i x_i^2\log r_i+4\sigma y\sum_i x_i\theta_i\right]\quad . \quad . \quad (21)$$

and approach those of the zero order dislocation at large distances :

$$u \to \frac{b}{8\pi(1-\sigma)}[\sin 2\theta+4(1-\sigma)\theta]$$

$$v \to \frac{-b}{8\pi(1-\sigma)}[\cos 2\theta+2(1-2\sigma)\log r].$$

The distributions of $\widehat{xx}'$, $\widehat{xy}$ and u' along the slip plane are sketched in fig. 5.

Fig. 5

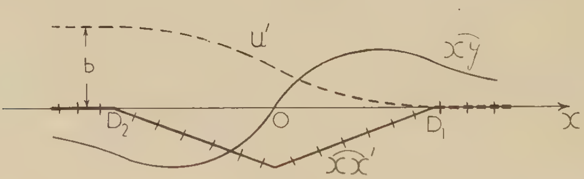

Curves drawn to an arbitrary scale for the edge dislocation expressed in terms of second order dislocations. The shear stress is finite and continuous all along the slip plane.

On comparing this with fig. 4 it is seen that there is now no discontinuity in $\widehat{xx}'$, nor singularity in $\widehat{xy}$. The smooth curve of u' is given by :

$$\begin{aligned} u' &= 0 \quad \text{for } x \geqslant h \\ &= \frac{b(h-x)^2}{2h^2} \quad \text{for} \quad 0 \leqslant x \leqslant h \qquad . \quad . \quad . \quad . \quad . \quad (22) \\ &= \frac{b(h^2-2hx-x^2)}{2h^2} \quad \text{for} \quad -h \leqslant x \leqslant 0 \\ &= b \quad \text{for} \quad x \leqslant -h. \end{aligned}$$

The maximum shear stress is about $1{\cdot}76b/2\pi(1-\sigma)h$ and occurs at $x=\pm\frac{1}{2}\sqrt{2}h$. This may be compared with the result of Foreman *et al.* (1951)

$$p_{\max} \doteqdot \frac{\mu b}{2\pi(1-\sigma)w}$$

where w is the width of the dislocation and approaches $0{\cdot}6h$ for large h.

§ 5. The Law of Force

From the values of u and $\widehat{xy}$ near the slip plane a curve may be drawn showing the relation between the relative displacement ∇u of adjacent atoms and the shear stress acting at their centres. Peierls and Nabarro called this relation the Law of Force although, as shown in § 1, it is a law which changes form on changing the external stress field.

Fig. 6

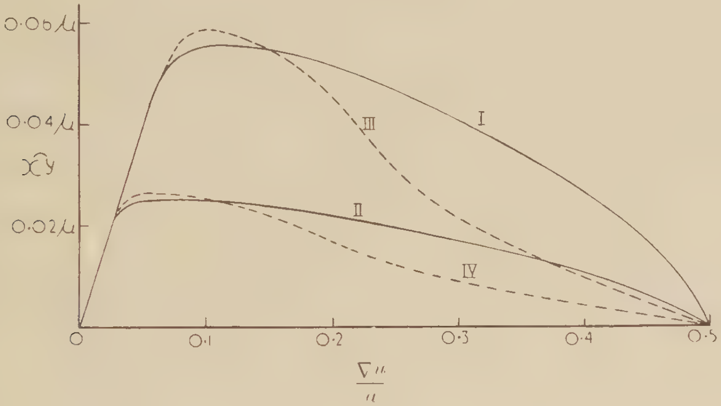

The Law of Force for various dislocations.

Curve I	$h=6{\cdot}7b$	$w=5b$	formulae (23) and (24)
II	$h=15b$	$w=10b$	
III	$h=6{\cdot}7b$	$w=5{\cdot}7b$	formulae (25) and (26).
IV	$h=15b$	$w=12b$	

For comparison with previous work the Law of Force is again plotted in fig. 6. The ordinate is the value of $\widehat{xy}$ on the slip plane. For convenience in varying h the shear stress may be expressed as a function of $t=x/h$;

$$\widehat{xy}=\frac{\mu b}{2\pi(1-\sigma)h}T \qquad \text{. . . . . . .} \quad (23)$$

where

$$T\equiv\tfrac{1}{2}[(t-1)\log(t-1)^2-2t\log t^2+(t+1)\log(t+1)^2].$$

Similarly $\nabla u/a$, for small a/h, is given by

$$\frac{\nabla u}{a}=\frac{u'}{a}+\frac{(3-2\sigma)b}{4\pi(1-\sigma)h}T+0\left(\frac{a}{h}\right)^2 \qquad \text{. . . . . .} \quad (24)$$

where

$$
\begin{aligned}
u' &= 0 & t &\geqslant 1 \\
&= \tfrac{1}{2}b(1-t)^2 & 0 &\leqslant t \leqslant 1 \\
&= \tfrac{1}{2}b(1-2t-t^2) & -1 &\leqslant t \leqslant 0 \\
&= b & t &\leqslant -1.
\end{aligned}
$$

These formulae have been used in plotting curves I and II of fig. 6, with $a=b$, $\sigma=\frac{1}{4}$. For other values of h, a and σ the curves are readily obtained from the table.

t	0	0·1	0·2	0·3	0·4	0·5	0·6	0·7	0·8	0·9	1	2	3	∞
T	0	0·66	1·04	1·31	1·51	1·65	1·73	1·76	1·74	1·64	1·39	0·54	0·34	$1/t$
u'/b	0·5	0·40	0·32	0·245	0·18	0·125	0·08	0·042	0·02	0·005	0	0	0	0

Curves III and IV have been added to show how the form of the Law of Force may be varied by altering the positions of the second order dislocations. The two dislocations at $x=0$ are moved to $x=\frac{1}{2}h$ and $x=-\frac{1}{2}h$ respectively, and the constants are adjusted to keep the stress field unaltered at large distances. Then the shear stress on the slip plane is given by

$$\widehat{xy}=\frac{2\mu b}{3\pi(1-\sigma)h}T_1 \quad . \quad . \quad . \quad . \quad . \quad . \quad . \quad . \quad (25)$$

where

$$T_1=\tfrac{1}{2}[(t-1)\log(t-1)^2-(t-\tfrac{1}{2})\log(t-\tfrac{1}{2})^2-(t+\tfrac{1}{2}) \times\log(t+\tfrac{1}{2})^2+(t+1)\log(t+1)^2]$$

and

$$\frac{\nabla u}{a}=\frac{u'_1}{a}+\frac{(3-2\sigma)b}{3\pi(1-\sigma)h}T_1 \quad . \quad . \quad . \quad . \quad . \quad . \quad . \quad (26)$$

with

$$
\begin{aligned}
u'_1 &= \frac{2b}{3}(1-t)^2 & \tfrac{1}{2} &\leqslant t \leqslant 1 \\
&= \frac{2b}{3}(\tfrac{3}{4}-t) & -\tfrac{1}{2} &\leqslant t \leqslant \tfrac{1}{2} \\
&= \frac{2b}{3}(\tfrac{1}{2}-2t-t^2) & -1 &\leqslant t \leqslant -\tfrac{1}{2} \\
&= b & t &\leqslant -1.
\end{aligned}
$$

Further variations may readily be obtained by choosing other positions for the central dislocations. In the limit as the inner dislocations approach those at $x=\pm h$ the solution reduces to that of two first order dislocations as in § 3.

Narrower dislocations are obtained by decreasing h, but the width as measured along $y=\pm\frac{1}{2}b$ does not decrease indefinitely. Even for the limiting case $h=0$, when the stress field reduces to that of a zero order dislocation (Read *loc. cit.*) the displacement u on $y=\pm\frac{1}{2}b$ gives the width $1{\cdot}8b$. The width $1{\cdot}5b$ used by Peierls is obtainable only by taking $a=0{\cdot}8b$ or less in the zero order dislocation.

The elastic solution given in this paper cannot be expected to give so narrow a dislocation. The width $1{\cdot}5b$ implies that the first row of atoms has been compressed or extended by the amount $\frac{1}{4}b$ within a distance $1{\cdot}5b$, an average strain of 1/6, to which elasticity theory can scarcely apply.

§ 6. THE STRAIN ENERGY

The strain energy W per unit length of the dislocation is estimated from the work done on the sides of a cut from $x=h$ to $x=-R$ along the slip plane, assuming an outer boundary of large radius R. It is readily shown to be independent of the width h except for the usual term in $\log (R/h)$

$$W=-\tfrac{1}{2}\int_{-R}^{h} \widehat{xy}.u'dx+W_R$$

where W_R represents the contribution from the outer surface and is independent of h if R is sufficiently large. From (23) and (24),

$$\begin{aligned}
-\tfrac{1}{2}\int_{-R}^{h} \widehat{xy}.u'\,dx &= \tfrac{1}{2}\int_{-h}^{-R} \widehat{xy}.u'\,dx+\tfrac{1}{2}\int_{h}^{-h} \widehat{xy}.u'dx \\
&= \frac{\mu b^2}{4\pi(1-\sigma)h}\left\{\int_{-1}^{\frac{-R}{h}} T.h\,dt+\int_{0}^{1}(2t-t^2)T.h\,dt\right\} \\
&= \frac{\mu b^2}{4\pi(1-\sigma)}\log\frac{R}{h}+\text{ terms independent of } R,\ h \\
&= \frac{\mu b^2}{4\pi(1-\sigma)}\left(\log\frac{R}{h}+1{\cdot}3\right).
\end{aligned}$$

§ 7. CONCLUSION

Having calculated the stress fields from various assumed distributions of relative displacement, it is desirable to compare the result with experiment and so choose the solution closest to reality. Unfortunately this seems difficult to do. The properties most apparent in experiment depend on long range effects, and at large distances the fields of all these dislocations are identical.

The Law of Force at least provides a comparison with previous theories and has been calculated for that purpose. The curves I and II of fig. 6 are similar in form to those of Foreman *et al.*, although with a different initial slope for reasons discussed in § 1. Curves III and IV are more nearly of the form proposed by Orowan (1954). The maximum shear stress on the slip plane is of the same order as that obtained by Foreman *et al.* at the first row of atom centres. It is about $\mu b/3h$, the central singularity having entirely disappeared.

The chief result of this calculation therefore appears to be a change in the initial slope of the force curve.

But the method itself is of wider application and opens up a whole new field of problems of plane elasticity. Of particular interest are those concerned with inclusions, such as deposits of solute atoms along certain planes. If the dislocations of this paper are replaced by those of the second type where the discontinuity is v' instead of u', the same method gives the stresses around an inclusion of very general shape. The problem of a narrow slit opening only very gradually from each end is now readily soluble, whereas previously it was treated as the limit of an ellipse with consequent difficulties and complications. The stress field of such a dilated slit is treated in a subsequent paper.

ACKNOWLEDGMENTS

I wish to thank Dr. P. B. Hirsch for very helpful discussion and criticism, Dr. J. S. Koehler for reading the manuscript, and the Atomic Energy Research Establishment, Harwell, for a grant.

REFERENCES

FOREMAN, A. J., JASWON, M. A., and WOOD, J. K., 1951, *Proc. phys. Soc. Lond.* A, **64,** 156.
FRENKEL, J., 1926, *Z. Phys.*, **37,** 572.
MANN, E. H., 1949, *Proc. roy. Soc.* A, **199**, 376.
NABARRO, F. R. N., 1947, *Proc. phys. Soc. Lond.*, **59,** 256; 1952, *Advanc. Phys.*, **1,** 352.
OROWAN, E. O., 1954, *Dislocations in Metals A.I.M.M.E.*, 74.
PEIERLS, R. E., 1940, *Proc. phys. Soc. Lond.*, **52,** 34.
READ, W. T., 1953, *Dislocations in Crystals* (New York: McGraw-Hill), p. 116.

Photodisintegration of the Alpha Particle†

By B. H. Bransden and A. C. Douglas
Department of Natural Philosophy, University of Glasgow

and H. H. Robertson
CERN, European Organization for Nuclear Research, Geneva

[Received June 21, 1957]

Abstract

The cross section for the two particle, $^4He(\gamma, p)^3H$, photodisintegration of the alpha particle is calculated, taking into account the interaction between the proton and triton in the final state. It is shown that this is insufficient to remove the discrepancy between the experimental cross section, and cross sections calculated with wave functions that are consistent with the binding energy of the alpha particle, even when the tensor force is included in the two body interaction.

§ 1. Introduction

The study of the photodisintegration of the lightest nuclei may, in principle, yield valuable information about the nuclear wave functions and interactions. One of the most suitable reactions for investigation is the two particle, (γ, p) or (γ, n) photodisintegration of ^4He, as the cross section has been measured in detail at low energies (Fuller 1954, Perry and Bame 1955, Atkinson *et al.* 1957). The cross section (fig. 2) rises rapidly from the threshold (at 19·8 MeV), to a maximum value of $\sim 1{\cdot}8 \times 10^{27}$ cm² at 6 to 7 MeV above threshold. The theory of the reaction has been developed by Flowers and Mandl (1951) and by Gunn and Irving (1951), who were able to account for the qualitative features of the observed cross section, without assuming the existence of an excited state of ^4He. Gunn and Irving described the ejected proton by a plane wave and used simple analytic wave functions for ^3He and ^3H of the form :

Gaussian

$$\phi = N \exp\{-\mu^2(\sum_{i>j} r_{ij}^2)\} \quad . \quad . \quad . \quad . \quad (1\,a)$$

Irving

$$\phi = N \exp\{-\mu(\sum_{i>j} r_{ij}^2)^{1/2}\}/(\sum_{i>j} r_{ij}^2)^{1/2} \quad . \quad . \quad . \quad . \quad (1\,b)$$

They found that if the parameters μ (denoted subsequently by μ_T for the triton and μ_α for helium), were determined variationally to give the best ^{3}H and ^{4}He binding energies, using central forces, the calculated (γ, p) cross section exhibited a maximum at an energy much higher than that observed. To obtain a maximum at the correct energy, the size of the ^{4}He nucleus had to be increased considerably (μ_α decreased), but when this was done the value of the calculated cross section at maximum became several times too large.

---

† Communicated by the Authors.

In the present paper, the interaction in the final state is taken into account and it is found that the position of the calculated maximum is not significantly altered, although the detailed shape of the cross section does depend on the exchange nature of the nuclear force. Wave functions consistent with the binding energy of ^{4}He, for two body interactions containing a tensor component are used to recalculate the (γ, p) cross section. It is found that the consistency problem remains and that it is impossible to choose wave functions, of this type, that give both the correct position of the maximum cross section and also the correct binding energy of ^{4}He.

§ 2. GENERAL THEORY

The electric dipole transition matrix element for the (γ, p) reaction is

$$\mathscr{M}=\sum_{\text{spin}}\int \Psi_b^*(z_1+z_2)\Psi_a\,d\tau \qquad . \quad . \quad . \quad . \quad . \quad . \quad (2)$$

and the total cross section $\sigma(\gamma, \mathrm{p})$ is

$$\sigma(\gamma,\mathrm{p})=\tfrac{1}{2}\left(\frac{me^2}{\hbar^2}\right)kK\,|\,\mathscr{M}\,|^2. \qquad . \quad . \quad . \quad . \quad . \quad . \quad (3)$$

where z_1, z_2 are the z components of the coordinates of the protons, referred to the centre of mass of the system, Ψ_a, Ψ_b are initial and final nuclear wave functions, m is the nucleon mass and K, k the photon and ejected proton wave numbers, respectively.

By the conservation of energy, if the binding energies of ^{4}He and ^{3}H are denoted by ϵ_α, ϵ_{T} then

$$\hbar cK=\frac{2\hbar^2}{3m}k^2+\epsilon_{\mathrm{T}}-\epsilon_\alpha. \qquad . \quad . \quad . \quad . \quad . \quad . \quad . \quad (4)$$

Assuming for the moment central forces, the initial ^{4}He wave function may be written

$$\Psi_a=\phi_\alpha(1234)\sigma_0(1234) \qquad . \quad . \quad . \quad . \quad . \quad . \quad (5)$$

and the final (proton+triton) state may be represented by a resonating group wave function

$$\Psi_b=\frac{1}{\sqrt{2}}(1-P_{12})\phi_{\mathrm{T}}(234)F(1)\sigma_0(1234) \qquad . \quad . \quad . \quad . \quad (6)$$

where ϕ_α, ϕ_{T} are the ^{4}He and ^{3}H spatial wave functions, $F(1)$ describes the motion of the proton relative to the triton, P_{12} is the exchange operator and the singlet spin function σ_0 is

$$\sigma_0(1234)=\tfrac{1}{2}\{\alpha(1)\beta(2)-\beta(1)\alpha(2)\}\{\alpha(3)\beta(4)-\beta(3)\alpha(4)\}.$$

If ϕ_α, ϕ_T are symmetrical functions of the coordinates of all particles, then

$$\mathscr{M}=\frac{1}{\sqrt{2}}\int \phi_\alpha(\mathbf{r}, \mathbf{X}, \mathbf{R})\phi_T(\mathbf{X}, \mathbf{R})F(\mathbf{r})(r_z+\tfrac{4}{3}X_z)d\mathbf{r}\, d\mathbf{X}\, d\mathbf{R} \quad . \quad . \quad (7)$$

where the coordinates

$$\mathbf{r}=-\mathbf{r}_1+\tfrac{1}{3}(\mathbf{r}_2+\mathbf{r}_3+\mathbf{r}_4)\,; \quad \mathbf{X}=-\mathbf{r}_2+\tfrac{1}{2}(\mathbf{r}_3+\mathbf{r}_4),$$

$\mathbf{R}=\mathbf{r}_3-\mathbf{r}_4$ have been introduced. As ϕ_α, ϕ_T represent S states, the proton is ejected into a p state, so that

$$F(\mathbf{r})=(kr)^{-1}f_1(r)P_1(\cos\theta)$$

and

$$f_1(r)\sim\sin\left(kr-\tfrac{1}{2}\pi+\alpha\log(2kr)+\delta\right),$$

and

$$\alpha=-\frac{2me^2}{3\hbar^2k}.$$

§ 3. The Interaction in the Final State

Bransden *et al.* (1956) have calculated wave functions for neutron–triton scattering by the resonating group method assuming central two body interactions of either the Serber or symmetrical exchange type. This work is being extended to proton–triton scattering and radial functions $f_1(r)$ have been found over a range of proton energies up to 40 MeV (Bransden and Robertson 1957). The triplet even two body interaction is Gaussian

$$V(x)=A\exp(-\lambda^2x^2) \quad . \quad . \quad . \quad . \quad (8)$$

$$A=-45\text{ MeV}, \quad \lambda^2=0{\cdot}267\times10^{26}\text{ cm}^{-2}$$

and the triton is represented by the Gaussian function (1 *a*), with $\mu_T^2=0{\cdot}0718\times10^{26}$ cm^{-2}.

Comparison of the calculated n–H^3 and n–He^3 scattering cross sections with experiment suggests that (8) is a reasonable equivalent central interaction for the four body problem when a Serber exchange factor is used.

The initial ^{4}He ground state wave function is also taken to be of Gaussian form (1 *a*), and the constant μ_α is chosen so that the maximum of the (γ, p) cross section occurs at ~7 MeV above the threshold for a plane wave final state ($f_1=rj_1(kr)$). This gives $\mu_\alpha^2=0{\cdot}021\times10^{26}$ cm^{-2}, a value which leads to a very large root mean square radius, $R=2{\cdot}5\times10^{-13}$ cm for the helium nucleus.

In fig. 1, comparison is made between (γ, p) cross sections calculated with plane wave final state wave functions and those calculated with wave functions $f_1(r)$ determined from Serber and symmetrical two body interactions, (8). It is seen that the interaction between proton and triton in the final state alters the shape of the (γ, p) cross section appreciably, but that the position of the maximum given by the $f_1(r)$ determined from the Serber potential (which is consistent with the n–t scattering data), is quite close to that given by the plane wave. The use of the symmetrical interaction gives a maximum at an energy about 2 MEV higher.

Fig. 1

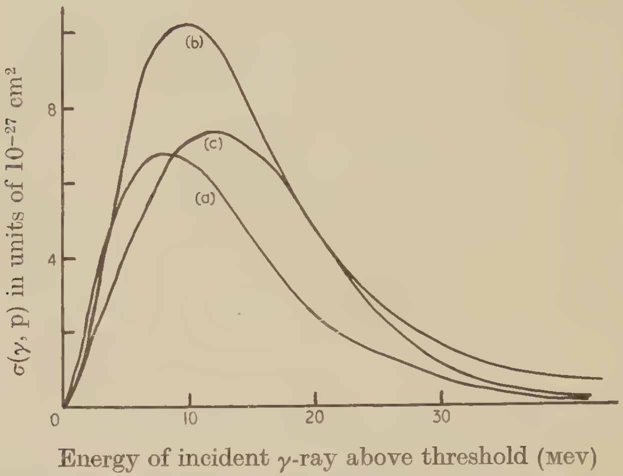

Calculated ^{4}He$(\gamma, p)^3$H cross sections for Gaussian wave functions: (*a*) with a plane wave final state, (*b*) interacting final state—Serber potential, (*c*) interacting final state—symmetrical potential.

If μ_α is altered to the value that gives the best ^{4}He binding energy, for the potential (8) ($\mu_\alpha^2=0{\cdot}0789\times10^{26}$ cm^{-2}, $\epsilon_\alpha=-26{\cdot}7$ MEV), then the position of the (γ, p) maximum cross section is much higher (~30 MEV above threshold). A resonating group ground state wave function of form (6) for ^{4}He has also been investigated. This wave function gives a binding energy as good as the Gaussian function ($\epsilon_\alpha=-26$ MEV) but has a much better asymptotic form. However, in this case the maximum cross section occurs at an energy which is still too high (~20 MEV above threshold), for both plane wave and interacting final states.

It must be concluded that the interaction in the final state is not responsible for the discrepancy between wave functions that are consistent with the binding energy of ^{4}He, and those that are consistent with the (γ, p) cross section. In investigating the consistency problem, it should be sufficient to employ plane wave final states and this has been done in the following sections.

§ 4. THE TENSOR FORCE

It has been suggested (Gunn and Irving 1951) that the discrepancy might be removed, if ^{4}He wave functions consistent with a two body interaction containing the tensor force (which is known to be important for the binding energy problem), were used in calculating the cross section In the presence of a tensor force, D state wave functions are directly coupled to the S state wave functions in both the ^{3}H and ^{4}He ground states. The electric dipole matrix elements (3) vanish for an S $\rightleftharpoons$ D transition and the D $\rightleftharpoons$ D transition is unimportant as the percentage D state of ^{3}H and ^{4}He is less than 4-6% and as the S $\rightleftharpoons$ S transition is not abnormally small. Thus only the S parts of the ^{3}H and ^{4}He wave functions are considered and are used in the expression (7), which still holds.

Irving (1953) and Abraham *et al.* (1955) have investigated the binding energies of ^{3}H, ^{4}He with two body potentials containing central and tensor components, with Yukawa radial shapes. The S and D wave parts of the ^{3}H and ^{4}He were represented by the exponential form

$$\phi = N \exp -\mu\Big(\sum_{i>j} r_{ij}^2\Big)^{1/2} \quad . \quad . \quad . \quad . \quad . \quad (9)$$

where μ is a variational parameter.

With this wave function, and with a plane wave final state

$$\sigma(\gamma, \mathrm{p}) = \tfrac{1}{3}\left(\frac{e^2}{\hbar c}\right) k^3 \left\{ k^2 + \frac{3m}{2\hbar^2}(\epsilon_\mathrm{T} - \epsilon_\alpha) \right\}$$

$$\times \frac{\mu_\alpha^{11}\mu_\mathrm{T}^{8}}{\left\{\dfrac{k^2}{12} + \dfrac{\mu_\alpha^{2}}{4} - \dfrac{3\mu_\mathrm{T}^{2}}{16}\right\}^{13}} \cdot \frac{11^2 \,.\, 9^2 \,.\, 7^2 \,.\, 5 \,.\, 3^{1/2}}{2^{25}} \{f(z)\}^2 \quad . \quad . \quad (10)$$

where

$$f(z) = \frac{1}{24}\, \frac{1}{\sqrt{z-1}}(585z^2 - 975z + 422)$$

$$- \frac{1}{11 \,.\, 9 \,.\, 7} \cdot \frac{1}{z^3\sqrt{z-1}}(594z^2 + 66z + 8)$$

$$- \frac{5}{8}(39z^2 - 52z + 16)\sin^{-1}\left(\frac{1}{\sqrt{z}}\right)$$

and

$$z = \frac{\mu_\alpha^{2} + k^2/3}{\mu_\alpha^{2} + k^2/3 - 3\mu_\mathrm{T}^{2}/4}.$$

Abraham *et al.* considered that if the nuclear potential is of the form

$$V(x) = -A[1 + \tfrac{1}{2}g(\boldsymbol{\sigma}_1 \,.\, \boldsymbol{\sigma}_2 - 1)]\frac{\exp(-\lambda x)}{\lambda x} - BS_{12}\frac{\exp(-\eta x)}{\eta x} \quad . \quad (11)$$

then the set of constants, consistent with the binding energy of ^{2}H, and with the low energy nucleon-nucleon scattering data, that is most likely to be also consistent with the ^{3}H and ^{4}He binding energies is

$$A = 39{\cdot}51 \text{ MeV}, \qquad B = 33{\cdot}03 \text{ MeV}$$

$$\lambda^{-1} = 1{\cdot}1847 \times 10^{-13} \text{ cm}, \qquad \eta^{-1} = 1{\cdot}5315 \times 10^{-13} \text{ cm}.$$

The variationally determined parameter (including the principal D state only) is for this case $\mu_\alpha = 1{\cdot}134 \times 10^{13}$ cm^{-1}, giving a binding energy $\epsilon_\alpha = -16{\cdot}6$ MeV. (This increases when further D states are included in the wave function.) The (γ, p) cross section calculated from (10) with $\mu_\alpha = \mu_\mathrm{T} = 1{\cdot}134 \times 10^{13}$ cm^{-1} is shown in fig. 2, where it is compared with cross sections calculated with $\mu_\alpha=\mu_\tau=0{\cdot}8\times10^{13}$ cm and $\mu_\alpha=\mu_T=0{\cdot}5\times10^{13}$ cm and the experimental cross section. The cross section for $\mu_\alpha=1{\cdot}134\times10^{13}$ cm rises much too slowly. If the tensor range is decreased slightly, the calculated binding energy can be raised to -28 Mev, but in this case μ_α is larger and the disagreement with the experimental cross section is worse. For $\mu_\alpha=0{\cdot}5\times10^{13}$ cm, the calculated cross section is in harmony with the experimental cross section, but this value of μ_α is far outside any value consistent with ^{4}He binding energy.

Fig. 2

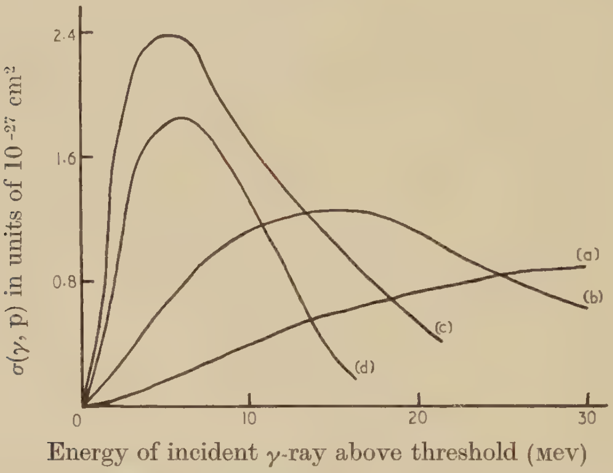

Calculated ^{4}He(γ, p)^{3}H cross sections for exponential wave functions: (*a*) $\mu_\alpha=1{\cdot}134\times10^{13}$ cm^{-1} consistent with binding energy of ^{4}He, (*b*) $\mu_\alpha=0{\cdot}8\times10^{13}$ cm^{-1}, (*c*) $\mu_\alpha=0{\cdot}5\times10^{13}$ cm^{-1}, (*d*) the experimental cross section (this is subject to an error of ±20%) taken from Perry and Bame (1955).

§ 5. CONCLUSION

To summarize the results of Gunn and Irving (1951) and of the present work, fig. 3 shows the variation of the position of the maximum cross section with the size of the ^{4}He nucleus for the exponential (9) and the Gaussian and Irving (1 *a*, b) wave functions. (The approximation $\mu_\alpha=\mu_T$ has been made, but it should be noted that $\sigma(\gamma, p)$ is relatively insensitive to μ_T.) It is clear that for wave functions that are functions of $(\sum_{i>j} r_{ij}^2)$ only, the position of the maximum depends sensitively on R, the root mean square radius of ^{4}He, but is not very dependent on the shape of the wave function.

The electron scattering experiments of McAllister and Hofstadter (1956) give a mean radius of $1{\cdot}61\times10^{13}$ cm for ^{4}He. Wave functions that agree with this value are not consistent with either the calculated binding energy (which requires a lower value of R for the type of wave function considered) or with the calculated (γ, p) maximum (which requires a larger R). The former result is true even for the more elaborate six parameter wave function of Clark (1954) (also a function of $(\sum_{i>j} r_{ij}^2)$) where for a calculated binding energy of −29·87 MeV, the mean radius is about $\frac{2}{3}$ of the observed value. It seems likely that these inconsistencies may be resolved when hard core interactions are introduced into the nuclear potential, which tend to push out the wave function, for a given binding energy, thus increasing R and at same time decreasing the calculated (γ, p) maximum†. Kikuta *et al.* (1956) have considered the effects of hard core interactions on the binding energies of ^{3}H and ^{3}He and they find that because of the increased value of R for these nuclei, the well known discrepancy between the coulomb and binding energies of ^{3}He can be removed. The construction of ^{4}He wave functions from two body interactions containing a repulsive core is being undertaken and the photodisintegration of ^{4}He will be investigated with the new wave functions.

Fig. 3

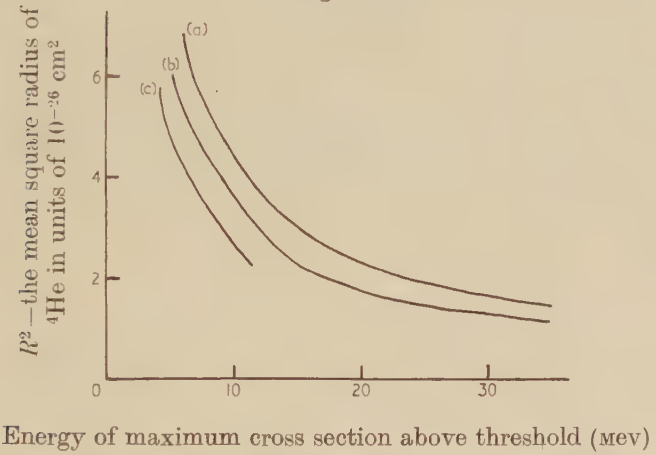

The variation of the position of the (γ, p) maximum cross section with nuclear size: (*a*) Gaussian wave functions, eqn. (1 *a*), (*b*) Exponential wave function, eqn. (19), (*c*) Irving wave functions, eqn. (1 *b*).

ACKNOWLEDGMENTS

The authors are indebted to Professor J. C. Gunn for his continued interest in this work and for helpful discussions. One of us (A. C. D.) is indebted to the Department of Scientific and Industrial Research for a grant.

---

† Since this work was completed, a paper by Rustgi and Levinger (1957) has appeared in which the total and bremsstrahlung weighted cross sections $\sigma_T = \int \sigma \, dE$, $\sigma_b = \int (\sigma/E) dE$, are calculated for the Irving (1953) wave function. Although these cross sections relate to the sum of all dipole reactions in ^{4}He, they find that the σ_b inferred from the experimental (γ, p) and (γ, n) measurements is already considerably larger than that calculated, and they draw conclusions from this result similar to our own.

References

ABRAHAM, G., COHEN, L., and ROBERTS, A. S., 1955, *Proc. phys. Soc., Lond.* A, **68,** 265.

ATKINSON, J. R., REID, J. M., and SWINBANK, P., 1957 (to be published).

BRANSDEN, B. H., ROBERTSON, H. H., and SWAN, P., 1956, *Proc. phys. Soc., Lond.* A, **69,** 877.

BRANSDEN, B. H., and ROBERTSON, H. H., 1957 (to be published).

CLARK, A. C., 1954, *Proc. phys. Soc., Lond.* A, **67,** 323.

FLOWERS, B. H., and MANDL, F., 1951, *Proc. roy. Soc.* A, **206,** 131.

FULLER, E. G., 1954, *Phys. Rev.*, **96,** 1306.

GUNN, J. C., and IRVING, J., 1951, *Phil. Mag.*, **42,** 1353.

IRVING, J., 1953, *Proc. phys. Soc., Lond.* A, **66,** 17.

KIKUTA, T., MORITA, M., and YAMADA, M., 1956, *Progr. theor. Phys., Osaka*, **15,** 222.

MCALLISTER, R. W., and HOFSTADTER, R., 1956, *Phys. Rev.*, **102,** 851.

PERRY, J. E., and BAME, S. J., 1955, *Phys. Rev.*, **99,** 1368.

RUSTGI, M. L., and LEVINGER, J. S., 1957, *Phys. Rev.*, **106,** 530.

Nuclear Forces and the Structure of the Lithium Isotopes[†]

By J. M. Soper
Cavendish Laboratory, Cambridge[‡]

[Received July 30, 1957]

Abstract

By consideration of the observed spectrum of ^{6}Li in intermediate coupling, values are obtained for the p-shell radial integrals, the spin–orbit force parameter and two of the three independent parameters of the exchange character of the central force. These results are used to calculate the spectrum and properties of ^{7}Li in intermediate coupling. Fresh evidence is found for the assignment of the 7·46 Mev level in ^{7}Li to the $5/2^-$ level of the ^{24}P term, indicating the probable presence of a further $5/2^-$ level (from the ^{22}F term) in the 5 to 7 Mev region.

§ 1. Introduction

The success of the intermediate coupling shell model in the interpretation of spectra, magnetic moments and a wide variety of reaction properties of light nuclei leads us to consider the problem of obtaining, from available experimental data, information about a two-body central force mixture which, together with the well-known spin–orbit term of the model, will describe the spectra of such nuclei. Previous work on the model has almost invariably started with some assumption about the force mixture to be used and in the majority of cases this has been that of Rosenfeld (1948) as far as the central forces are concerned.

We shall show in this paper that it is possible to derive from the observed spectrum of ^{6}Li a number of conditions on the exchange parameters of the force mixture which reduce them to a single one which cannot be predicted from the available data. Values of the p-shell radial integrals L and K are also obtained for this nucleus, together with the strength parameter a of the spin–orbit force. These results are applied to the structure problems of ^{7}Li.

Recently Meshkov and Ufford (1956) attacked a problem related to this by applying the method of Bacher and Goudsmit to the calculation of the elements of the energy matrix of ^{7}Li from those of ^{6}Li. The ^{6}Li elements were estimated by assuming a central force mixture and using a successive approximation method to find the values of the radial integrals and the strength of the spin–orbit force which gave the best fit to the (over-determined) set of conditions obtained from the experimental data. These values were taken over by the Bacher–Goudsmit method into the calculation of the ^{7}Li levels. The condition that these should correspond to experimentally observed levels is then used to give a revised estimate of the central force mixture.

[†] Communicated by Dr. B. H. Flowers.

[‡] Present address : Atomic Energy Research Establishment, Harwell.

Apart from its uncertainties, this approach suffers, as its authors point out, from the assumption that all the parameters involved remain unaltered from nucleus to nucleus In view of the fact that other studies suggest that the intermediate coupling situation changes systematically from nucleus to nucleus through the p-shell, it would seem desirable to devise a method which is potentially free from this restriction.

In the present paper we calculate all but one of the unknowns directly from the spectrum of ^{6}Li. The remaining parameter has a comparatively small effect on the low-energy spectrum of many nuclei, and an arbitrary choice is made for it before applying the results to ^{7}Li. We are then able if need be to treat the radial integrals and spin–orbit strength as free parameters in the spirit of the intermediate coupling model. We find in fact that a satisfactory fit to the known spectrum and properties of ^{7}Li is possible using virtually the same values of the spin–orbit strength and the direct radial integral L, when expressed in units of K, as were found for the nucleus ^{6}Li ; only the value of K (which determines the overall scale of the predicted spectrum) needs to be altered appreciably.

The derivation of the unknowns from the ^{6}Li spectrum is given in § 2 of this paper. § 3 goes on to deal with the application of these results to ^{7}Li.

§ 2. The Force Mixture

In this section we calculate a single-parameter force mixture to describe ^{6}Li exactly in its low-energy features, on the assumption that these can be described in terms of a pure p^2 configuration. It may be hoped that such a mixture may prove valuable in the study of other light nuclei. We shall ignore any possible effects of the presence of tensor forces, since, although Elliott (1956) has shown that some tensor force is necessary to explain the beta-decay of ^{14}C on the shell model, there is no evidence to show that the strength of such a force is in any way comparable with the central and spin–orbit terms. The extra parameters which would have to be introduced in order to include this force might well lead to serious errors in the calculation, even if we could find sufficient experimental data to determine them formally.

The data we shall use on the spectrum of ^{6}Li are given in fig. 1 which is extracted from the compilation of Ajzenberg and Lauritsen (1955). The diagram also shows (where these are not known experimentally) the spin and parity assignments we shall make on the basis of the shell model for the first six levels. In L–S coupling they are the levels, $^{13}S_1$, $^{13}D_{3,2,1}$, $^{31}S_0$, $^{31}D_2$.

Confining ourselves to central and spin–orbit forces, we see that we must consider six independent parameters. These are three out of the four parameters W, M, B, H of the central mixture (their sum is normalized to unity), the spin–orbit strength a which occurs in the expression

$a\sum_i \mathbf{l}_i \cdot \mathbf{s}_i$ for this force, and the radial integrals L and K. The first six levels appear to give us five equations (for the spacings), although the breadth of the level at 5·4 MeV will introduce some uncertainty which we shall consider below; a further equation may be obtained by computing the energy zero for the theoretical calculation from known data. This zero represents the energy of a proton and neutron in the presence of the central core, but in the absence of forces not due to this core.

Fig. 1

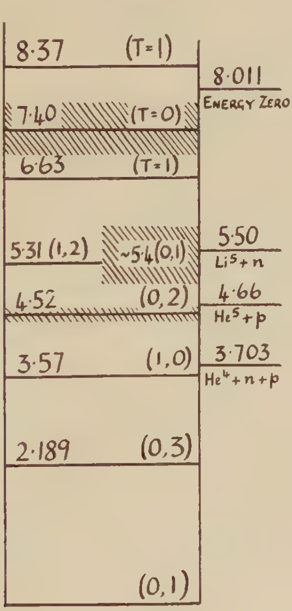

Spectrum of ^{6}Li (after Ajzenberg and Lauritsen 1955).

We denote this zero by $^6\mathrm{Li}_0$. We then have the energy equation:

$$^6\mathrm{Li}_0 = {}^4\mathrm{He} + \mathrm{p} + \mathrm{n} + C(\mathrm{n}s^4) + C(\mathrm{p}s^4)$$

where the last two terms represent the energy of interaction (including the Coulomb energy which, though we assume it to be common to all terms of a given nucleus, must be taken into account when relating different nuclei) of the p-shell neutron and proton with the core of four s-particles. To evaluate these terms we consider the observed resonances that represent the ground states of ^{5}He and ^{5}Li. These have the form of split ^{22}P terms with very broad upper levels. We are interested in the positions of the ground states of these nuclei in the absence of this splitting, i.e. in:

$$^5\mathrm{Li}_0(+\mathrm{n}) = {}^4\mathrm{He} + \mathrm{p}(+\mathrm{n}) + C(\mathrm{p}s^4)$$

$$^5\mathrm{He}_0(+\mathrm{p}) = {}^4\mathrm{He}(+\mathrm{p}) + \mathrm{n} + C(\mathrm{n}s^4)$$

where we have added a nucleon on each side of each equation for the sake of comparison with ^{6}Li. As it is impossible to obtain the spin–orbit splitting in these nuclei with any accuracy directly from the resonances concerned, we assume it to have the value given directly by the splitting between the $J=2, 3, T=0$ levels in ^{6}Li (see below), namely $\frac{3}{2}a=2{\cdot}331$ MeV. This gives us the $^5\mathrm{Li}_0$ and $^5\mathrm{He}_0$ levels lying at $\frac{1}{2}a=0{\cdot}777$ MeV above the observed ground states, i.e. (with the added nucleon) at 6·277 and 5·437 MeV respectively above ^{6}Li ground. Also we have on this scale :

$$^4\mathrm{He}+\mathrm{p}+\mathrm{n}=3{\cdot}703 \text{ MeV}.$$

These equations show $^6\mathrm{Li}_0$ to lie at 8·011 MeV above ^{6}Li ground. The table lists the states of ^{6}Li, giving their energies measured (downwards) from this zero.

All energies in MeV

Level	Energy from zero	T	J
Ground	8·011	0	1
2·189	5·822	0	3
3·57	4·441	1	0
4·52	3·491	0	2
5·31	2·701	1	2
5·4	2·611	0	1

We now consider the energy matrices themselves. These have been given, for example, by Elliott (1953), who uses parameters slightly different from ours. The simplest are the $T=0$, $J=2$, 3 matrices which consist each of a single term :

$$^{13}\mathrm{D}_2 : L-K-\tfrac{1}{2}a\,; \qquad ^{13}\mathrm{D}_3 : L-K+a.$$

Equating these to the observed energies we obtain :

$$a=1{\cdot}554\,; \qquad L=K+4{\cdot}268$$

where here and subsequently all energies are expressed in MeV.

With the remaining matrices we proceed by substituting the values above for a and L into the elements and subtracting from the diagonal elements the observed root given in the table. On writing down the conditions that the resulting determinants are zero we obtain four simultaneous equations in K and the three central force parameters, which can be solved.

This procedure however is to some extent nullified by the great width of the level at 5·4 MeV. Analysis of the equations involved shows† that, while the parameters a, L, K and the combinations :

$$^{31}O=W+M-B-H$$
$$^{33}O=W-M+B-H$$

---

† I am very grateful to Dr. J. P. Elliott for pointing this out to me.

(note ${}^{13}O = W + M + B + H = 1$ in this notation) are extremely insensitive to variations in the exact position assumed for this level, the combination :

$$ {}^{11}O = W - M - B + H $$

shows extremely critical dependence on the position, and remains, for practical purposes, undetermined by the data. The values obtained for the remaining parameters are :

$$ a = 1\cdot554 \text{ Mev} : {}^{31}O = 0\cdot46 $$
$$ L = 5\cdot45 \text{ Mev} : {}^{33}O = 0\cdot15 $$
$$ K = 1\cdot18 \text{ Mev} : ({}^{13}O = 1). $$

These values are not consistent with those of the Rosenfeld (1948) mixture which is based on saturation conditions. It would seem preferable to use values based on experiment in light nuclei rather than those which are obtained by extrapolation from heavier nuclei where, indeed, saturation may be due to properties of the forces other than their exchange character.

§ 3. APPLICATION TO ^{7}Li

The difficulty of obtaining a value for the parameter ${}^{11}O$ persists throughout the p-shell and into the (2s-1d) shell, as Elliott and Flowers have found in their work on the nuclei of masses 18 and 19 (Elliott and Flowers 1955) and on the odd parity states of ^{16}O and ^{16}N (Elliott and Flowers 1957). In the latter paper they do obtain a value ${}^{11}O \simeq 0\cdot5$, but this estimate is not directly applicable to our case as they use values of ${}^{31}O$ and ${}^{33}O$ which differ considerably from those we have found. The difficulty arises from the fact that the parameter ${}^{11}O$ (which in the two-particle case refers to an antisymmetric space state) does not occur in most of the matrix elements of the highly symmetric wave functions that provide the main components of the low-energy states of these nuclei. Conversely it follows that many of the properties of these states will be largely independent of the value we choose for it. This is the case for example in ^{7}Li. Meshkov and Ufford (1956) observed that variations of the assumed position of the 5·4 Mev level in ^{6}Li did not make any appreciable difference to their ^{7}Li results, although, as we have seen, this assumption affects the value of ${}^{11}O$ critically. The reason is that the ${}^{11}P(11)$ state of p^2, which involves ${}^{11}O$, is not a parent state for the ${}^{22}P(3)$, ${}^{22}F(3)$ and ${}^{24}P(21)$ terms in ^{7}Li which give rise to the low-energy spectrum in L–S coupling, and the resulting insensitivity will persist for some way into the intermediate coupling region.

Bearing this in mind, we make the arbitrary choice ${}^{11}O = 0$, which gives rise to the force mixture :

$$ W = 0\cdot40, \quad M = 0\cdot33, \quad B = 0\cdot17, \quad H = 0\cdot10. $$

It is interesting to note that this force from ^{6}Li is very similar to the approximate mixture obtained by Meshkov and Ufford from the spectrum of ^{7}Li ($W = M = 0\cdot4$, $B = 0\cdot2$). We may thus expect it to give good results when applied to this nucleus.

In intermediate coupling the L–S states of ^{7}Li listed above give rise to the level sequence

$$J=3/2,\ 1/2,\ 7/2,\ 5/2,\ 5/2$$

in that order. The size of the ^{7}Li energy matrices makes any 'fitting' procedure such as that described above prohibitively tedious, and a further deterrent is the fact that the experimental situation is by no means so clear-cut as in ^{6}Li. Accordingly we have adopted the procedure of fixing the value of the ratio L/K at the value (4·62) that we found for ^{6}Li, and treating a and K as free parameters. On general grounds we do not expect the value of this ratio to vary greatly, though it is possible that evidence of variation may be found in further studies of the systematics of the p-shell.

On writing the parameter a in units of K, the latter quantity appears only as a factor determining the overall energy scale. The matrices were set up in this form and latent roots and vectors extracted for ten values of the ratio a/K. This work was largely carried out on EDSAC, the Cambridge Mathematical Laboratory's digital computer.

Meshkov and Ufford have discussed the experimental situation in ^{7}Li in the light of shell-model theory and have reached the same conclusion as ourselves, namely that the 7·46 MeV level observed is the $^{24}P_{5/2}$ level, and that the existence of a further 5/2 level between 4·61 and 7·46 MeV is indicated, possibly masked by the broad positive parity level at 6·6 MeV. With this assumption the spectrum was fitted to the theoretical curves, and the best overall fit was found to occur with a/K approximately equal to 1·4. This is so close to the value (1·32) found for ^{6}Li that the two may be taken to be equal to within the accuracy of the calculation, though the increase may be a genuine reflection of that found by Inglis (1953) and Kurath (1956) to occur throughout the p-shell. The observed and predicted spectra are shown in fig. 2 where it is seen that a very satisfactory account of the spectrum may be given in this manner. The value of K necessary for this fit is 1·56 MeV, rather larger than that found for ^{6}Li.

Some of the reaction and electromagnetic properties of these nuclei have been considered by Lane using Rosenfeld forces with $L=6K$. We have carried through similar calculations and many more with our present wave functions and find complete consistency with the parameter values given above except in calculations involving the usual form of the Ml operator, i.e. magnetic moments and Ml transition widths. We hope to discuss these anomalies in a subsequent paper.

One reaction property of this nucleus is however of considerable interest in that it supports the identification of the $5/2^-$ level at 7·46 MeV with that from the $^{24}P_{5/2}$ term. Calculation of the reduced width of this level for nucleon emission to ^{6}Li ground in intermediate coupling agrees with the experimental value for the 7·46 MeV level, while that of the level from $^{22}F_{5/2}$ differs from this by a factor of three. The evidence for this identification thus appears to be strong on a number of grounds.

We thus see that a consistent and satisfactory account of these nuclei may be given in terms of the force parameters we have deduced. On going from ^{6}Li to ^{7}Li the effective strengths of the forces appear to increase in much the same ratio, due probably to a modification in the radial shape of the wave functions, an effect we should expect to be in the direction observed.

Fig. 2

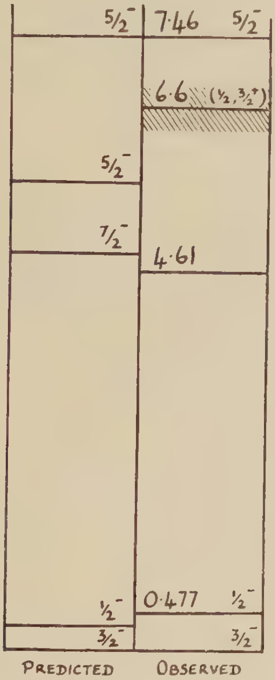

Spectrum of ^{7}Li. In the observed spectrum only states known with certainty are included.

ACKNOWLEDGMENTS

My warmest thanks are due to Dr. B. H. Flowers for suggesting this analysis and for his continued help and encouragement, and to Dr. J. P. Elliott for very helpful discussions. This work was carried out during the author's tenure of a D.S.I.R. Maintenance Award.

REFERENCES

AJZENBERG, F., and LAURITSEN, T., 1955, *Rev. mod. Phys.*, **27,** 77.
ELLIOTT, J. P., 1953, *Proc. roy. Soc.* A, **218,** 345 ; 1956, *Phil. Mag.*, **1,** 503.
ELLIOTT, J. P., and FLOWERS, B. H., 1955, *Proc. roy. Soc.* A, **229,** 536 ; 1957, *Ibid.* (to be published).
INGLIS, D. R., 1953, *Rev. mod. Phys.*, **25,** 390.
KURATH, D., 1956, *Phys. Rev.*, **101,** 216.
MESHKOV, S., and UFFORD, C. W., 1956, *Phys. Rev.*, **101,** 734.
ROSENFELD, L., 1948, *Nuclear Forces* (Amsterdam : North-Holland Publishing Company).

Electrostatic Fields round Localized Defects in Metals†

By P. M. Lee and N. H. March
Department of Physics, The University, Sheffield

[Received June 17, 1957, and in revised form July 9, 1957]

Abstract

A procedure for dealing with localized defects in metals is proposed, based on three main assumptions. First, the validity of the Thomas–Fermi approximation is assumed, secondly departures of the perturbing potentials from spherical symmetry are neglected, and thirdly, no account is taken of any relaxation of the lattice which may occur on the introduction of localized defects. However, the framework outlined is sufficiently general to enable the second assumption to be avoided, should this turn out to be necessary.

It is expected that the method will be useful for foreign atoms entering the lattice substitutionally, provided the atomic size is such that no serious distortion of the lattice is produced, and also for vacancies, although in this latter case it will no doubt eventually prove necessary to consider relaxation effects.

The method proposed is illustrated by studying numerically the case of a vacancy in copper, and an approximate self-consistent field is established for the perturbed lattice, based on the method of Slater and Krutter for the unperturbed crystal. A partial wave analysis using the free-electron approximation has then been carried out. The resistivity comes out considerably larger than that obtained by previous workers and possible reasons for this are discussed.

§ 1. Introduction

While many problems remain to be solved in connection with the perfect periodic lattice, a good deal of attention is now being devoted to the perturbations introduced in originally perfect crystals by foreign atoms, interstitials, vacancies and dislocations. Particularly with the current importance of the problem of assessing the effects of irradiation on metals, the theoretical study of vacancies and interstitials especially seems a matter of some urgency. The present investigation represent an attempt to devize a somewhat general method of approximating to the self-consistent field and the electron distribution in metals in which localized defects have been introduced. Thus, dislocations are immediately excluded from the present discussion. Furthermore, and of more immediate concern, it will emerge that the assumptions which at this stage it turned out to be highly desirable, if not entirely essential, to make, probably also exclude interstitials, or rather preclude the possibility of obtaining a realistic description of the perturbed crystal in this case. However, a modification of the present scheme appears possible for this case, and we hope to deal with this later. Thus, we think that the present approach will provide a first approximation for foreign atoms entering substitutionally in the lattice, and for vacancies.

---

† Communicated by the Authors.

It is appropriate first of all to review the most important attempts which have so far been made to deal with the problems of concern to us here. Most of these have been based on the treatment introduced by Mott (1936), in which only the conduction electrons are considered, the Sommerfeld free-electron model being used to describe the unperturbed metal. The effect of foreign atoms in a monovalent metal say, was then described by introducing a point singularity with charge Ze at the position of the foreign atom, the impurity atom having $(Z+1)$ electrons outside a closed shell. The redistribution of the conduction electrons and the self-consistent perturbing field were then determined by the Thomas-Fermi method, and this approach has been the basis of a good deal of more recent work. A detailed review has been given by Friedel (1954), and for the most important developments since this was written the article by March (1957) may be consulted.

While such an approach has a good deal of value, particularly from the point of view of obtaining physical insight into the problems with a relatively simple model, it is apparent that there are cases with which, by its very nature, it cannot deal. Thus, such an approach, without modification, cannot explain why small concentrations of gold atoms in a silver lattice lead to an increase in the resistivity. Furthermore, when dealing with vacancies in other than metals formed of light atoms, any incorporation in the valence scheme inevitably involves approximations which must be rather drastic, particularly concerning the form of the perturbing potential near the vacancy. Such a situation, in fact, also obtains when the valence treatment is used for substitutional impurities which are not immediately adjacent to the solvent atom in the periodic table.

Previous workers have made attempts of various kinds to overcome these limitations, and brief reference to their work will now be made. Thus Huang (1948) in an important early paper, attempted to calculate the excess resistivity due to a monovalent atom in a monovalent metal. In this work also, use was made of the Thomas–Fermi approximation, but in a rather less fundamental way than in the present paper. In connection with the objections to dealing with a vacancy in the valence scheme above, attempts have been made by Jongenburger (1953), and more recently by Blatt (1955 a) to improve the approximation to the perturbing potential by using the negative of the Hartree potential for a positive ion for copper, and adjusting this in order to satisfy the sum rule of Friedel (1952). These treatments appeared to lead to quite reasonable results for the excess resistivity due to vacancies (about 1·3–1·5 micro-ohm cm per atomic %), but the fields obtained in this manner can hardly be justified in a fundamental way. Further, although these authors concluded that the exact form of the perturbing field did not appear to matter very much in the calculation of the excess resistivity (Friedel 1954), Blatt (1955 b) has shown it to be of some importance when changes in thermoelectric power due to vacancies and interstitials are calculated.

Finally, we should mention some unpublished work of Howell, which was kindly made available to us, and undoubtedly has considerably influenced the course of the present study. Howell attempted to deal with the vacancy problem from the point of view of calculating the energy needed to create a vacancy in copper. He concluded that the method he proposed, based on the Thomas–Fermi approximation, was not satisfactory for the calculation of this quantity. However, we think that the present work circumvents the main difficulties associated with Howell's approach, although we focus attention on the perturbing potential and do not attempt energy calculations.

§ 2. THE PERFECT LATTICE

For the perfect metallic lattice we have to solve the fundamental Thomas–Fermi (TF) equation

$$\nabla^2(V-V_0)=\mu(V-V_0)^{3/2} \quad . \quad . \quad . \quad . \quad . \quad . \quad . \quad (1)$$

where

$$\mu=\frac{32\pi^2 e}{3h^3}(2m)^{3/2},$$

subject to appropriate boundary conditions. Hence V is the electrostatic potential and $-eV_0$ is the Fermi energy. For a metal in which we construct the usual atomic polyhedra surrounding the atoms, the problem of finding an exact solution of (1) is a formidable task and has not as yet been solved for any lattice. However, as Slater and Krutter (1935) emphasized in their original paper on the application of the TF method to metals, in many cases the atomic polyhedron is of high symmetry and may, to a good approximation, be replaced by a sphere of equal volume. It is then consistent to suppose that within each atomic sphere the potential V is spherically symmetrical, and the condition that V is given by (1) is periodic with the period of the lattice is replaced by the simpler requirement that

$$\left(\frac{dV}{dr}\right)_R=0, \quad . \quad . \quad . \quad . \quad . \quad . \quad . \quad . \quad (2)$$

where R is the radius of the atomic sphere. This also ensures that the sphere is electrically neutral.

At the centre of the sphere, where there is a nucleus of charge Ze, we have

$$V-V_0 \to \frac{Ze}{r} \text{ as } r \to 0. \qquad (3)$$

In this case, eqn. (1) reduces to the ordinary dimensionless TF equation

$$\frac{d^2\phi}{dx^2}=\frac{\phi^{3/2}}{x^{1/2}} \qquad (4)$$

where

$$V-V_0=\frac{Ze}{r}\phi, \qquad (5)$$

$$r=bx, \qquad (6)$$

with

$$b=\left(\frac{3}{32\pi^2}\right)^{2/3}\frac{h^2}{2me^2Z^{1/3}}.$$

The boundary conditions are now

$$\phi(0)=1 \qquad (7)$$

$$\frac{\phi(x_0)}{x_0}=\left(\frac{d\phi}{dx}\right)_{x_0} \qquad (8)$$

where x_0 is the radius of the atomic sphere in dimensionless units. This type of solution has been made the basis of the present treatment of defects in metals; should it eventually prove to be necessary to go beyond the sphere approximation for the perfect lattice, the method described by March (1957) may be used to calculate the effect of angular terms in the potential.

§ 3. THE PERTURBED LATTICE

In this case, suppose a single defect is introduced at a lattice site which we take as origin of coordinates, and let the nuclear charge change from Ze to $Z'e$ at this point. The new TF equation to be solved is

$$\nabla^2(V+V_p-V_0)=\mu(V+V_p-V_0)^{3/2} \qquad (9)$$

where V_p is the change in electrostatic potential caused by the introduction of the defect. Then we must solve (9) subject to the new boundary conditions

$$V+V_p \to \frac{Z'e}{r} \text{ as } r \to 0, \qquad (10)$$

$$V_p \to 0 \text{ at infinity.} \qquad (11)$$

The neighbouring atoms are assumed unaffected by the introduction of the defect; that is, any relaxation of the lattice is neglected in this approximation. We can therefore focus attention on an atomic sphere of radius R centred on the origin, and within this sphere we should expect that both V_p and V are spherically symmetrical to a good approximation. Then (9) again reduces to the dimensionless TF equation, although the boundary conditions are now different. However, the boundary condition at infinity cannot be applied without examining the solution outside the central sphere and we shall now proceed to do this†.

Since we are then rather far from the defect we may assume

$$V-V_0 \gg V_p, \quad . \quad . \quad . \quad . \quad . \quad . \quad . \quad . \quad (12)$$

and this must eventually be checked in practical applications. Then we may write (9) in the form

$$\nabla^2(V+V_p-V_0)=\mu(V-V_0)^{3/2}\left[1+\frac{3}{2}\left(\frac{V_p}{V-V_0}\right)+0\left(\left\{\frac{V_p}{V-V_0}\right\}^2\right)\right], \quad (13)$$

or using (1)

$$\nabla^2 V_p \doteqdot \tfrac{3}{2}\mu(V-V_0)^{1/2}V_p. \quad . \quad . \quad . \quad . \quad . \quad . \quad . \quad . \quad (14)$$

To solve (14), we now imagine V_p and $(V-V_0)^{1/2}$ to be expanded in spherical harmonics about the origin. Of course, $(V-V_0)^{1/2}$ is not a spherically symmetric function when it is expanded about any other origin than the centre of the atomic sphere in which the point under consideration lies. However, we assume that the angular terms in V_p are unimportant, and then if the radial term is indeed a sufficient approximation, we obtain this by solving the equation

$$\frac{1}{r}\frac{d^2}{dr^2}(rV_p) \doteqdot \frac{3}{2}\mu\overline{(V-V_0)^{1/2}}V_p, \quad . \quad . \quad . \quad . \quad . \quad . \quad (15)$$

where $\overline{(V-V_0)^{1/2}}$ is the average of $(V-V_0)^{1/2}$ over the angular variables, and this may be obtained numerically as discussed in §4.

It will be seen that once the solution of (15) which tends to zero at infinity is known, the remaining constant is a simple multiplier, and this greatly simplifies the problem. It means that only one solution of (15) is needed, and the arbitrary constant is then obtained by matching at R with the solution for V_p in the central sphere. The way this works out in practice for a particular case is discussed in §5.

§4. DETERMINATION OF $\overline{(V-V_0)^{1/2}}$

$\overline{(V-V_0)^{1/2}}$ is given as a function of r by

$$\frac{\displaystyle\int_0^{2\pi}\int_0^{\pi}(V-V_0)^{1/2}\sin\theta\,d\theta\,d\phi}{\displaystyle\int_0^{2\pi}\int_0^{\pi}\sin\theta\,d\theta\,d\phi} \quad . \quad . \quad . \quad . \quad . \quad . \quad (16)$$

where r, θ and ϕ are spherical polar coordinates. This may be evaluated numerically for values of $r>R$ by considering a network of points on the surface of a sphere of radius r with the origin as centre. Each of these points may be associated with the appropriate atomic sphere, and the corresponding value of $(V-V_0)^{1/2}$ may be obtained by the method of Slater and Krutter†. The integrations in (16) may thus be carried out numerically for spheres of increasing radii, although it is necessary to employ a series solution for $(V-V_0)^{1/2}$ in the regions very near to atomic nuclei. For $r<R$, $(V-V_0)^{1/2}$ is the same as $\overline{(V-V_0)^{1/2}}$ in the present approximation.

---

† The following treatment is quite different from that of Howell and, we believe, avoids the difficulties associated with his approach.

Fig. 1

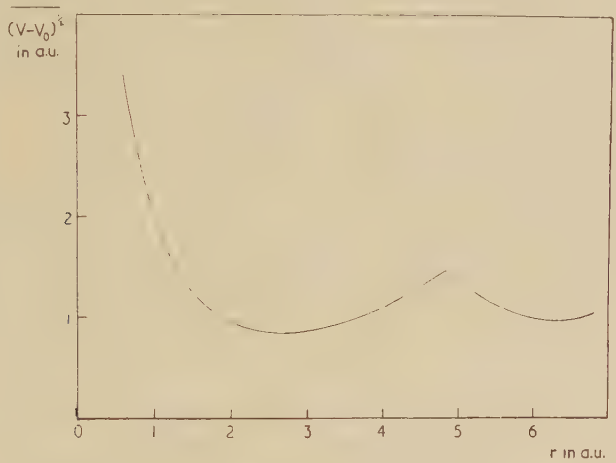

$\overline{(V-V_0)^{1/2}}$ as a function of r (atomic units used).

The results thus obtained for copper are displayed in fig. 1. The radius R of the atomic sphere corresponds to the point of zero derivative of $\overline{(V-V_0)^{1/2}}$, the discontinuity in the derivative occurs at the nearest neighbour distance and the curve is drawn out to the next nearest neighbour distance. In view of the sphere approximation employed to obtain $(V-V_0)^{1/2}$, it was found necessary to make a slight adjustment of the curve between R and the nearest neighbour distance‡ in order to match satisfactorily with the results in the central sphere. The correct lattice structure (face-centred cubic) enters the calculation of $\overline{(V-V_0)^{1/2}}$, although it probably has a minor effect on the form of the final curve.

§ 5. CASE OF A VACANCY IN COPPER

5.1. *Calculation of Perturbing Potential*

We shall now illustrate the general method outlined in §2–4 by describing a calculation we have made for vacancies in a copper lattice. As remarked earlier, relaxation of the lattice, which undoubtedly occurs when an atom is removed, is neglected in the present work; some discussion of the errors which are thereby involved will be given later.

---

† A solution of eqn. (4) corresponding to a value of $R=2{\cdot}66$ atomic units was kindly made available to us by Dr. R. A. Ballinger.

‡ At no point was $\overline{V-V_0})^{1/2}$ changed by more than 3 or 4%.

In the central sphere, where $V+V_p$ is assumed spherically symmetrical, (9) may be transformed to the usual dimensionless form (4) by putting

$$(V+V_p-V_0)=\frac{Ze}{r}y(x), \quad . \quad . \quad . \quad . \quad . \quad . \quad . \quad (17)$$

where x is defined by (6). To give the required behaviour of V_p near the origin, the boundary condition for y is

$$y(0)=0. \quad . \quad . \quad . \quad . \quad . \quad . \quad . \quad (18)$$

Near the origin the following series solution may be used†

$$y=A^2x[1+b_3x^2+b_5x^4+b_7x^6+\ldots] \quad . \quad . \quad (19)$$

where the coefficients are given in table 1, and A^2 is the slope of y at the origin.

Table 1

$b_3=\dfrac{A}{6}$	$b_{11}=\dfrac{19A^5}{14256000}$
$b_5=\dfrac{A^2}{80}$	$b_{13}=\dfrac{2719\,A^6}{53374464000}$
$b_7=\dfrac{A^3}{1440}$	$b_{15}=\dfrac{20621A^7}{11208637440000}$
$b_9=\dfrac{A^4}{31104}$	

The convergence of this series is good; for example for $A \sim 0{\cdot}06$ it can be used out to $x=8$.

Next eqn. (14) is solved outside the atomic sphere. The boundary condition that V_p shall be zero at infinity was approximated by putting it zero at the next nearest neighbour distance. The averaging described in § 4 was thus needed out to this point. The function $\overline{(V-V_0)^{1/2}}$ has a discontinuous derivative at the values of r equivalent to nearest and next nearest neighbour distances, due to the presence of the atomic nuclei. This complicates the solution of (14) somewhat, but the difficulty was overcome by first solving it in the region between the nearest and next nearest neighbours by the relaxation method (see, for example, Fox 1949) with the boundary condition that V_p was zero at the next nearest neighbour point. A Taylor series was then developed around the nearest neighbour point and the integration extended inwards to the surface of the central atomic sphere by a method due to Fox and Goodwin (1949). The solution was thus determined for the outer region apart from a multiplying constant.

---

† This solution was obtained in connection with the present problem by Howell, and independently, as far as b_{13}, by one of us (N.H.M.) during the course of earlier unpublished work on the molecules P_4 and As_4.

In practice the solution of (9) inside the atomic sphere was tabulated for a chosen value of the slope of y at the origin, using the series given in (19). This solution can then be transformed very simply to obtain the correct matching of solutions across the surface of the central atomic sphere. This is possible since, if $y(x)$ is a solution of the dimensionless TF equation, then it is easily shown that $y_1(x_1)$ is also a solution provided

$$\left.\begin{aligned} y_1&=ay \\ x_1&=dx \\ ad^3&=1 \end{aligned}\right\} . \qquad (20)$$

By suitable choice of a, matching of the two solutions was achieved. The perturbing potential due to a vacancy is then determined uniquely and is shown as a function of r in fig. 2.

Fig. 2

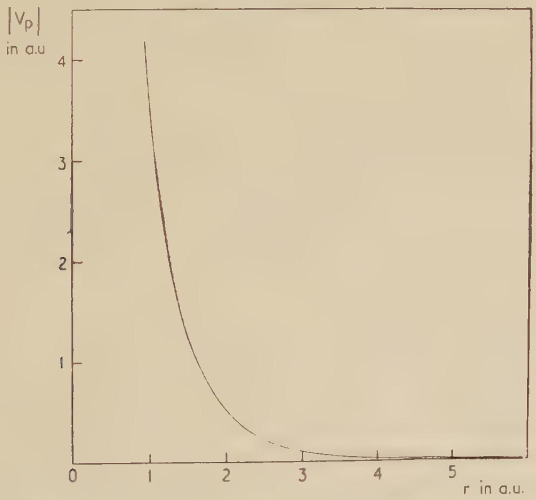

Magnitude of perturbing potential as a function of r (atomic units used).

5.2. *Electron Distribution round Vacancy*

We also thought it of interest to examine the electron distribution in the atomic sphere surrounding the vacancy. In atomic units, the electron density in the perturbed lattice is given by

$$n(r)=\frac{2^{3/2}}{3\pi^2}[V+V_p-V_0]^{3/2}. \qquad (21)$$

Using the results obtained here for V_p and the Slater and Krutter values of $V-V_0$, we find that there are very nearly two electrons inside the central atomic sphere. Thus, on removing an atom, there is a significant movement of electrons into the 'vacancy sphere' according to the present model (see, however, the remarks in § 5.3 below).

5.3. *Comments on Approximations Involved*

In the vacancy case, the form of the perturbing potential is such that the application of the unmodified Thomas–Fermi approximation seems open to some question. The introduction of a correction along the lines proposed by von Weizsäcker (1935) therefore merits consideration, but the problem is then much more formidable than that considered here. In view of this, and bearing in mind that there is a degree of uncertainty with regard to (*a*) the magnitude of the angular terms in the perturbing potential and (*b*) the effect of relaxation of the lattice, we have not attempted to make quantitative calculations of such a correction. However, in the light of previous work using the von Weizsäcker method, it seems that while the results for the electron density (which depends on the second derivative of the potential) discussed in § 5.2 above may be rather significantly modified, the perturbing potential, which is our main concern here, is unlikely to be markedly changed. If energy calculations were to be made eventually on the basis of the present treatment, much more careful study of the von Weizsäcker correction would seem to be called for.

A less fundamental approximation, the linearization employed outside the central atomic sphere, may be checked for the vacancy case using our numerical values for V_p, and at the boundary of the central sphere we find $V_p/(V-V_0)=0{\cdot}19$. The first neglected term is $(V_p/\{V-V_0\})^2$ in eqn. (13) and it is soon verified that this approximation is not serious.

§ 6. CONNECTION WITH PREVIOUS WORK ON VACANCIES IN COPPER

Particularly with a view to establishing some relationship between the perturbing potential we have obtained and the forms used earlier by Jongenburger and Blatt, we have made calculations by the partial wave method of the scattering cross section due to V_p. Following these workers, we have adopted the free-electron model for the conduction electrons in calculating this cross section. However, it should certainly be borne in mind that for vacancies in copper the perturbing potential is so strong and has such a marked effect on the electronic wave functions near the vacant site that it may turn out to be a drastic approximation to compute the excess resistivity by treating the conduction electrons as free. Thus the phase shifts calculated by this means may differ significantly from those which would result when the same perturbing potential V_p was used in conjunction with more realistic wave functions for the conduction electrons. The present calculations should therefore be regarded as semi-quantitative only, but some interesting points emerge from a comparison with previous work and we shall therefore briefly report our findings.

The first four phase shifts corresponding to $l=0$, 1, 2 and 3 were determined and these are given in table 2, together with the value obtained for the excess resistivity for 1 atomic % of vacancies. This is considerably larger than the values obtained by the earlier workers (in the range 1·3–1·5 micro-ohm cm per atomic %), and we shall now attempt to analyze the possible reasons for this. We note first that previous workers have made no attempt to obtain the perturbing fields from first principles, but invoked the Friedel sum rule as an aid in constructing the potential. This may be stated (Friedel 1952) in the form

$$N=\frac{2}{\pi}\sum_{l=0}^{\infty}(2l+1)\eta_l \quad . \quad . \quad . \quad . \quad . \quad . \quad . \quad . \quad (22)$$

where η_l is the phase shift for the partial wave order l for electrons at the Fermi surface, N being the 'screening charge'. For the case of a vacancy in a monovalent metal, N has been taken as -1 by previous workers. However, in the present calculation the perturbing potential is completely determined by our approximate self-consistent field calculation, and using the phase shifts given in table 2 we find

$$N=-2{\cdot}25.$$

Whereas previously the conclusion had been reached that the form of the perturbing potential was not very important for the calculation of the excess resistivity, provided the phase shifts satisfy the sum rule (see, however, Fujiwara 1955, 1956), it is not surprising that we find a considerably greater increase in resistivity with a potential which leads to $N=-2{\cdot}25$. We feel therefore that until the status of the sum rule is clarified, some caution should be exercised in using it as a means of determining perturbing fields.

Table 2. Phase Shifts and Excess Resistivity

l	0	1	2	3
η_l	$-1{\cdot}32$	$-0{\cdot}44$	$-0{\cdot}12$	$-0{\cdot}04$

$\Delta_\rho=3{\cdot}09$ micro-ohm cm/atomic %.

Finally, we must attempt to assess briefly the possible effect of allowing for relaxation of the lattice. Here there appears to be some measure of disagreement between various writers. For example, Roth (1957) suggests that the work of Overhauser and Gorman (1956) overestimated the effect of relaxation by an order of magnitude. From some rough estimates we have made, we do not feel that the resistivity as calculated here will change by more than 0·5 micro-ohm cm per atomic % due to relaxation effects. It seems highly probable therefore that the use of the free-electron approximation for the calculation of the scattering cross section is much more serious than the neglect of relaxation, and is causing the excess resistivity to come out too high (see especially the discussions of Blatt (1955 a) and Overhauser and Gorman (1956)). A calculation of the excess resistivity using the present perturbing potential together with a more realistic description of the conduction electrons would be of very considerable interest.

ACKNOWLEDGMENTS

We wish to thank a referee for some helpful remarks on the application to vacancies. One of us (P.M.L.) wishes to acknowledge the award of an Ellison Fellowship by the University of Sheffield.

REFERENCES

BLATT, F. J., 1955 a, *Phys. Rev.*, **99,** 1708 ; 1955 b, *Ibid,* **100,** 666.
FOX, L., 1949, *Proc. Camb. phil. Soc.*, **45,** 50.
FOX, L., and GOODWIN, E. T., 1949, *Proc. Camb. phil. Soc.*, **45,** 373.
FRIEDEL, J., 1952, *Phil. Mag.*, **43,** 153 ; 1954, *Advanc. in Physics*, **3,** 446.
FUJIWARA, H., 1955, *J. phys. Soc. Japan*, **10,** 339, 727 ; 1956, *Ibid.*, **11,** 376.
HUANG, K., 1948, *Proc. phys. Soc. Lond.*, **60,** 161.
JONGENBURGER, P., 1953, *Appl. Sci. Res.* B, **3,** 237.
MARCH, N. H., 1957, *Advanc. in Physics*, **6,** 1.
MOTT, N. F., 1936, *Proc. Camb. phil. Soc.*, **32,** 281.
OVERHAUSER, A. W., and GORMAN, R. L., 1956, *Phys. Rev.*, **102,** 676.
ROTH, L. M., 1957, *Bull. Am. Phys. Soc.*, **2,** 214.
SLATER, J. C., and KRUTTER, H. M., 1935, *Phys. Rev.*, **47,** 559.
VON WEIZSÄCKER, C. F., 1935, *Z. Phys.*, **96,** 431.

On the Mechanism of Work Hardening in Face-Centred Cubic Metals with Special Reference to Polycrystalline Copper : II†

By P. FELTHAM and J. D. MEAKIN
The University, Leeds

[Received April 26, 1957 ; and in revised form July 2, 1957]

ABSTRACT

Rods of annealed polycrystalline copper (99·991%) were deformed in tension at 77, 195 and 293°K. The initial mode of hardening was linear up to a temperature-depended tensile stress σ_C ; the mechanism was the same as the one leading to linear hardening (stage II) in single crystals. The assumption that at stresses above σ_C 'yielding' took place by the spread of slip from some of the small slip zones characteristic of the linear stage, and that this resulted in interaction hardening, is shown to account satisfactorily for the parabolic shape of the stress-strain curves above σ_C.

§ 1. INTRODUCTION

IN a recent paper (Feltham and Meakin 1957 a), which will be referred to as I, the present authors showed that a linear stage of hardening‡ preceeds parabolic hardening in annealed polycrystalline copper deformed in tension at room temperature. This hardening was interpreted in terms of the model proposed by Friedel (1955), while hardening in stage III was thought to be of the interaction type, and to arise from dislocation pile-ups as formed above a characteristic temperature-dependent stress σ_C at which Cottrell–Lomer barriers ceased to be effective in confining slip to the small rectangular slip-zones active in stage II.

The primary object of the present work was to study work hardening in copper under similar experimental conditions but at lower temperatures, and to examine in how far hardening in stage III could be accounted for in terms of a simple model based on the interaction mechanism. The choice of low temperatures was made in an endeavour to minimize interference from relaxation and creep phenomena ; for similar reasons the tensile strain ϵ was in no case allowed to exceed about 10%.

§ 2. MATERIAL AND METHOD

Polycrystalline rods drawn from oxygen-free high-conductivity copper (99·991%), which were used in the experiments, had a diameter of 2 mm and were 10 cm long. They came from the same stock as the rods used in I. After annealing *in vacuo* for 2 hours at 600°C and furnace cooling, the rods were extended in liquid nitrogen, powdered carbon dioxide, or in air, by means of a motor-driven Hounsfield Tensometer at a constant tensile strain rate of 10^{-3} sec^{-1}. The spatial mean grain diameter D was $2{\cdot}84 \times 10^{-3}$ cm. A more detailed account of the experimental procedure has been given previously (I).

---

†Communicated by the Authors.

‡This linear hardening is now generally referred to as stage II, to distinguish it from linear hardening due to easy-glide : stage I. The parabolic hardening discussed in this paper will be referred to as stage III.

§ 3. EXPERIMENTAL RESULTS

The stress–strain curves obtained at 77, 195 and 293°K are shown in the figure. The strains up to the tensile yield stress σ_Y were too small to be measured reliably, and the measured points have not been recorded in the figure. The curves were found to be reproducible to a high degree of accuracy.

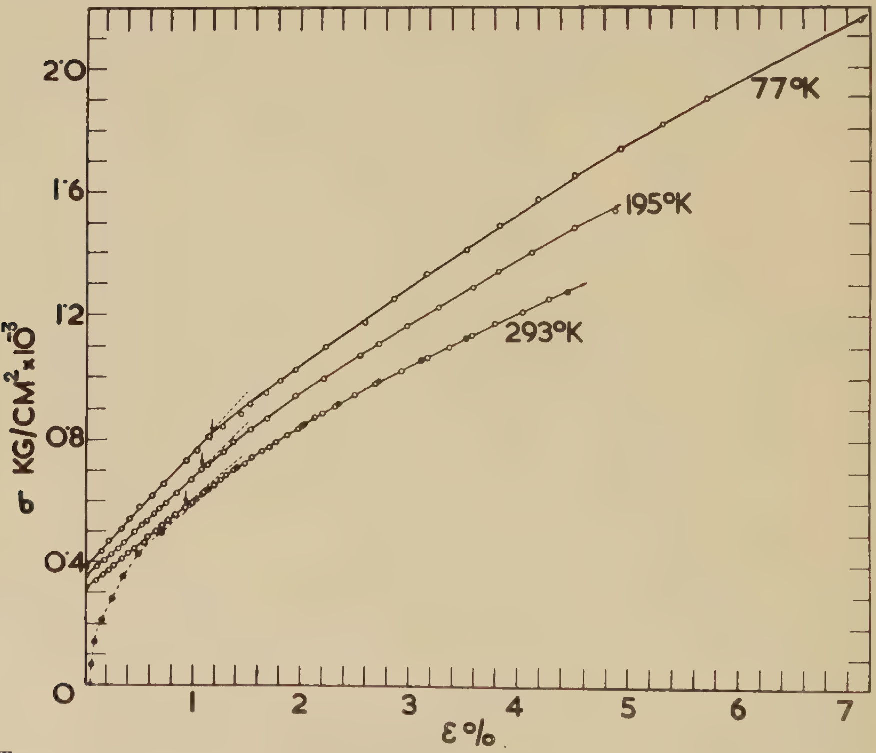

True stress–strain curves of annealed polycrystalline copper. Full circles represent the parabola given by eqn. (1).

A linear part, terminating at a tensile stress σ_C indicated by arrows in the figure, is seen to extend up to tensile strains of about 1% in all cases. This part of the curve is then followed by a parabolic section. The origins (σ_0, ϵ_0) of the parabolae and the coefficients of work hardening χ_p were derived by analysing the curves by means of the equation

$$(\sigma-\sigma_0)^2=\chi_p(\epsilon-\epsilon_0)$$

as in I. Again, the parabolae seemed to have their origins close to the origin of the coordinate system; the parabola

$$\sigma^2 = 3{\cdot}62 \times 10^7(\epsilon - 5 \times 10^{-4})\ (\mathrm{kg/cm}^2)^2 \qquad . \quad . \quad . \quad (1)$$

for example is shown fitted to the lowest curve in the figure. The values of σ_Y, σ_C, σ_C/σ_Y and of the shear modulus G are given in table 1. G is the unrelaxed modulus, the temperature-dependence of which was assumed to be equal to that of Young's modulus at low temperatures as given by Lozinskii (1956).

Table 1

T °K	σ_Y kg/cm^2	σ_C kg/cm^2	σ_C/σ_Y	$G \times 10^{-5}$ kg/cm^2
77	384	800	2·09	5·18
195	351	670	1·91	5·00
293	313	550	1·76	4·83

§ 4. THEORY

4.1. *The Yield Stress* σ_Y

On the basis of the theoretical treatments of the relations between the parameters characterizing yielding and work hardening in single crystals and polycrystals respectively (e.g. Sachs 1928, Taylor 1938, Kochendörfer 1947, 1950, Bishop and Hill 1951) the tensile yield stress σ_Y should be given by

$$\sigma_Y = c\tau_f + S, \qquad . \quad . \quad . \quad . \quad . \quad . \quad . \quad (2)$$

where τ_f is the critical resolved shear stress of the single crystal, and $2 \leqslant c \leqslant 3$. No adequate explanation of the significance of the stress S exists. Kochendörfer sought to relate it to elastic deformations due to hydrostatic stresses near grain boundaries. He shows that such an interpretation associates S with the Bauschinger effect, i.e. a polycrystal which had been deformed in tension just above σ_Y should subsequently have a yield stress in compression given numerically by

$$(\sigma_Y)_{\mathrm{comp}} = c\tau_f - S.$$

Such an interpretation of the significance is however untenable in the present case, for σ_Y is about ten times greater than τ_f as obtained by Blewitt *et al.* (1955) with single crystals of copper of purity comparable with that of our polycrystals, so that S is numerically about three times greater than $c\tau_f$, leading to the inadmissible result of a negative numerical value for $(\sigma_Y)_{\mathrm{comp}}$. As it is reasonable to assume that stresses due, for example, to cooling from the annealing temperatures, are induced near grain boundaries in an elastically highly anisotropic metal such as copper, a small plastic deformation, possibly involving slip on several slip systems in each grain and the formation of some Cottrell–Lomer barriers, may have occurred. Such a hypothesis would not be open to the same objections as Kochendörfers ; a detailed theory of the structure of grains in annealed polycrystals has not however been developed as yet.

4.2. *Linear Hardening*

The small temperature-dependence of the coefficient of linear hardening $\chi_l(=d\sigma/d\epsilon)_{\mathrm{I}}$, apparent from table 2, supports the earlier conclusion (I) that hardening in stage II arose through the locking of slip by Cottrell–Lomer barriers (Friedel 1955, Seeger *et al.* 1957). Friedel pointed out that the product $\sigma_C T^{1/2}$ should vary but little with temperature if σ_C is the stress at which Cottrell–Lomer barriers give way under the shear stress due to arrays of dislocations piled up against them. Table 2 shows this to be the case except at 77°K. (The product $\chi_p T^{1/2}$ shows the same trend, indicating a linear relation between σ_C and χ_p.) Stroh's (1956) more detailed analysis of the strength of Cottrell–Lomer barriers shows however that this simple criterion cannot apply at low temperatures. The approximate constancy of $\sigma_C T^{1/2}$ would however also be expected if transition from stage II to stage III were due to the circumvention of Cottrell–Lomer barriers by dislocations, facilitated by cross-slip (Seeger *et al.* 1957) ; the numerical value of the product does not, at present, enable one to discriminate between the two processes.

Table 2

T °K	$\sigma_c T^{1/2}\times 10^{-3}$ (kg/cm²)°K$^{1/2}$	$\chi_p T^{1/2}\times 10^{-8}$ (kg/cm²)²°K$^{1/2}$	$\chi_l\times 10^{-4}$ kg/cm²	$\chi_P\times 10^{-7}$ (kg/cm²)²	
				Measured	Eqn. (8)
77	7·0	5·8	3·6	6·7	6·2
195	9·4	6·7	3·2	4·8	4·9
293	9·4	6·2	2·8	3·6	3·8

The observations of Blewitt *et al.* (1955) that single crystals of copper with orientations favouring slip on a conjugate glide system harden more rapidly in stage II than crystals with orientations away from the [100]–[111] great circle seems to show that Cottrell–Lomer barriers are being formed also in the process of hardening, and not only at the beginning of stage II as originally proposed by Friedel. This point of view is also expressed by Diehl (1956) and Seeger *et al.* (1957). Schmid's Law is thus not strictly true in face-centred crystals, and allowance for this must be made in deriving work hardening curves of polycrystals from single crystal data on the basis of theories in which Schmid's Law is implicit, e.g. Sachs's (1928) and Kochendörfer's (1947).

Now, the coefficient of shear hardening in stage II, derivable from the curves for copper single crystals of various orientations deformed between 4 and 300°K (Blewitt *et al.* 1955) lie in the range† $1{\cdot}6$–$2{\cdot}4 \times 10^3$ kg/cm^2. Sachs's theory requires the coefficient of linear hardening of the polycrystalline copper to be equal to $(2{\cdot}24)^2$ times the shear hardening coefficient of the single crystal, i.e. at most $1{\cdot}2 \times 10^4$ kg/cm^2, on using the highest value obtained from Blewitt's data, which applies to a crystal with an orientation close to [100].

Reference to table 2 shows that χ_l as measured is 2–3 times greater than this estimate. Allowing for the possibility that the factor $(2{\cdot}24)^2$ may be an underestimate, it still appears as if the complex system of stresses acting on the grains of the polycrystal lead to a somewhat greater hardening rate in the individual grains than would be found in similar grains subject to uniaxial tension, the complexity of the stress systems resulting in slip on several ' primary ' slip systems. However, in aluminium and dilute aluminium alloys Jaoul (1957) found a somewhat better correlation between the shear hardening rates of single crystals and the hardening of corresponding polycrystals in tension, also on the basis of the factor $(2{\cdot}24)^2$.

The shear strain over which stage II extends in single crystals is also considerably greater than the tensile strain up to σ_C in polycrystals ; but σ_C and the stress $2\tau_C$, where τ_C is the shear stress at the end of stage II in single crystals, are approximately equal (I), as is to be expected from the identity of the mechanisms leading to the onset of stage III.

4.3. *Parabolic Hardening*

It was pointed out in I that certain features of the distribution of dislocation pile-ups in alpha brass (Jacquet 1954) and the similarity between alpha-brass and copper suggested to the present authors that hardening in copper in stage III might be of the interaction type which leads to a parabolic work hardening law (Mott 1952). The stress strain curves of copper polycrystals in stage III were in fact shown to be sections of parabolae, the latter having their origins close to the origin of the coordinate system, as the parabolae fitted to the curves in the figure. Also, an attempt to apply some relations derivable from Mott's theory lead to the conclusion that hardening early in stage III was probably due to interaction between pile-ups which had originated from the small rectangular slip zones characteristic of hardening in stage II at stresses above σ_C, when Cottrell–Lomer barriers ceased to be effective in confining slip to the interior of such zones. The additional experimental results obtained in the present work permit a somewhat more detailed examination of this hypothesis. In deriving the parabolic hardening law we shall adopt the method used by Mott (1952), with a different interpretation however of the origin of the pile-ups responsible for hardening. We shall make the following assumptions:

---

† This was erroneously stated to be $1{\cdot}6$–$2{\cdot}4 \times 10^4$ kg/cm^2 in I.

(*a*) At the end of stage II the structure of any grain is as given by Friedel's (1955) model, i.e. a random distribution of rectangular slip zones of linear dimensions $2L_F \simeq 10\,\mu$, locked on all sides by Cottrell–Lomer barriers; on account of their size interaction between them is small (Friedel 1955).

(*b*) As the stress σ_C is reached the non-uniformity of the internal stress will result in the breakdown or circumvention of Cottrell–Lomer barriers containing the dislocations of some of these slip zones.

(*c*) The pile-up in any given zone which has become active in this manner will expand to give a ' large ' slip zone of linear dimensions $2L$ and slip distance L.

(*d*) The stress relaxation in such a pile-up, resulting from the expansion, will facilitate renewed locking of the expanded slip zone by Cottrell–Lomer barriers.

(*e*) The ' large ' slip zones cannot be regarded as dislocation dipoles (Friedel 1955), and their long-range stress fields, which oppose the applied stress, necessitate an increase in stress above σ_C if further ' large ' slip zones are to be formed.

(*f*) The major source of hardening is the increase in the density of ' large ' slip zones with increasing stress, at least in the early stages of stage III here under consideration; hardening due either to any increase in the slip distance L, or in the thickness of these L-zones due to band-formation—if such effects occur—is negligible.

(*g*) The number of dislocations, n, in the L-zones is constant and equal to that in the L_F-zones, such that (Mott 1952)

$$n=\pi(\sigma_C-\sigma_f)L_F/Gb, \quad . \quad . \quad . \quad . \quad . \quad . \quad (3)$$

where we have written $\frac{1}{2}\sigma_C$ and $\frac{1}{2}\sigma_f$ in place of the shear stress τ_C, and the initial yield stress in shear τ_f of a single crystal respectively. G is the shear modulus, b the Burger's vector, and the slip distance in an L_F-zone has been taken to be equal to L_F.

We shall also make the simplifying assumption that the internal stress pattern in any grain above σ_C is the same as would have been obtained if interaction hardening only had taken place right from the beginning, i.e. starting with $\sigma=0$. This assumption amounts to replacing the whole hardening curve (e.g. the lowest curve in the figure) by a parabola passing through the origin. No physical significance is, of course, attached to this model at stresses below σ_C. It also implies that as a small stress is applied to the hypothetical model in its undeformed state a number of fully formed L-zones will appear instantly, with an average spacing between adjacent bands given by x. As the yield stress of the undeformed material is assumed to be negligible (the curve passing through the origin) the internal stress σ_i due to a random distribution of L-zones of this type, given by (Mott 1952)

$$\sigma_i = nGb/\pi(xL)^{1/2}, \quad . \quad . \quad . \quad . \quad . \quad . \quad . \quad (4)$$

must be exceeded before further hardening can take place. Thus the internal stress is equal also to the external applied stress σ which must be exceeded before additional L-zones are formed.

The tensile strain corresponding to σ is given by

$$\epsilon = nb/x, \quad . \quad . \quad . \quad . \quad . \quad . \quad . \quad . \quad . \quad (5)$$

where, as in I, we take the tensile and shear strains to be equal. From eqns. (4) and (5) we have

$$\sigma^2 = \chi_p \epsilon, \quad . \quad . \quad . \quad . \quad . \quad . \quad . \quad . \quad . \quad . \quad (6)$$

where

$$\chi_p = nG^2b/\pi^2L, \quad . \quad . \quad . \quad . \quad . \quad . \quad . \quad . \quad . \quad (7)$$

or, on using eqn. (3):

$$\chi_p = (G/\pi)(L/L_F)(\sigma_C - \sigma_f). \quad . \quad . \quad . \quad . \quad . \quad . \quad (8)$$

The values of χ_p evaluated from eqn. (8) with $L/L_F = 2$ and $\sigma_f = 60$ kg/cm^2 (Blewitt *et al.* 1955) are given in table 2 together with the measured values. The agreement is satisfactory both from the point of view of the order of magnitude, as well as in relation to the temperature-dependence. (The linear relation between χ_p and σ_C, already referred to above, is also apparent from eqn. (8).) The coefficient of shear hardening of single crystals in stage III should be equal to about $(2.24)^{-3}$ times χ_p. This estimate is in fact of the right order (I).

4.4. *Cottrell–Lomer Barriers*

By using the measured values of σ_C and χ_p respectively it is possible to deduce from eqn. (3) and eqn. (7) two independent values of the number, n, of dislocations which will lead to the break-down or other mode of failure of Cottrell–Lomer barriers. Both estimates, together with their mean, are given in table 3.

Table 3

T °K	n			R	$R_{\min}$	$R_{\max}$	$R/R_{\min}$	$R/R_{\max}$
	Eqn. (3)	Eqn. (7)	Mean					
77	88	91	90	0·070	0·041	0·20	1·7	0·35
195	70	75	73	0·049	0·031	0·15	1·6	0·33
292	62	61	62	0·035	0·027	0·13	1·3	0·27

Now, Stroh (1956) has plotted the ratio $n\sigma_C/2G$ as a function of the temperature for the two possible modes of breakdown of a Cottrell–Lomer barrier in copper. The maximum value of this ‘ breakdown ’ ratio $R_{\max}$, given by Stroh, relates to breakdown by ‘ dissociation ’; the width of the core of a dislocation is taken to be $0{\cdot}2b$. The minimum $R_{\min}$ relates to breakdown by ‘ recombination ’, the assumed core-width being $0{\cdot}3b$. The values of the ratio, denoted by R in table 3, obtained with n and σ_C as given in table 3 and table 2 respectively, lie between the limits of Stroh's estimates (table 3). The present results do not therefore rule out the possibility that a ‘ breakdown ’ mechanism of the type visualized by Stroh may be operative at the end of stage II as well as in stage III.

However, Seeger *et al.* (1957) have recently suggested that as

(*a*) the activation energy for cross-slip is less than that for ‘ breakdown ’ and as

(*b*) the breakdown mechanism would be expected to result in the appearance of long slip lines on the surface of crystals entering stage III, a phenomenon not observed by them in copper, dislocations piled up against Cottrell–Lomer barriers would surmount the barriers by cross-slip rather than break through them. These arguments do not appear to us to be fully convincing for the following reasons:

(*a*) The relation between the magnitudes of two activation energies is not a decisive criterion for discriminating between two processes in the absence of a detailed model of the mechanisms of both; such a model is not yet available for the mechanism involving cross-slip.

(*b*) Dislocations which have broken through a Cottrell–Lomer barrier could either again be stopped by a new barrier, as suggested in this paper in dealing with hardening in stage III, or they could be deflected to other slip-planes by cross-slip. Cross-slip, occurring *subsequent* to ‘ break-through ’ could thus account for the fragmentation of slip-bands observed for example by Seeger *et al.* (1957) in copper, and by the present authors (Feltham and Meakin 1957 b) in single crystals of lead, while the break-through process itself could provide a rational explanation of some characteristics of slip in metals, e.g. the occurrence of slip-ledges several thousand Å high in metals with low stacking-fault energies such as alpha-brass (Wilsdorf and Towrie 1956), or the sudden appearance of fully-formed slip steps about 200 Å high early in the process of band-formation in aluminium (Kuhlmann 1950).

It may well be that within a certain domain of the variables, i.e. temperatures, stress and strain rate, one of the processes may be operative, outside that domain the other.

REFERENCES

Bishop, J. F. W., and Hill, R., 1951, *Phil. Mag.*, **42**, 1298.
Blewitt, T. H., Coltman, R. R., and Redman, J. K., 1955, *Defects in Crystalline Solids* (London: The Physical Society), p. 369.
Diehl, J., 1956, *Z. Metallk.*, **47**, 331, 411.

FELTHAM, P., and MEAKIN, J. D., 1957 a, *Phil. Mag.*, **2,** 105., 1957 b, *Acta Met.* (in the Press).
FRIEDEL, J., 1955, *Phil. Mag.*, **42,** 1169.
JACQUET, P., 1954, *Acta Met.*, **2,** 752, 770.
JAOUL, B., 1957, *J. Mech. Phys. Solids*, **5,** 95.
KOCHENDÖRFER, A., 1947, *Metallforschung*, **2,** 173 ; 1950, *Z. Metallk.*, **41,** 322.
KUHLMANN, D., 1950, *Z. Metallk.*, **41,** 129.
LOZINSKII, M. G., 1956, *High-Temperature Metallography* (Moscow : Mashgiz), p. 222.
MOTT, N. F., 1952, *Phil. Mag.*, **43,** 1151.
SACHS, G., 1928, *Z. Ver. dtsch. Ing.*, **72,** 734.
SEEGER, A., DIEHL, J., MADER, S., and REBSTOCK, H., 1957, *Phil. Mag.*, **2,** 323.
STROH, A. N., 1956, *Phil. Mag.*, **1,** 489.
TAYLOR, G. I., 1938, *J. Inst. Met.*, **62,** 307.
WILSDORF, H., and TOWRIE, J. T., 1956, *Acta Met.*, **4,** 271.

The Atomic Heats of Titanium, Zirconium and Hafnium†

By N. M. Wolcott
Clarendon Laboratory, Oxford, England‡

[Received June 3, 1957]

Abstract

The specific heats of the metals titanium, zirconium, and hafnium have been measured between 1·2 and 20°K. Values of γ, the electronic specific heat coefficient, have been determined for these metals as 8·5, 7·25 and $6\cdot 3\times 10^{-4}$ cal/mole deg^2, while the corresponding values of the Debye θ in the continuum region are 430°, 310° and 261°. The variation of θ with temperature has been investigated, and it is shown that there is a similarity in this variation for all three elements when a suitably reduced scale of temperature is used.

§ 1. Introduction

The availability of high purity titanium, zirconium, and hafnium in recent years has made possible the investigation of the thermal properties of these metals. As the information on these elements is not complete below 20°K, it was thought of interest to extend the specific heat measurements from liquid hydrogen to liquid helium temperatures with the aim in particular of determining the electronic specific heat of hafnium which has not previously been reported.

The elements titanium, zirconium, and hafnium in Group IVA of the periodic table all crystallize in the hexagonal close-packed structure with almost equal axial ratios ($c/a=1\cdot 59$). For close-packed spheres c/a would be 1·633. All three elements also have body-centred cubic modifications which are stable at high temperatures. Some similarity in their thermal properties may therefore be expected.

§ 2. Previous Measurements

The specific heats of titanium and zirconium have been measured by Johnston and Kothen (1953) and Johnston and Skinner (1951) respectively between 15° and 300°K. Other measurements down to liquid nitrogen temperatures are those of Kelley (1944) on titanium, and Todd (1950) on zirconium. Johnston's work has been used here for comparison as he had the purer sample available, and the measurements extend over a wider temperature range. For hafnium only the results of Simon and

---

† Communicated by the Author.

‡ Now at U.S. Naval Research Laboratory, Washington, D.C.

Cristescu (1934) are available, but it is now thought that their sample was largely hafnium oxide.

At liquid helium temperatures there are only the measurements of Estermann *et al.* (1952) on the specific heat of titanium and zirconium. Recently some measurements have appeared on titanium between 4° and 15°K (Aven *et al.* 1956).

§ 3. Experimental Details

The samples of the elements were provided by A.E.R.E. Harwell and were all made by the van Arkel process in which the crystals are formed by condensation from the iodide. It is possible that the zirconium contained 1% hafnium, but the hafnium was said to be zirconium free. Other impurities were stated to be less than 0·1%. The samples consisted of about one mole of material for each element.

The calorimeter used in these experiments has been described in detail by Smith and Wolcott (1956). Since the technique of measurements is also described by these authors it will not be further elaborated.

§ 4. Results

In the helium region the specific heat can be described by the formula $C_p=\gamma T+464T^3/\theta^3$ cal/mole deg where the linear term in T is the electronic

Fig. 1

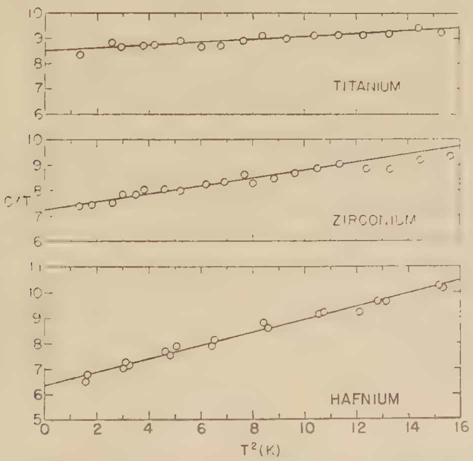

Plot of C_p/T against T^2 for titanium, zirconium, and hafnium. The ordinate is plotted in units of 10^{-4} cal/mole deg².

specific heat and the cubic term the lattice contribution. Above 4° the Debye characteristic temperature, θ, decreases with rising temperature for all three elements. The following values of γ and θ were appropriate for these substances below 4°K : titanium, $\gamma=8{\cdot}5\times10^{-4}$, $\theta=430°$; zirconium, $\gamma=7{\cdot}25\times10^{-4}$, $\theta=310°$; hafnium, $\gamma=6{\cdot}3\times10^{-4}$ cal/mole deg², $\theta=261°$. Graphs of C_p/T vs T^2 from which these values are derived appear in fig. 1, while the experimental points are given in the table. Since the

Measured values of C_p and corresponding values of the Debye θ. The values in parentheses are determined in the plot of C_p/T against T^2 in the liquid helium region. C_p is expressed in units of cal/mole deg.

Titanium

T	C_p	θ	T	C_p	θ	T	C_p	θ	T	C_p	θ
1·17	0·000989	(430)	3·64	0·00335		8·15	0·0104	417	12·65	0·0234	420
1·60	0·00142		3·80	0·00358		8·46	0·0109	425	13·18	0·0258	419
1·71	0·00148		3·91	0·00361		8·74	0·0116	420	13·74	0·0282	419
1·94	0·00169		4·50	0·00404		9·03	0·0122	424	14·25	0·0313	414
2·05	0·00179		5·11	0·00503		9·35	0·0129	427	14·85	0·0345	412
2·28	0·00204		5·40	0·00556	440	9·64	0·0138	422	15·52	0·0384	411
2·45	0·00212		5·74	0·00605	423	9·93	0·0145	423	16·18	0·0433	405
2·62	0·00230		6·05	0·00648	425	10·22	0·0150	429	16·85	0·0485	401
2·76	0·00246		6·66	0·00746	425	10·52	0·0164	419	17·58	0·0549	400
2·89	0·00264		7·00	0·00793	430	10·80	0·0170	421	18·29	0·0620	394
3·05	0·00275		7·30	0·00841	434	11·15	0·0181	421	19·00	0·0692	391
3·22	0·00294		7·58	0·00923	419	11·52	0·0191	426	19·66	0·0777	387
3·36	0·00308		7·85	0·00976	416	11·90	0·0207	421	20·32	0·0839	388
3·50	0·00320					12·28	0·0217	424	20·95	0·0945	382

Zirconium

T	C_p	θ	T	C_p	θ	T	C_p	θ	T	C_p	θ
1·16	0·000856	(310)	3·52	0·00315		8·23	0·0172	285	12·80	0·0579	271
1·34	0·000994		3·65	0·00322		8·52	0·0189	284	13·15	0·0608	274
1·62	0·00122		3·81	0·00351		8·82	0·0204	284	13·50	0·0678	270
1·73	0·00136		3·96	0·00371		9·11	0·0222	283	13·85	0·0759	266
1·88	0·00147		4·55	0·00433		9·42	0·0245	280	14·27	0·0805	269
1·95	0·00157		4·88	0·00508	328	9·70	0·0262	282	14·82	0·0899	268
2·14	0·00173		5·32	0·00641	302	10·00	0·0284	280	15·27	0·0968	268
2·28	0·00182		5·80	0·00779	294	10·33	0·0314	278	15·78	0·1121	264
2·49	0·00206		6·15	0·00859	298	10·62	0·0333	279	16·25	0·1251	260
2·63	0·00220		6·45	0·00942	298	10·90	0·0356	279	16·70	0·140	257
2·77	0·00239		6·73	0·01036	297	11·18	0·0386	277	17·38	0·160	255
2·83	0·00234		7·05	0·0116	294	11·48	0·0404	280	17·95	0·177	254
2·97	0·00252		7·36	0·0132	287	11·82	0·0445	278	18·45	0·193	254
3·10	0·00270		7·65	0·0141	290	12·15	0·0496	274	19·05	0·215	252

T	C_p	θ	T	C_p	θ	T	C_p	θ	T	C_p	θ
1·25	0·000813	(261)	3·48	0·00321		7·40	0·0179	242	11·83	0·0739	225
1·29	0·000873		3·58	0·00346		7·68	0·0197	242	12·28	0·0825	225
1·75	0·00123		3·63	0·00350		7·97	0·0220	243	12·72	0·0944	224
1·77	0·00129		3·90	0·00401		8·26	0·0243	240	13·25	0·1067	222
1·83	0·00131		3·92	0·00401		8·56	0·0266	240	13·75	0·122	220
2·15	0·00166		4·62	0·00546	262	8·85	0·0294	238	14·30	0·140	218
2·20	0·00166		4·96	0·00650	257	9·16	0·0329	237	14·91	0·163	218
2·25	0·00178		5·30	0·00766	252	9·47	0·0358	237	15·57	0·188	214
2·54	0·00201		5·65	0·00886	251	9·75	0·0402	233	16·22	0·217	213
2·56	0·00209		5·95	0·00995	251	10·04	0·0440	232	16·95	0·248	212
2·90	0·00256		6·22	0·01154	245	10·35	0·0481	231	17·70	0·291	209
2·93	0·00252		6·50	0·0128	243	10·70	0·0535	230	18·48	0·334	208
3·25	0·00297		6·80	0·0143	245	11·06	0·0597	229	19·25	0·385	206
3·28	0·00302		7·12	0·0157	246	11·45	0·0651	229	20·15	0·441	205

Smoothed Values of C_p and θ

Specific Heat				Debye θ			
T	Ti	Zr	Hf	T	Ti	Zr	Hf
1·5	0·00122	0·00107	0·00100	0	430	310	261
2·0	0·00175	0·00155	0·00147	5	430	304	257
3·0	0·00265	0·00255	0·00255	6	430	300	251
4·0	0·00368	0·00375	0·00400	7	430	295	246
5·0	0·00485	0·00535	0·00660	8	428	290	241
6·0	0·00639	0·00825	0·0102	9	427	285	237
8·0	0·0100	0·0157	0·0223	10	426	280	233
10·0	0·0146	0·0284	0·0480	12	422	274	226
12·0	0·0210	0·0470	0·0770	14	415	267	219
14·0	0·0295	0·0781	0·130	16	407	261	213
16·0	0·0422	0·118	0·207	18	398	255	208
18·0	0·0596	0·180	0·308	20	388	249	205
20·0	0·0810	0·243	0·434				

lattice contribution is less than 10% of the total specific heat of titanium and zirconium in the liquid helium region, θ for these elements can only be specified to ±3% below 4°K.

§ 5. DISCUSSION

5.1. *Lattice Specific Heats*

In order to determine the true lattice contribution to the specific heat and hence the corresponding Debye θ, it is necessary first of all to correct the measured values of C_p to C_v and then to allow for the electronic term, γT. As an indication of the relative magnitude of these corrections, neglecting the electronic term for zirconium at 150°K or T/θ about 3/5 would introduce an error of 10% to the Debye θ, while ignoring the C_p–C_v correction would add another 4%. The correction for the electronic term is easily made using the value of γ determined in the helium region where $C_p = C_v$ and the lattice contribution is proportional to T^3. The C_p–C_v correction can be determined from the approximate relation $C_p - C_v = AC_p^2T$ where A is determined by comparison at room temperature with the exact thermodynamic expression $C_p - C_v = \alpha^2VT/\beta$, where α is the bulk thermal expansion coefficient, β the compressibility, and V the atomic volume. For zirconium the value of A was determined to be $8{\cdot}9 \times 10^{-6}$ mole/cal using the room temperature values of the thermal expansion and compressibility (van Arkel 1939, Reynolds 1952). Since expansion data are not available for titanium the empirical formula of Nernst and Lindemann (1911) was used in which $A = 0{\cdot}0214/T_s$, where T_s is the melting temperature, giving $A = 1{\cdot}07 \times 10^{-5}$ mole/cal. The Nernst–Lindmann formula also gives the value of $A = 8{\cdot}9 \times 10^{-6}$ for zirconium, so that the value obtained for titanium in this way is expected to be reasonable. Below 20°K, C_p–C_v is negligible, and so no correction has been made for hafnium in this temperature range.

The θ–T relations for these three elements are shown in figs. 2 to 4.

The results are in general accord with the present theory (e.g. Blackman 1955) from which a temperature variation of the Debye θ may be expected at temperatures above about $\theta/50$ where the non-continuum portion of the vibration spectrum becomes reasonably excited. For titanium θ does not change very much with temperature up to 13°K; this is in agreement with the results of Aven *et al.* who find a value of $\theta = 421$ between 4° and 13° while the present measurements indicate an average θ value of 425° in this temperature range. The present results connect quite well with those of Johnston, as figs. 2 and 3 indicate. Aven commented that the θ values calculated from Johnston's data seemed much too low; however, he apparently neglected to allow for the electronic specific heat when calculating the Debye θ from Johnston's measured values of C_p. When correction is made for the electronic term the higher values of θ shown in fig. 2 are obtained. On the other hand the θ's in the 2°–4° region given by Estermann *et al.* for titanium (280°) and zirconium (265°) appear to be much too low compared with the present value of 430° (Ti) and 310° (Zr).

Fig. 2

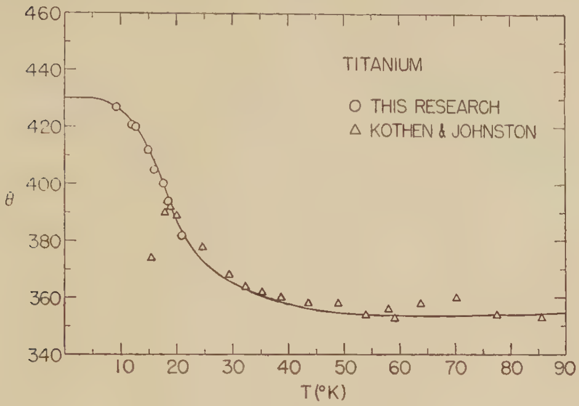

Debye θ of titanium as a function of temperature.

Fig. 3

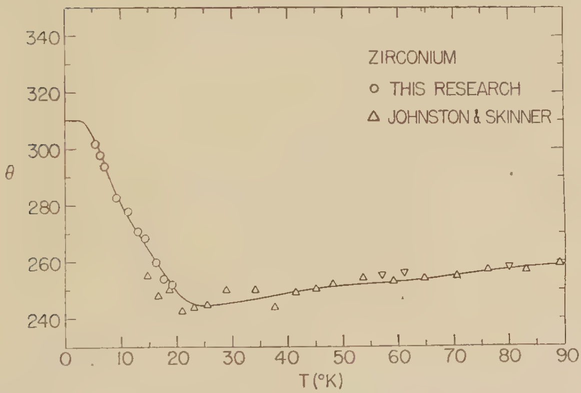

Debye θ of zirconium as a function of temperature.

Fig. 4

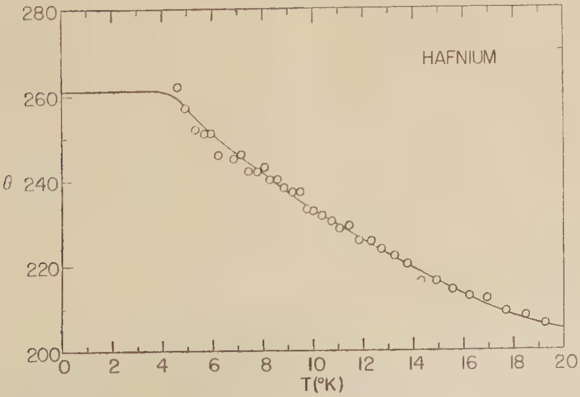

Debye θ of hafnium as a function of temperature.

However, these authors also obtain θ values which appear low for copper (Corak *et al.* 1955) and magnesium (Smith 1955), so that the discrepancy may be a systematic one.

The similarity in the θ–T curve of these elements is further brought out by fig. 5 in which the reduced values θ/θ_∞ and T/θ_∞ have been plotted. Here θ_∞ is a characteristic value of θ at high temperatures. For titanium θ_∞ was taken as 360°, for zirconium 260°, and for hafnium 200°. (The results of Friedberg (private communication) have been used in determining θ_∞ and the shape of the reduced θ curve at high temperatures for hafnium.) Exact coincidence in the curves is not to be expected however, for as Hill and Smith (1953) have pointed out, this would imply that the ratios of the interatomic force constants were identical as well as the axial ratios.

Fig. 5

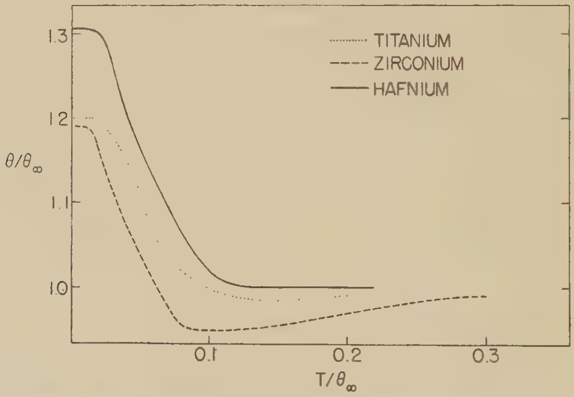

Reduced θ plotted as a function of reduced temperature for Ti, Zr, and Hf.

The reduced θ curves may be compared with those for the hexagonal metals of Groups II and IIB of the periodic table (Hill and Smith 1953, Smith 1955, Smith and Wolcott 1956). When this is done it appears that there is a similarity among the Group II elements beryllium and magnesium, and the Group IVA metals, all of which have axial ratios slightly less than the ideal $\sqrt{8/3}=1{\cdot}633$. The temperature variation of θ for zinc and cadmium ($c/a=1{\cdot}9$) is much more pronounced. One might be tempted to conclude from this that for the hexagonal metals large axial ratios are associated with large temperature variations of the Debye θ. However, rhenium with an axial ratio of 1·6 has a Debye θ which changes over 60% below 20° (Wolcott 1955), so it appears that other variables as well as the c/a ratio must be significant in determining the θ behaviour of the various hexagonal metals.

It is interesting to note that the high temperature θ's closely follow the Lindemann (1910) formula which requires that θ be proportional to $(T_s/M)^{1/2}V^{-1/3}$, where T_s is the melting temperature, M the atomic mass, and V the atomic volume. For the elements titanium, zirconium, and hafnium this quantity has the proportion 1 : 0·70 : 0·54, while the actual high temperature θ's are in the proportion 1 : 0·72 : 0·55. This correspondence might be expected in view of the similar physical properties of these elements.

As no complete theoretical calculations of the vibration spectra have been carried out for the hexagonal close-packed lattice, no detailed comparison of the θ–T curves with theory can be made. However, Barron and Domb (1955) have made some calculations using a central force model and conclude that the Debye θ at 0°K shifts about 1% when the lattice structure changes from hexagonal to cubic close-packed. In view of this agreement at low temperatures there may be some justification in comparing qualitatively the experimental θ–T curves for the h.c.p. metals with the theoretical calculations for the cubic close-packed structure. When this is done, it is seen that the 20% drop in θ with rising temperature is indeed similar to that found by Leighton (1948) for the f.c.c. lattice. It should be mentioned though that there are f.c.c. metals (thorium) as well as h.c.p. metals (rhenium) which show much larger θ variations than those indicated by Leighton. When the single crystal elastic constants for these metals become available a more detailed check of the adequacy of the Leighton model can be made.

A θ may also be calculated from the isotropic Debye model using the room temperature longitudinal and transverse wave velocities of Reynolds (1952). When this is done values of $\theta = 380°$ for titanium and $\theta = 264°$ for zirconium are obtained. The agreement with the high temperature θ's (which also occurs in the case of copper) must, of course, be considered fortuitous, as the continuum theory is not applicable in this temperature region.

5.2. *Electronic Specific Heats*

The electronic specific heats may be related to the density of electronic states at the Fermi surface, $g(\epsilon)$, since quite generally $\gamma = 2/3\pi^2 k^2 g(\epsilon)$. The present values of γ give the density of states to be 0·755 levels/atm ev for titanium, 0·644 levels/atm ev for zirconium, and 0·56 levels/atm ev for hafnium. These results are about two and one half times the free electron values assuming four free electrons per atom, and are therefore qualitatively in agreement with Mott's (1935) theory of the transition metals. However, as no theoretical calculation of the density of states has been made for any of these elements, no real comparison with theory is possible. From the theoretical density of state calculations that have been made for other transition metals, the value of γ for the elements in Group IVA would be expected to be larger than the free electron value, but smaller than that for the later transition elements in Groups V and VIII, which is in fact what is observed. In common with other transition metal series, it appears that the heavier elements have the lower density of states; in fact, for Group IVA the density of states is very nearly proportional to $Z^{-1/4}$, where Z is the atomic number.

The actual values of the electronic coefficient γ obtained here for titanium and zirconium are a few per cent higher than those reported by

Estermann *et al.* and Aven *et al.*, but the discrepancies are probably within the combined experimental error.

As titanium and zirconium are superconductors, estimates of γ may be obtained from their magnetic threshold field curves. For titanium the measurements give $\gamma=35\times10^{-4}$ (Hein *et al.* 1957), and for zirconium $\gamma=4\times10^{-4}$ cal/mole deg^2 (Smith and Daunt 1952). These values are derived from theoretical formulae which treat the critical magnetic field curve as representing a phase boundary between the normal and superconducting states of the metal. This picture is idealized in as much as it admits no intermediate state. In the case of hard superconductors such as titanium and zirconium which have broad transitions and therefore large intermediate states, the application of thermodynamics to the critical field curves is questionable, and hence the disagreement with calorimetric values of γ is not surprising.

§ 6. CONCLUSION

The low temperature heat capacities of the Group IVA metals have now been fairly thoroughly investigated. The electronic specific heats and Debye θ's are in agreement with the general theoretical picture, whilst there is a similarity in the thermal properties of these elements which is not unexpected in view of their similar physical and chemical properties.

REFERENCES

AVEN, M. H., CRAIG, R. S., WAITE, T. R., and WALLACE, W. E., 1956, *Phys. Rev.*, **102,** 1263.

BARRON, T. K. H., and DOMB, C., 1955, *Proc. roy. Soc.* A, **227,** 447.

BLACKMAN, M., 1955, *Handbuch der Physik* (Berlin: Springer Verlag), Vol. VII, Part I, p. 325.

CORAK, W. S., GARFUNKEL, M. P., SATTERTHWAITE, C. B., and WEXLER, A., 1955, *Phys. Rev.*, **98,** 1699.

ESTERMANN, I., FRIEDBERG, S. A., and GOLDMAN, J. E., 1952, *Phys. Rev.*, **87,** 582.

HEIN, R. A., HENRY, W. E., and WOLCOTT, N. M., 1957, *Phys. Rev.* (to be published).

HILL, R. W., and SMITH, P. L., 1953, *Phil. Mag.*, **44,** 636.

JOHNSTON, H. L., and KOTHEN, C. W., 1953, *J. Amer. chem. Soc.*, **75,** 3101.

JOHNSTON, H. L., and SKINNER, G. B., 1951, *J. Amer. chem. Soc.*, **73,** 4549.

KELLEY, K. K., 1944, *Ind. Eng. Chem.*, **36,** 865.

LINDEMANN, F. A., 1910, *Physik. Z.*, **11,** 609.

MOTT, N. F., 1935, *Proc. phys. Soc. Lond.*, **47,** 571.

NERNST, W., and LINDEMANN, F. A., 1911, *Z. Elektrochem.*, **17,** 817.

REYNOLDS, M. B., 1952, *Communication* P-181, Knolls Atomic Power Laboratory, Schenectady, N.Y.

SIMON, F. E., and CRISTESCU, S., 1934, *Z. physik. Chem.* B, **25,** 273.

SMITH, P. L., 1955, *Phil. Mag.*, **46,** 744.

SMITH, T. S., and DAUNT, J. G., 1952, *Phys. Rev.*, **88,** 1172.

SMITH, P. L., and WOLCOTT, N. M., 1956, *Phil. Mag.*, **1,** 854.

TODD, S. A., 1950, *J. Amer. chem. Soc.*, **72,** 2914.

VAN ARKEL, A. E., 1939, *Reine Metalle* (Berlin: Julius Springer Verlag).

WOLCOTT, N. M., 1955, *Bulletin de l'Institute International du Froid*, Supplement 1955–3 (Jan. 1956), p. 286.

The Angular Correlation of the Gamma Cascade in Sulphur 34†

By P. S. Fisher and G. G. Shute
Department of Physics, University of Birmingham

[Received June 19, 1957]

Abstract

The angular correlation of the gamma cascade in ^{34}S has been measured to be $1+(0{\cdot}332\pm0{\cdot}032)P_2(\cos\theta)-(0{\cdot}017\pm0{\cdot}011)P_4(\cos\theta)$ and this is interpreted in terms of a spin-sequence 2^+, 2^+, 0 with a mixture of 1·4% of E2 radiation in the first transition. A new angular correlation apparatus and fast coincidence system is briefly described.

§ 1. Introduction

The ^{34}Cl nucleus is the lightest nucleus with $A=4n+2$ to have the level with total isotopic spin zero ($T=0$) higher in energy than the $T=1$ level, which forms the ground state. Consequently, the beta decay of both the isomeric level ($t_{1/2}=33$ min) and the ground state ($t_{1/2}=1{\cdot}5$ sec) are of particular interest, and the mode of decay is well established (see fig. 1).

Angular correlation measurements for the gamma ray cascade in ^{34}S can be used to assign spins to the energy levels. Measurements were published for this correlation by Handler and Richardson in 1956 whilst the present work was in progress, but it was thought that the information was of sufficient interest, and the measurements sufficiently complicated by the short half life and by the presence of the abundant annihilation radiation, to make an independent measurement and analysis of the results desirable.

This paper contains some details of a new angular correlation apparatus built to make measurements on isotopes with half lives as short as 10 minutes. It includes a new and simple fast coincidence arrangement. Measurements of the angular correlation for the gamma rays from ^{34}S are considered in association with the other data on the decay scheme to assign spins to the ^{34}S energy levels.

§ 2. Apparatus

Two scintillation counters were mounted on the movable arms of a table so that they could be set at any angle from 45° (when they were in contact) up to 180°. Each counter consisted of a $1\frac{1}{2}$ in. × 2 in. sodium iodide (Tl) crystal mounted on an E.M.I. Type 6262, 14-stage photomultiplier, with a lead shield 2 in. long defining the half angle of acceptance to 10°. The mounts which held the counters to the table were provided with fine adjustments so that each counter and shield could be directed accurately at the table centre, where the source was situated.

---

† Communicated by the Authors.

Fig. 1

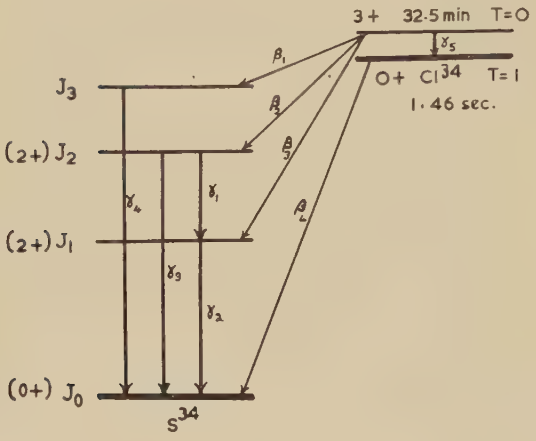

γ	E MeV.	%	α
1	1·16	15	
2	2·10	39	
3	3·22	7	
4	4·0	0·2	
5	0·145	38	0·14

α is the conversion coefficient

β	E_{max} MeV.	%	log ft
1	0·53	0·1	>5·6
2	1·33	26	4·82
3	2·48	28	6·08
4	4·50	46	3·50

The decay scheme of ^{34}Cl to ^{34}S. This decay scheme summarizes the results of the following authors: Ruby and Richardson (1951), Ticho (1951), Aber and Stahelin (1953), Stahelin and Preiswerk (1953), Peaslee (1953), Green and Richardson (1954), Handler and Richardson (1956), Bleuler and Morinaga (1956). The spin assignments resulting from the present measurements are shown on the left in parentheses.

To form a fast–slow coincidence system (Bell and Petch 1949), two output signals were taken from the 14-stage photomultipliers. The first, which came from the 9th dynode, was given conventional amplification and was used for pulse height selection and spectroscopic purposes. The second signal came from the final electrode (collector) and was used for the fast coincidence work. With 1·5 kv applied to the photomultiplier the final stages tended to saturate, particularly for large pulses, resulting in preferential amplification of smaller signals, and reduction of all pulses to approximately uniform amplitude. The negative output pulse rose to 0·3 v in 10^{-8} sec when fed directly into a load of 100 ohms and a 110 ohm cable. At the far end the cable was unterminated and fed pulses into an E.F.P. 60 secondary emission pentode with an inductive load in the anode, which in turn drove a low level trigger circuit using another E.F.P. 60 pentode. This trigger circuit has been described by Moody and McLusky (1952). It has accurate and low level triggering because the valve is passing appreciable cathode current in its quiescent state and consequently works under approximately optimum conditions. The feedback from secondary cathode to grid is a direct capacitative coupling involving only small strays, and the whole system is kept stable by interrupting the feedback path with a germanium diode just biased-off. The circuit was originally designed as a discriminator, for which the very low triggering voltage of 0·05 volts gives accurate selection of small pulses (0 → 10 v). The same factors which make it suitable as a low level discriminator (i.e. sensitive triggering and production of a standard output pulse) also make this circuit suitable for use in a coincidence arrangement. The circuit is triggered by very small pulses

Fig. 2

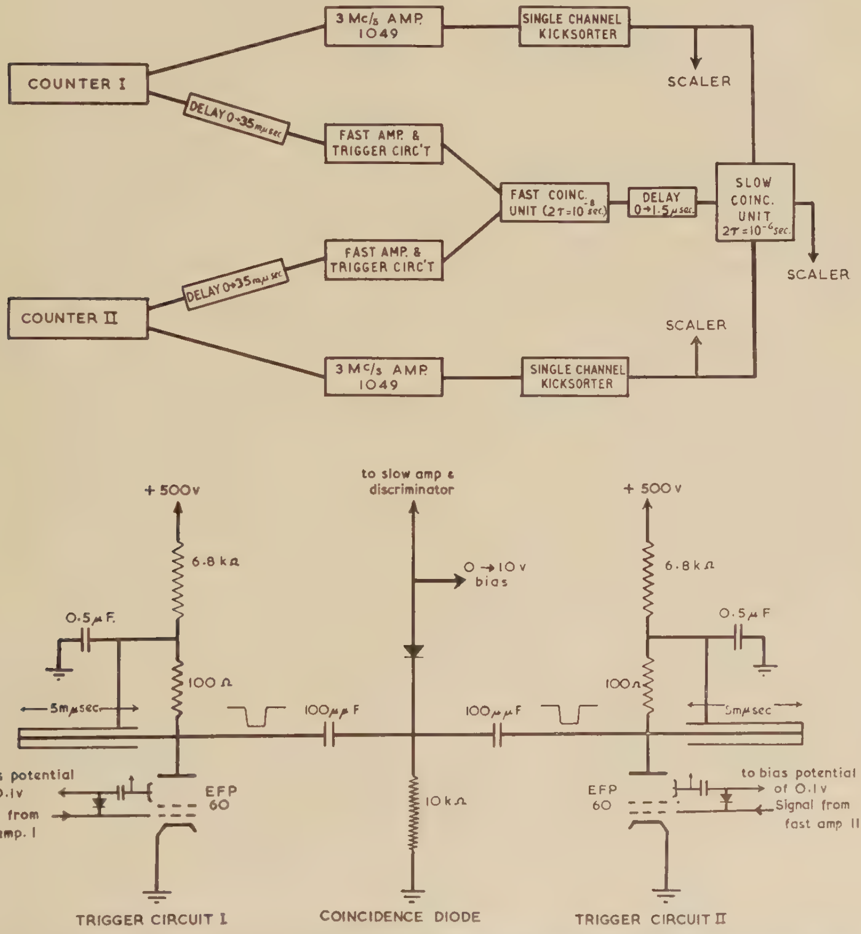

The fast–slow coincidence arrangement showing a detail of the fast coincidence system.

(about 0·05 v) and if the control grid is driven through even a few tenths of a volt in 10^{-9} sec the positive feedback, which has a very small lag, rapidly drives the valve into saturation current. The triggering point of the circuit depends upon the bias across the diode in the feedback path and when this bias is reduced to the minimum consistent with long term stability of the circuit, triggering by the signal from the photomultiplier (after amplification in the secondary emission pentode) is estimated to be accurate to within 2×10^{-9} sec. When triggered the circuit gives a 5 volt pulse across a 110 ohm line 5 mμsec long, shorted at the far end to clip the signals to 10^{-8} sec.

Clearly, two such signals mixed in a coincidence circuit will give a resolving time of about 10^{-8} sec. In the present apparatus, pulses from the trigger circuits are fed to a biased-off germanium diode followed by slow amplification. The schematic arrangement is shown in fig. 2; apart from the details of the fast coincidence circuit, it is a standard fast--slow coincidence assembly. Pulses selected for pulse height are put into slow coincidence ($2\tau=10^{-6}$ sec); the resulting coincidences are formed only between pulses of the required amplitude (and hence correspond to the energy range of interest) but a large proportion of random coincidences may be included at fast counting rates (10^5 per sec). The fast coincidence system gives coincidences regardless of pulse height, but includes a very low proportion of randoms. Coincidences common to both systems are selected in a further coincidence circuit, and these so called fast–slow coincidences occur only between pulses of the desired amplitude and contain the low proportion of random characteristic of the fast coincidence circuit.

The apparatus was checked as a whole using ^{60}Co for which the angular correlation is well established and the results of this measurement are given in fig. 3 together with the theoretical values; the agreement is satisfactory.

§ 3. OBSERVATIONS

$^{34\mathrm{m}}$Cl may conveniently be formed by the reaction

$$^{32}\mathrm{S}+{}^{4}\mathrm{He}\rightarrow{}^{34\mathrm{m}}\mathrm{Cl}+p+n$$

and this reaction was induced by bombarding a natural sulphur target with the external beam of 40 MEV He^{2+} ions from the 60 in. Nuffield cyclotron of this laboratory. The external beam is free from contamination by the low energy helium ions and deuterium ions which might be present in circulating beams within the cyclotron tank. The sulphur target, which was about 2 mm thick, adhered to a water cooled copper backing and was covered during bombardment by a 0·0003 in. tantalum foil. Bombardments of 0·5 μA for 10 minutes provided sufficient activity to make up sources of convenient strength. Preliminary experiments confirmed the prediction that under these conditions there would be no competing nuclear reactions induced which would produce activities comparable in intensity with that of the $^{34\mathrm{m}}$Cl after the lapse of a few minutes. Consequently it was possible to use the bombarded sulphur directly as the source, without chemical extraction of the $^{34\mathrm{m}}$Cl activity. Sulphur from the target was scraped off and sealed into a thin walled (0·002 in.) brass cylinder 2 mm in diameter and 5 mm long, extending from a 2 B.A. brass threaded rod at the lower end. This sealed source could then be screwed into the centre of the angular correlation table.

Direct use of the target sulphur in the source holder had the great advantage of shortening the time between the bombardement and the measurements, and also avoided the use of silver chloride from the standard chemical extraction of chlorine, with its attendant high density, as the source. Initial source strengths used for the angular correlation were of the order of 0·1 mc and these gave a ratio of real to random coincidences of about 20 with the resolving time of 10^{-8} sec. The pulse height analysers of both scintillation counters were set to receive pulses corresponding to an energy dissipation in the crystal in the range 0·7 to 2·5 Mev.

Fig. 3

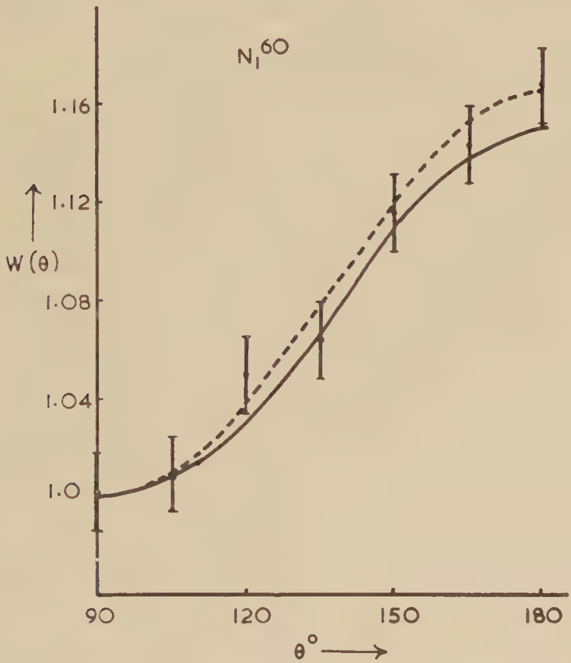

The angular correlation for ^{60}Ni. The broken line represents the least squares fit. The solid line is the theoretical correlation for a 4(2)2(2) 0 transition.

The half life of ^{34m}Cl is only 33 min, and to make the angular correlation measurements it was necessary to replace the source every 80 minutes and then to relate the measurements together. It was decided to take measurements with each source at 15° intervals for 7 angles for a period of 10 minutes at each angle. At each observation a period of 1 minute had to be allowed for reading and re-setting the scalers. For a given number of observations in a run this reading time was fixed, and to concentrate it in early stages of the measurements when the source was most active, which would have been the result of taking measurements after a constant count had been recorded, meant losing a great deal more information than in counting for constant time. The total number of coincidences at angles with $\cos^2\theta$ less than 0·40 was made roughly equal to the total number at angles with $\cos^2\theta$ greater than 0·40 by taking observations in the following sequence :

90°, 165°, 105° or 75°, 150°, 120° or 60°, 135° or 45°, 180°.

With each new source a start was made at the angle next in the sequence to the one which started the previous series.

Frequent checks were made during the course of the experiment on the resolving times of the coincidence circuits.

§ 4. TREATMENT OF RESULTS

The observed counting rates had to be corrected for the dead times of the circuits, which were determined in all cases by the 5 μsec dead time of the 1009 scaling units, and allowance had to be made for the inclusion of random coincidences in the coincidence count. To compensate for any slight decentring of the source, and small variations in the discrimination levels, the combination $Y=(C/N_1N_2)\exp(-\lambda t)$ was formed. C was the coincidence rate after subtraction of the calculated random coincidences, N_1 and N_2 were the single counting rates in the two counters after correction for the scaler dead time, and λ was the decay constant of $^{34\text{m}}$Cl. The quantity Y is not affected by the decay of the source, although it is strongly dependent upon the source strength at time $t=0$, and consequently relative values of the function at different angles are directly proportional to the correlation function $W(\theta)$ for those angles. Observations from different sources were related together by fitting the observations to a two parameter curve $Y=a_0+a_2\cos^2\theta$ and then using the a_0 as a normalizing factor. The results of the observations could then be collected together, averaged and fitted to a three parameter curve.

$$a_0+a_2\cos^2\theta+a_4\cos^4\theta$$

by the method of least squares. The observations at 180° were not used in the evaluation of the normalizing factor, or when fitting the observations to the curve, since the presence of annihilation radiation was likely to induce at this angle a rise in the coincidence rate which could not be readily estimated.

The (χ^2) significance test (Kendall 1945) was applied to the deviation of the observations from the least squares fit taking care to make allowance for the various constraints imposed during the calculations. The test gave a value for the chance deviation from the calculated curve as 80%, indicating that all the parameters a_0, a_2 and a_4 were significant. Having thus established the validity of the parameters, the errors in the coefficients a_0, a_2 and a_4 were computed from the mean square deviation of the observations from the fitted curve.

Each counter had a small but significant efficiency for the exceedingly abundant radiation resulting from the annihilation of the positrons. Much of this radiation was coincident with the various gamma rays of the decay, and it was necessary to correct the observed distribution for the inclusion of the isotropic contribution from gamma-annihilation coincidences. This contribution was estimated by carrying out a correlation experiment at 5° intervals from 150° through 180° to 150°, with each spectrometer in turn set upon the annihilation radiation photopeak. From the rise in the coincidence rate at 180° it was possible to estimate the relative efficiency of the unaltered counter for annihilation radiation. In this way the annihilation gamma contribution to the isotropic coincidence rate was estimated as 8·1±0·5%.

Fig. 4

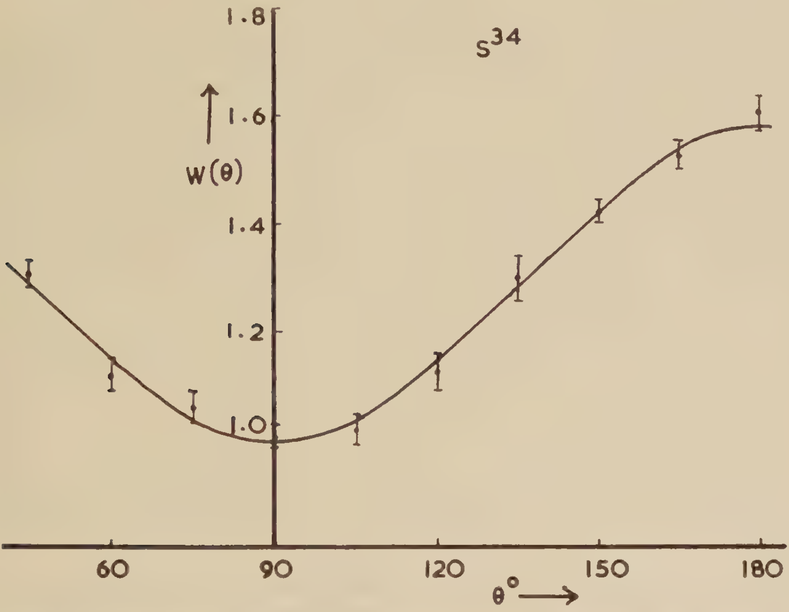

The Angular correlation for ^{34}S. The curve drawn through the observations is the least squares fit.

Finally, the result was converted to the standard form :

$$W(\theta)=A_0+A_2P_2(\cos\theta)+A_4P_4(\cos\theta) \quad . \quad . \quad . \quad (1)$$

and the coefficients A_2 and A_4 corrected for the finite solid angle subtended by the detectors. This correction has been treated by Rose (1953), and his correction factors Q for the geometry used are $Q_0=1$, $Q_2=0{\cdot}97$, and $Q_4=0{\cdot}88$. The experimental results after correction by all these factors then appear in the form (1) with

$$A_0=1, \quad A_2=0{\cdot}332\pm0{\cdot}032, \quad A_4=-0{\cdot}017\pm0{\cdot}011.$$

These results may be compared with those of Handler and Richardson (1956) if the latter are expressed in the same form (1) ; they give

$$A_0=1, \quad A_2=0{\cdot}330\pm0{\cdot}055, \quad A_4=-0{\cdot}018\pm0{\cdot}021.$$

§ 5. DISCUSSION

The presence of a strong crossover transition in the decay scheme of the even–even nucleus ^{34}S, together with the knowledge that the

3·32 MeV level does not have a long lifetime ($<10^{-7}$ sec), limits the spins which need be considered for the two excited states to 1, 2 or 3.

The experimental coefficients have been compared with the predictions from all permutations of these spins using the tables of Biedenharn and Rose (1953). Since a mixture of multipoles is possible in the first transition the mixing parameter δ has been introduced in accordance with the definition of Biedenharn and Rose. For a mixed transition the correlation function $W(\theta)$ may be written :

$$W(\theta)=W_1(\theta)+\delta^2 W_{11}(\theta)+2\delta W_{111}(\theta)$$

where $W_1(\theta)$ and $W_{11}(\theta)$ are correlation functions for the pure cascade, $W_{111}(\theta)$ takes into account interference between $W_1(\theta)$ and $W_{11}(\theta)$, and δ^2 is the mixing ratio. Values of δ have been found which bring the theoretical coefficient A_2 of eqn. (1) to the experimental value ($A_2=0{\cdot}332$). In general, two solutions for δ are obtained for each spin sequence, and to each δ there is a corresponding value for the coefficient A_4. In the table the spin sequences considered are listed with the corresponding values for δ and A_4. It is interesting to note that even with mixing the spin sequence 3, 2, 0 cannot be reconciled with the observed value for A_2. If the theoretical coefficient A_4 is required to lie within two standard deviations of the experimental values, only those entries in *italic* type in the table are acceptable.

The Values Tabulated for the Mixing Parameter δ give $A_2=0{\cdot}332$ for each Spin Sequence. The Predicted Value of A_4 is shown beside the Corresponding Value for δ.

J_2	J_1	J_0	δ	A_4	δ'	A'_4
1	1	0	*−0·477*	0	*−2·10*	0
2	1	0	*0·445*	0	*7·67*	0
3	1	0	*0·72*	0	*−13·2*	0
1	2	0	0·564	−0·184	6·73	−0·745
2	2	0	*0·12*	*0·0046*	1·67	0·240
3	2	0	no real solutions			
1	3	0	0·122	−0·0407	3·37	0·0764
2	3	0	0·411	0·0207	6·90	0·140
3	3	0	*−0·055*	*−0·00029*	*1·48*	*−0·0654*

Experimental values $A_0=1$, $A_3=0{\cdot}332\pm0{\cdot}032$, $A_4=-0{\cdot}017\pm0{\cdot}011$.

The assignments with spin 1 for the first excited state all require the postulate of strong mixing and it is hard to see how assignments 1, 1, 0 ; 2, 1, 0 or 3, 1, 0 could be reconciled with the observed mode of decay from the isomeric level in ^{34}Cl for which the 3+ assignment is well substantiated (see fig. 1). The assignments 3, 3, 0 and 2, 2, 0 remain.

For octopole crossover radiation (γ_3 of fig. 1) to compete with the dipole transition γ_1 in the spin sequence 3, 3, 0, it must be E3 competing with M1 in a sequence 3−(− = odd parity), 3−, 0+. On this assignment beta decay from the 3+ isomeric state of ^{34}Cl to the first two excited states of ^{34}S would be first forbidden, whereas the measured log *ft* values indicate that they are allowed. This spin sequence may therefore be excluded.

The spin sequence 2, 2, 0 requires the assumption of only slight mixing ($\delta^2 = 1{\cdot}4\%$) to bring the experimental and theoretical angular correlations into agreement. With a sequence 2+, 2+, 0+ the mixture would be M1 with E2 radiation in the 1·2 Mev transition between the levels of spin 2, followed by an E2 transition to the ground state. The crossover radiation from the 3·2 Mev 2+ level would also be E2 and this would be expected to compete favourably with the M1+E2 mixture. Beta decay to the 2+ levels from the 3+ isomeric state of ^{34}Cl would be allowed, and this agrees with the observed log *ft* values. The assignment 2+ for the first excited state is expected from comparison with similar nuclei and although mixing has to be introduced in order to fit the observed angular correlation, there appears to be no ambiguity in interpreting the results. The experimental and theoretical values for the coefficient A_4 can only just be reconciled however, and it is hoped soon to confirm this assignment by making polarization correlation measurements with the polarimeter now in use in this laboratory.

ACKNOWLEDGMENTS

We wish to thank Professor W. E. Burcham for proposing this problem, and for his help and advice during the course of the work. The cooperation of the workshop staff and of the cyclotron operators is gratefully acknowledged.

The authors wish to express their thanks for financial support: P. S. F. to the D.S.I.R. for a maintenance grant and G. G. S. to the University of Melbourne for a travelling scholarship.

REFERENCES

ABER, W., and STAHELIN, P., 1953, *Helv. phys. acta*, **26**, 433, 584.
BIEDENHARN, L. C., and ROSE, M. E., 1953, *Rev. mod. Phys.*, **25**, 749.
BELL, R. E., and PETCH, H. E., 1949, *Phys. Rev.*, **76**, 1409.
BLEULER, E., and MORINAGA, H., 1956, *Phys. Rev.*, **103**, 1423.
GREEN, D., and RICHARDSON, J. R., 1954, *Phys. Rev.*, **96**, 858.
HANDLER, H. E., and RICHARDSON, J. R., 1956, *Phys. Rev.*, **102**, 833.
KENDALL, M. G., 1945, *Advanced Theory of Statistics*, Vol. 1 (London: Griffin), p. 290.
MOODY, N. F., and MCLUSKY, G. J. R., 1952, *Millimicrosecond Pulse Techniques (Part 1) Electronic Engineering*, **24** (No. 291), 214.
PEASLEE, D. C., 1953, *Nuovo cim.*, **10**, 1349.
ROSE, M. E., 1953, *Phys. Rev.*, **91**, 610.
RUBY, L., and RICHARDSON, J. R., 1951, *Phys. Rev.*, **83**, 698.
STAHELIN, P. and PREISWERK, P., 1953, *Nuovo cim.*, **10**, 1219.
TICHO, H. K., 1951, *Phys. Rev.*, **84**, 847,

Helical Dislocations and Spiral Etch-Pits†

By S. Amelinckx, W. Bontinck and W. Dekeyser
Laboratorium voor Kristalkunde, Rozier, 6, Gent, Belgium

[Received July 8, 1957]

Summary

The etch-patterns due to helical dislocations are discussed. It is suggested that under certain conditions the etching of a helical dislocation gives rise to a spiral etch-pit of the kind observed on germanium and silicon crystals. Etch-patterns on (111) faces of fluorite crystals containing helical dislocations can readily be interpreted on the same basis.

§ 1. Introduction

It has been shown previously (Amelinckx, Bontinck, Dekeyser and Seitz 1957) that some dislocations can climb into a helical shape. Such dislocations have been made accessible to direct observation by various decoration processes in crystals of CaF_2 (Bontinck and Amelinckx 1957, Bontinck 1957), NaCl (Amelinckx, Bontinck and Maenhout-Van der Vorst 1957, Barber *et al.* 1957) and TiO_2 (Van Keymeulen and Dekeyser 1957).

Double rows of etch-pits which, on continued etching approach one another and finally coalesce, have been described by Bontinck (1957) on CaF_2. They have been interpreted as etch-patterns of helical dislocations having their axis parallel to the plane of observation. Other patterns which we interpret as being due to the etching of helical dislocations having their axis oblique with respect to the surface, have since been obtained. It is the object of this paper to discuss their general aspect for any orientation with respect to the observation plane.

§ 2. Theoretical

We consider first the ideal situation whereby the axis of the helix is perpendicular to the surface. During the etching process the pit will at every moment be centred on the dislocation line, and penetrate in depth at a constant speed v_n. Viewed from above, this means that the centre of the etch-pit describes a circle during the etching. Sideways etching proceeds simultaneously and uniformly at a speed v_t, once a pit is started. The resulting shape of this combined dissolution can roughly be described as a ‘ helical cone ’. Formulated more precisely, one can say that the surface of the pit is generated by a circle, lying in a plane parallel to the plane of observation, whose radius decreases linearly with depth and whose centre describes the helix. Figure 1 represents the projection of such surfaces on a plane parallel to the axis of the helix, for three different ratios of v_t/v_n.

---

† Communicated by the Authors.

Fig. 1

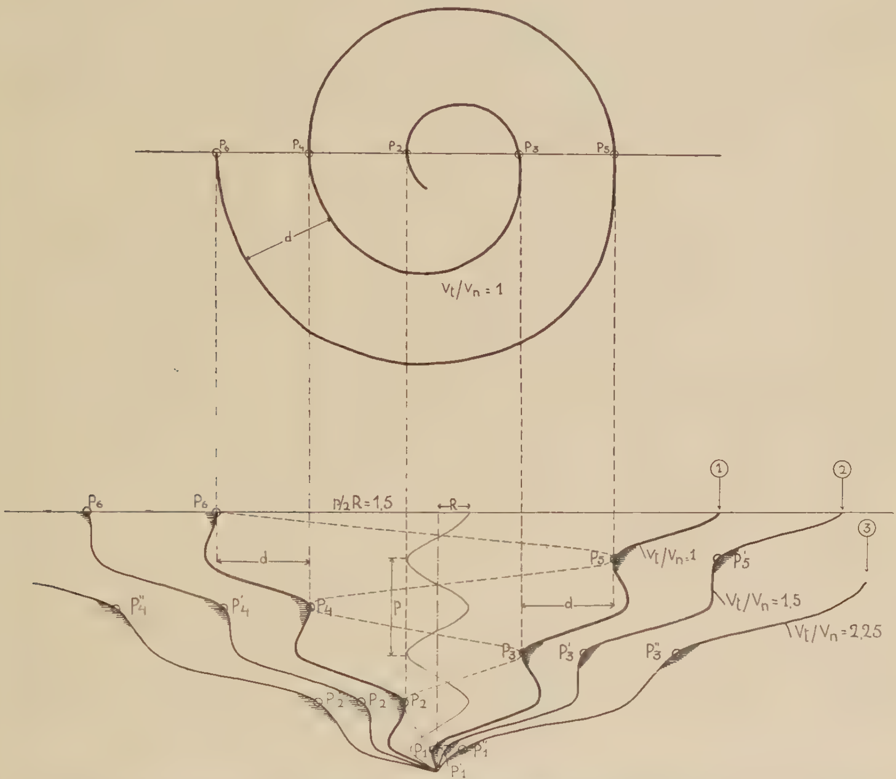

Projection of a spiral etch-pit on a plane passing through the axis of the helix, which is normal to the plane of observation.

It is possible to formulate quantitatively the characteristics of the resulting feature. If the dislocation line is given by

$$x = f_1(t) \quad \ldots\ldots\ldots \quad (1)$$

$$y = f_2(t) \quad \ldots\ldots\ldots \quad (2)$$

$$z = f_3(t) \quad \ldots\ldots\ldots \quad (3)$$

the equation for the surface of the etch-pit, assuming the observation plane to be (xy), can be obtained by eliminating t between (3) and (4)

$$[x - f_1(t)]^2 + [y - f_2(t)]^2 = (v_t/v_n)^2 z^2. \quad \ldots\ldots \quad (4)$$

In the specific case of the helical dislocations we can take as a parameter equation for the dislocation line

$$x = R\cos\phi\,; \quad y = R\sin\phi\,; \quad z = p\phi/2\pi \quad \ldots\ldots \quad (5)$$

ϕ being an azimuthal parameter; R the radius of the helix and p the step. It is easy to see that the projection of the etch-pit surface on the plane xz is

$$x = R \cos(2\pi z/p) \pm (v_t/v_n)z. \qquad (6)$$

This is the curve shown in fig. 1. The equation for a section with a plane through the axis of the helix is

$$x = R \cos(2\pi z/p) \pm [(v_t/v_n)^2 z^2 - R^2 \sin^2(2\pi z/p)]^{1/2}. \qquad (7)$$

For $z \gg R$ (2) and (3) become equivalent.

Fig. 2

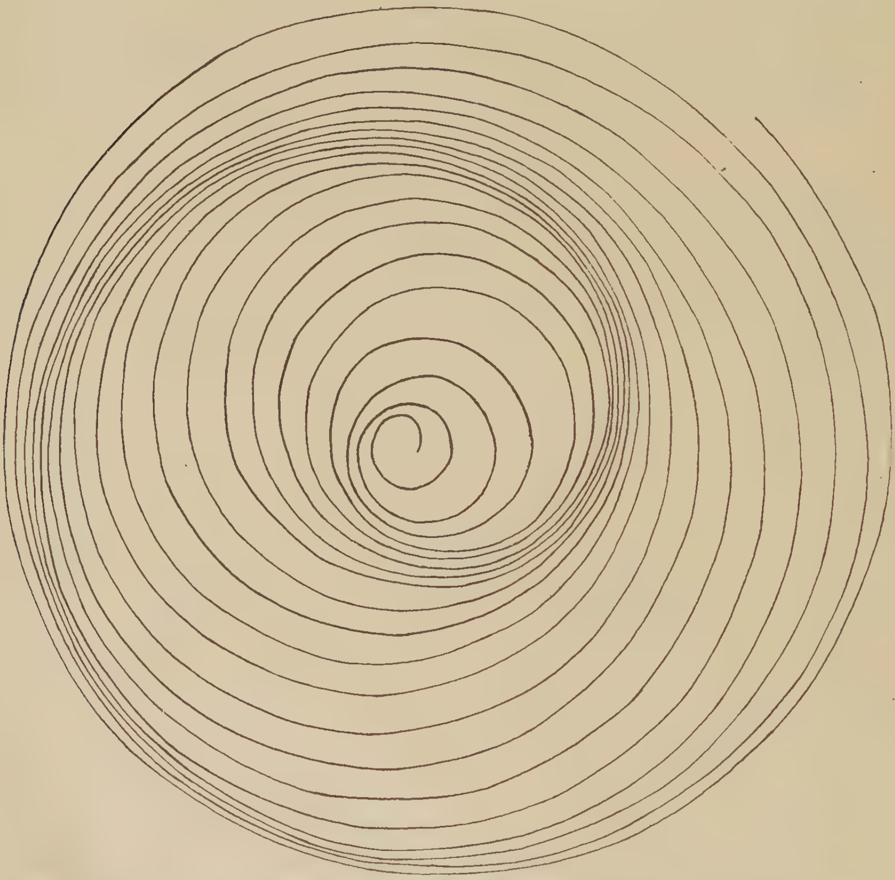

Shape of the monolayer step attached to the screw component of the emerging helical dislocation. Bunching of steps gives rise to a macroscopic spiral.

The lines seen when observing from above are evidently due to the steps marked by shading on fig. 1. We assume that the precise location of the step is in the points P_i. The spiral as observed (fig. 1) is then evidently the geometrical locus of the projection of all such points, for all possible cross sections. A simple, straightforward reasoning, shows that its equation in polar coordinates ρ and ϕ is:

$$\rho = R - a\phi \quad a = pv_t/2\pi v_n.$$

The spiral has Archimedian character, the distance d between successive turns being a constant: $d = pv_t/v_n$. The step height of the spiral turns out to be simply the step of the helix and it has, as a consequence, no direct relation with the Burgers vector of the underlying dislocation.

Fig. 3

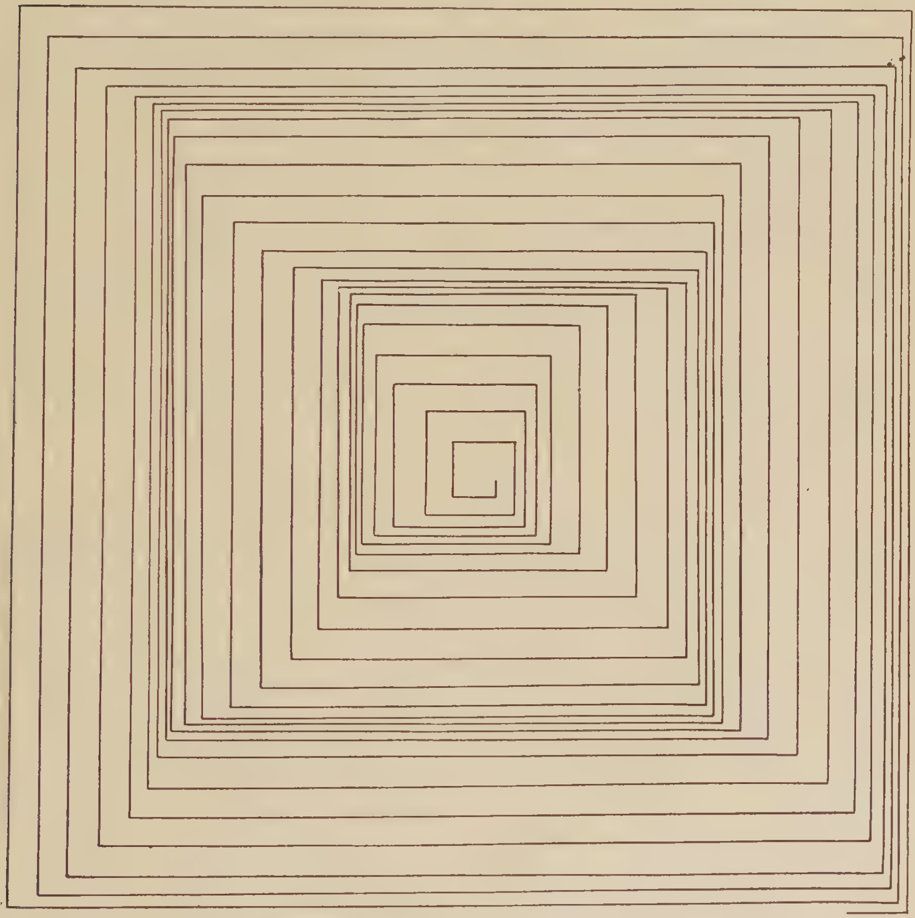

Polygonized spiral etch-pit.

From fig. 1 it is evident that the step, defining the spiral, becomes less and less well defined as v_t/v_n increases; one should observe a decreased contrast for such cases.

For small values of v_t/v_n (curve 1) the cross section presents concave parts, and the centre of the spiral will not be visible. For large values of v_t/v_n (curve 3) the steps which define the spiral are 'smeared out'.

The conditions for the occurrence of a vertical segment in the step is roughly $pv_t < 2\pi R v_n$. The centre of the spiral now becomes visible. For intermediate cases one can have rather well defined steps perpendicular to the plane of observation (curve 2).

When focusing attention on the unwinding of the monolayer step attached to the screw component of the dislocation, one finds that this step acquires the shape shown in fig. 2, i.e. a spiral of which the instantaneous centre describes a circle. This causes bunching of monolayers in the way shown and the macroscopic spiral now becomes visible.

If the anisotropy in v_t is pronounced one obtains polygonized spiral pits of the kind shown in fig. 3, for the case of tetragonal symmetry. Polygonization can also occur as a consequence of the polygonization of the helix itself (Bontinck 1957, Amelinckx, Bontinck and Maenhout-Van der Vorst 1957).

As in general helical dislocations have their axis parallel to a possible Burgers vector it is to be expected that the best developed spirals should be observed on planes perpendicular to a possible Burgers vector.

Etching of helices of which the axis is oblique with respect to the surface gives rise to patterns which can be deduced using similar reasoning as above. The step height is now the projection of p on the normal to the surface. The spiral will be deformed by bunching of the macroscopic steps, in the direction which is the projection of the axis of the helix on the observation plane.

§ 3. Experimental

Octahedral cleavage faces of CaF_2 crystals of which it was established previously by means of decoration methods, that they contained helical dislocations, were etched with concentrated sulphuric acid. Although the circumstances for the observation of spiral etch-pits due to helices are not favourable, because of the inclination of the axis of the helix (which is parallel to a [110] direction) with respect to the (111) plane, some features were observed, which are readily interpreted as being due to etching along helices. Figure 5, Pl. 48 shows an example; the spiral character is not apparent as a consequence of additional bunching of the large steps, in one sector. This is readily explained when considering the geometry in detail. The axis of the helix being, e.g. [110], the additional bunching, if due to the obliqueness of the axis of the helix, has to take place in the direction which is the projection of [110] on (111), i.e. in the $[\bar{1}2\bar{1}]$ direction. This is precisely what is observed.

Additional evidence that the described feature (fig. 4) originates from helical dislocations was obtained by the study of specimens from crystals presenting varying densities of helical dislocations, as deduced by the pecoration method. It was found that the number of pits of the shape of fig. 5 is proportional to the number of helices detected by the other method. It is further evident that the asymmetry of the terraced pits cannot be due to the geometry of the (111) face of fluorite; this would require a threefold axis of symmetry as presented by the majority of pits. The sector of bunched steps is moreover found with equal probability in any of the three sectors, which is again in agreement with the statistical distribution over all [110] directions, for the axis of the helices. A direct correlation of a decorated helix and the etch-pit centred on it proved to be difficult.

Attempts to study polished (110) faces were unsuccessful because of the difficulty of obtaining good etch-pits on this face.

Fig. 4

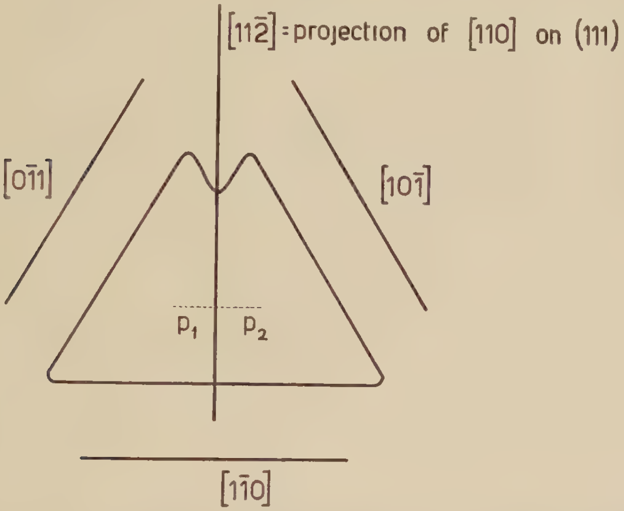

Etch-step on a (111) plane of fluorite due to a sequence of prismatic loops. The radial discontinuity in the $[11\bar{2}]$ direction results from the particular geometry of the 'twin' pits. P_1 and P_2 are the emergence points of the loop.

Occasionally one observes pits of the shape shown in fig. 6, Pl. 48, which present a radial discontinuity. It is thought that these originate in sequences of prismatic loops of the kind observed in CaF_2 (Bontinck 1957) and in NaCl (Barber *et al.* 1957) by means of decoration methods. It is clear that only sequences having their axis inclined with respect to the surface can be etched, and only if the following condition is satisfied $p/2R \leqslant tg\alpha$, where α is the angle between the axis of the sequence of loops and the normal to the surface. This condition is generally satisfied for the CaF_2 helices. The resulting feature is now a pit consisting of closed terraces; the centre of successive terraces being shifted along a $[11\bar{2}]$ direction, bunching of steps will again take place in this direction. An additional peculiarity results from the fact that each terrace is generated from two centres lying on a line in a [110] direction. As etch-pits develop [110] edges this means that the geometry of these 'twin' pits, is as shown in fig. 4. This explains the occurrence of the radial discontinuity in a $[11\bar{2}]$ direction.

During a recent discussion at Bell Telephone Laboratories W. G. Pfann raised the question of the origin of the spirally terraced etch-pits, which were first observed in germanium by Ellis (1955), and which have since then been observed in germanium and silicon by a number of other workers. One of us suggested that they might be due to helical dislocations. Although Mr. Pfann's suggestion has in part stimulated us to do the present work, we only have evidence for calcium fluoride.

The spirals on Ellis's photographs are very approximately Archimedean; he attributed them to large screw dislocations, the step height of the spiral being equal to the Burgers vector of the dislocation. Another explanation not based on the presence of dislocations was given by Lang (1957). There is however no reason why helical dislocations should not be present in germanium and silicon, which are also relatively rapidly cooled melt grown crystals. According to Apker (private communication), Dash (1956) using his copper decoration technique, has found some indication for helical dislocation in silicon.

ACKNOWLEDGMENT

This work is part of a research scheme supported by I.R.S.I.A. (Institut pour l'encouragement de la Recherche Scientifique dans l'Industrie et l'Agriculture ; Comité pour l'étude de l'état solide) Brussels.

REFERENCES

AMELINCKX, S., BONTINCK, W., DEKEYSER, W., and SEITZ, F., 1957, *Phil Mag.*, **2,** 355.
AMELINCKX, S., BONTINCK, W., MAENHOUT-VAN DER VORST, W., 1957, *Physica*, **23,** 270.
BARBER, D. J., HARVEY, K. B., and MITCHELL, J. W., 1957, *Phil. Mag.*, **2,** 704.
BONTINCK, W., 1957, *Phil. Mag.*, **2,** 561.
BONTINCK, W., and AMELINCKX, S., 1957, *Phil. Mag.*, **2,** 94.
DASH, W., 1956, *J. appl. Phys.*, **27,** 1193.
ELLIS, S. G., 1955, *J. appl. Phys.*, **26,** 1140.
LANG., A. R., 1957, *J. appl. Phys.*, **28,** 497.
VAN KEYMEULEN, J., and DEKEYSER, W., 1957 (to be published).

The Hardening and Embrittlement of Steel by Irradiation with Neutrons†

By A. T. CHURCHMAN‡
Associated Electrical Industries Limited, Aldermaston

I. MOGFORD and A. H. COTTRELL
Atomic Energy Research Establishment, Harwell

[Received July 15, 1957]

ABSTRACT

The tensile yield and fracture strengths of a structural steel have been measured before and after irradiation with neutrons. The fracture strength increases with irradiation at the same rate as the yield strength and the embrittlement cannot be ascribed to a loss of cohesive strength. Measurements have been made of the effects of grain size and testing temperature on the yield and fracture strengths; applied to Petch's equation they show that the radiation hardening is caused essentially by an increase in 'frictional' resistance in the slip planes, such as would be produced by dispersed islands of radiation damage, and that the cohesive strength of the lattice and the dislocation locking stress are not detectably changed by the irradiation. Notched-impact tests have also been made to show the embrittling effect of the irradiation.

§ 1. INTRODUCTION

THE hardening and embrittlement of structural steel by irradiation with neutrons (Kunz and Holden 1954, Sutton and Leeser 1954, Wilson and Billington 1955) raise several questions. For example, is the embrittlement caused by the hardening, or is there a loss of cohesive strength? To what extent is the hardening caused by the segregation of point defects to dislocations, or by the segregation of these defects into clusters dispersed through the lattice?

We have approached these questions experimentally by using a method developed originally by Petch (1953) for analysing the effect of grain size on the (tensile) yield and fracture stresses of steel. These stresses, which are denoted here by σ_y and σ_f respectively, have been shown by Hall (1951) and Petch (1953, 1954) to vary with the grain size l of the metal as

$$\sigma_y=\sigma_i+k_y l^{-1/2}, \qquad \sigma_f=\sigma_i+k_f l^{-1/2}. \quad . \quad . \quad . \quad . \quad (1)$$

---

† Communicated by the Authors.

‡ Work done while on attachment at A.E.R.E.

Here k_y measures the stress needed to start plastic yielding in the grains ahead of the plastic front and varies sensitively with the temperature and rate of straining, whereas k_f measures the stress needed to crack the metal at the tip of a slip band and is almost independent of the temperature and rate of straining. The stress σ_i measures the 'friction'—due for example to precipitates, other dislocations, or the lattice itself—that opposes the passage of a free dislocation across a slip plane. The theoretical interpretation of these formula is that, when a slip plane is made active by an applied stress σ, a part of this stress is used to overcome friction in the plane, and the rest of it, $\sigma-\sigma_i$, is free to pile dislocations against the grain boundary at the end of the plane. The stress concentration set up by these dislocations can become large enough, when $\sigma-\sigma_i$ is large, to trigger slip planes into activity in the next grain, or to open a crack at the end of the slip band. Equations (1) give σ_y and σ_f, the two values of σ at which these effects take place.

It follows that σ_i, k_y and k_f, can be determined from measurements of the yield and fracture stresses on specimens of different grain sizes. If σ_i is increased by irradiation we may conclude that the frictional resistance in the slip planes is increased by the presence of point defects dispersed, as individuals or clusters, throughout the lattice; and if k_y is increased then the locking of dislocations is increased by the irradiation. Similarly, if k_f is decreased then the cohesive strength is decreased by the irradiation. In this note we describe an experiment aimed to ascertain these effects.

§ 2. Method

Specimens were made from bars of En2 steel (0·15% C, 0·6% Mn, 0·12% Si) similar to that used by Petch. These were heat-treated to give two grain sizes, coarse (500 grains mm^{-2}) and fine (2000 grains mm^{-2}), and irradiated in aluminium cans filled with helium in the BEPO and Windscale reactors to integrated fluxes of $2{\cdot}5\times10^{17}$ to $5{\cdot}7\times10^{19}$ thermal neutrons cm^{-2} at temperatures of 50 to 100°C. The fast neutron flux above 1 MeV was about 75% of the thermal flux.

Notched impact specimens were used to show the embrittling effect of the irradiation and were tested in a balanced Hounsfield impact machine at various temperatures between −60°C and +180°C. The stresses σ_y and σ_f were measured on standard Hounsfield tensile specimens in a hard-beam machine at both room and liquid nitrogen temperatures.

§ 3. Results

The figure shows the embrittlement. Small irradiations are able to reduce the energy of ductile fracture and increase the temperature of brittle fracture appreciably in this steel.

The table summarizes the tensile measurements. Some specimens, particularly the fine grained ones, were ductile at the temperature of liquid nitrogen. It is known from the work of McAdam *et al.* (1945, 1947), Hollomon and Zener (1944), and Bridgman (1944), that plastic deformation raises the fracture stress. To obtain an undistorted measure of the direct effect of irradiation on the fracture stress it is thus necessary to separate the indirect effect which the irradiation exerts on the fracture stress through the change it produces in the ductility of the metal. We have, therefore, used the method of Petch (1953) to reduce the fracture stresses given in the table to zero elongation.

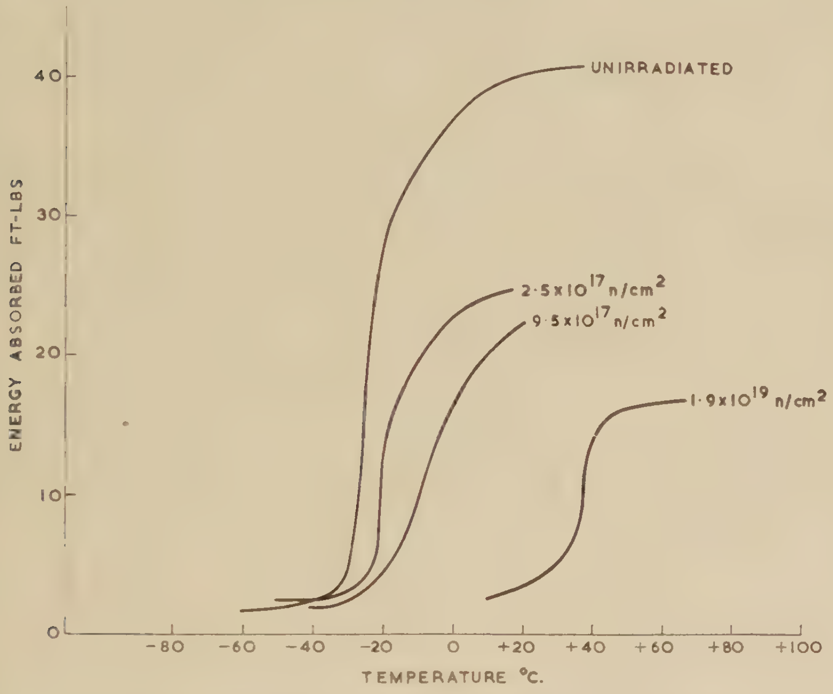

Effect of irradiation on the impact transition of En2 steel.
(Grain size 2000 grains/mm^2.)

§ 4. Discussion and Conclusions

The main feature of the results in the table can be seen by comparing the unirradiated and heavily irradiated specimens. Irrespective of grain size, temperature, or whether yield or fracture is considered, the strength of the metal is increased by about 32 000 lb in^{-2} by the irradiation. The only term in eqns. (1) that could give such behaviour is the friction stress, σ_i, and so we conclude that the irradiation has increased this term by about 32 000 lb in^{-2}. This strongly suggests that radiation hardening in these specimens is caused by dispersed regions of radiation damage, such as clusters of point defects, that are sufficiently large to withstand thermally-activated movements of dislocations.

It is clear that the irradiation has not significantly changed the cohesive strength of the metal, since the effect of grain size on the fracture stress is practically unaltered by the irradiation. The value of k_f, about $2{\cdot}5\times10^8$ c.g.s. units, obtained by fitting the results to eqn. (1) agrees reasonably with the theoretical value 2×10^8, deduced by Stroh (1954, 1955) from the cohesive properties of iron, and also with Petch's experimental value.

Effects of irradiation on the tensile strength of En2 steel. Each value of strength is averaged from three or more specimens

Integrated neutron Flux cm^{-2}	Lower yield stress σ_y at room temperature (lb in.$^{-2}$)		Lower yield stress σ_y at liq. N temperature (lb in.$^{-2}$)	
	Coarse grain	Fine grain	Coarse grain	Fine grain
Unirradiated	28 500	36 500	106 000	120 000
10^{18}	Not tested		↑	123 000
$1\cdot5\times10^{19}$	48 500	54 500	↑	143 000
$5\cdot7\times10^{19}$	60 500	68 000	Fractured ⟶	

Integrated Neutron Flux cm^{-2}	Reduced fracture stress σ_f at liq. N temperature (lb in.$^{-2}$)		Reduction in Area, per cent at liq. N temperature	
	Coarse grain	Fine grain	Coarse grain	Fine grain
Unirradiated	102 500	124 000	8	42
10^{18}	115 000	124 000	0–5	36
$1\cdot5\times10^{19}$	127 000	146 000	0	0–35
$5\cdot7\times10^{19}$	133 000	157 000	0	0–20

It also appears that the irradiation has not significantly changed the dislocation locking stress, i.e. the stress to start a slip band, since there is practically no change in the effect of grain size on the yield stress. However, in the tests at room temperature k_y is so small, about 9×10^7 c.g.s. that all but large changes in this term would remain undetected and the most we can infer from the present results in that k_y remains constant to within 15%. We hope to make further measurements at low temperatures, where k_y is large, to determine whether smaller changes occur.

It seems reasonable to expect some change in k_y in view of the well known effect of irradiation in suppressing internal friction due to dislocations in metals such as copper, which has been attributed to the pinning of dislocations by point defects (Thompson and Holmes 1956). However, the irradiations used in the present work are two to four orders of magnitude greater than those at which the pinning effect appears, and under these conditions the change in σ_i is predominant. It may be difficult to detect the effect of pinning on k_y in iron, even after light irradiations, in view of the strong pinning already produced by carbon and nitrogen atoms segregated to dislocations.

§ 5. ACKNOWLEDGMENTS

Thanks are due to D. Wynne for help in the experimental work and to many colleagues for useful discussion.

REFERENCES

BRIDGMAN, P. W., 1944, *Trans. Amer. Soc. Metals*, **32,** 553.
HALL, E. O., 1951, *Proc. phys. Soc. Lond.* B, **64,** 747.
HOLLOMAN, J. H., and ZENER, C., 1944, *Trans. Amer. Inst. min.* (*Metall.*) *Engrs*, **158,** 283.
KUNZ, F. W., and HOLDEN, A. N., 1954, *Acta Met.*, **2,** 816.
McADAM, D. J., GEIL, G. W., and MEBS, R. W., 1945, *Proc. Amer. Soc. Test. Mater.*, **45,** 448 ; 1947, *Trans. Amer. Inst. min.* (*Metall.*) *Engrs*, **172,** 323.
PETCH, N. J., 1953, *J. Iron St. Inst.*, **174,** 25 ; 1954, *Progress in Metal Physics* (London : Pergamon Press), **5,** 52.
STROH, A. N., 1954, *Proc. roy. Soc.* A, **223,** 404 ; 1955, *Ibid.*, **232,** 548.
SUTTON, C. R., and LEESER, D. O., 1954, *Nucleonics*, **12,** 8.
THOMPSON, D. O., and HOLMES, D. K., 1956, *J. appl. Phys.*, **27,** 713.
WILSON, J. C., and BILLINGTON, D. S., 1955, *Nuclear Eng. and Science Congress* (Cleveland), Preprint 91.

On the Electronic Conductivity of Crystals of Silver Halides†

By J. W. MITCHELL
H. H. Wills Physical Laboratory, University of Bristol

[Received August 28, 1957]

ABSTRACT

Crystals of silver halides which have been grown and annealed in air have always been used for measurements of photoconductivity. Such crystals, which are dilute solutions of silver oxide in the silver halide, have a much greater photoconductive response at room temperature than crystals of the highest purity. The mechanism responsible for the sensitization of the photoconductivity by silver oxide is discussed. The relationship of the model which is proposed to that developed by Newman, Tyler and Woodbury for the interpretation of sensitized photoconductivity in n-type germanium is indicated.

THE photoconductive sensitivity of crystals of silver halides is increased by annealing them at a temperature near 400°C in air or in oxygen, and decreased by annealing them in halogen or in vacuum. The purpose of this note is to suggest an interpretation of this behaviour, aspects of which have been recognized by all who have studied electronic conductivity in silver halide crystals (Toy and Harrison 1930, Hecht 1932, Lehfeldt 1935, van Heerden 1945, 1950, Haynes 1948, Haynes and Shockley 1948, 1951, Allemand and Rossel 1954, Brown 1955).

The experimental basis of the model which will be proposed is provided by observations made at Bristol on the displacement in electric fields of the photoelectrons which are liberated when light is absorbed in silver halide crystals at room temperature. The techniques used were introduced by Haynes and Shockley (1948, 1951) who mounted air annealed silver chloride crystals (Haynes 1948) between two glass plates, the outer surfaces of which were coated with platinum to form the two plates of a condenser. The front surface of the crystal was illuminated with short duration light flashes through gaps in the platinum coating and, simultaneously, voltage pulses appeared across the condenser. The lines of force of the resulting electric field were normal to the surfaces of the crystal, and the field was in the direction which would cause electrons

---

† Communicated by the Author.

to drift from the front to the rear surface. After many hours of repetitive flashing and pulsing a deposit of silver became visible on the rear surface. From this observation, Haynes and Shockley concluded that electrons were liberated by the absorption of the light flashes, displaced through the crystal by the voltage pulses, and trapped at the rear surface.

At an early stage in the experimental work on photographic sensitivity at Bristol, this method was employed to displace latent images, which are formed by much shorter exposures, to the rear surfaces of silver halide crystals. The thin single crystal silver halide sheets which were being used at that time (Keith and Mitchell 1953 a, b) were probably not very different in composition from the air annealed material used by Haynes and Shockley (1951), and a high surface density of specks of silver (fog specks in photographic terminology) always appeared when they were treated with photographic developers without previous exposure to light (compare, Haynes 1948, Allemand and Rossel 1954). With such sheets, Hedges and Mitchell (1953) were able to produce a developable latent image in the areas between the fog specks on the rear surfaces of the crystals after about ten light flashes with synchronized applied voltage pulses.

The material used for these experiments was, however, known to be a dilute solid solution of silver oxide in the silver halide and the experimental work was next concentrated on the purification of the silver halide (see Clark and Mitchell 1956 for a detailed account). The density of fog specks was reduced to a negligible value by methods of purification and crystallization designed to eliminate silver and silver oxide from the fused silver halide and from the crystals grown from it. The progress made can be assessed by a comparison of the surface density of fog specks in the photomicrographs reproduced in the papers by Keith and Mitchell (1953 a, b) with that in the photomicrographs in the paper by Evans *et al.* (1955). The quality of the large single crystals and thin single crystal sheets which were grown from this material, as judged from insensitivity to light and the absence of spontaneous reduction on immersion in active photographic developers, was probably as great as that of any previously prepared.

Evans (1955) then spent many months in attempts to displace the latent image at room temperature in crystals grown from this highly purified silver halide by the application of electric fields as in the previous work of Hedges and Mitchell (1953). He used precisely the same apparatus for producing short duration light flashes and synchronized voltage pulses but was finally forced to conclude that it was not possible to displace photoelectrons at room temperature *through* well annealed crystals of pure silver bromide, free from silver and silver oxide, to produce a developable latent image on the rear surface. A large number of these experiments were carried out with sheet crystals, $150\,\mu$ in thickness which had been annealed, first in vacuum to break down any residual silver oxide, then in bromine to convert any silver present to silver bromide, and finally in vacuum again to remove excess bromine. If it was assumed that the drift mobility of the electrons was about 50 cm^2 volt^{-1} sec^{-1}, the detailed analysis of the characteristics of the electrical circuit showed that their transit time would have been 5×10^{-9} sec. The fact that no latent image was ever formed on the rear surfaces of the pure crystals showed that, if electrons were actually liberated, their mean lifetime was considerably less than 5×10^{-9} sec. This was in striking contrast to the lifetimes of 10 μsec which had been observed in air annealed crystals of silver chloride by Haynes and Shockley (1951). As already stated, Hedges and Mitchell (1953) had experienced no difficulty in displacing the photoelectrons in silver bromide crystals containing silver oxide in solid solution by the application of electric fields; the lifetimes of the photoelectrons in these crystals were probably of the same order as those measured by Haynes and Shockley (1951) and Allemand and Rossel (1954).

The crystals of silver halides which had previously been used for observations of photoconductive phenomena had always been grown in air and annealed in air at a temperature of about 400°c (Hecht 1932, van Heerden 1945, 1950, Haynes 1948, Allemand and Rossel 1954, Brown 1955). It was believed that air annealing (1) removed internal strains introduced during crystal growth and preparation of specimens and (2) removed the photochemical products responsible for the discoloration produced by exposure to light and thus restored the crystal to its original state (see, for example, Hecht 1932, van Heerden 1950, Allemand and Rossel 1954). When the reasons for the increased range of the electrons in the crystals which were grown and annealed in air were discussed, emphasis was placed on the removal of internal strains by annealing (Haynes 1948, Brown 1955) and the possibility that the crystals might be sensitized by chemical changes occurring during annealing was not considered. A crystal of pure silver halide which has been exposed to light to liberate halogen and to form particles of colloidal silver can, however, never be restored to its original state by annealing in air; the colloidal silver is oxidized to silver oxide which passes into solid solution in the silver halide. An exposed crystal of silver halide can be restored to its original state by annealing in air only if it was already a solid solution of silver oxide in the silver halide before exposure. Annealing in air does, however, remove positively charged groups of silver atoms which furnish traps for conduction electrons (Mitchell 1957) and consequently decrease their lifetimes and limit their ranges (Lehfeldt 1935). It is now clear that crystals which were in fact dilute solid solutions of of silver oxide in the silver halides have been used for all the experiments on photoconductivity and on crystal counters which have been recorded in the literature. Brown and Waifan (1957) have recently observed that the ranges of the electrons which are liberated by γ-rays are greater in silver chloride crystals grown in air, and annealed in air at a temperature of 400°c than in crystals grown in vacuum and annealed in vacuum, in an inert atmosphere or in chlorine. Brown (1957) has also found that crystals of silver chloride, grown and annealed in air, have a greater photoconductive response when illuminated with short duration light flashes at room temperature.

We are of the opinion that dissolved silver oxide plays an essential role in the photoconductive process which has not previously been recognized and we shall propose an interpretation of the high photoconductive sensitivity of the air sensitized crystals. At low temperatures, crystals of silver halides containing silver oxide in solid solution have a higher ionic conductivity than pure crystals. This suggests that at least some of the silver oxide is dissolved in the form of doubly charged oxide ions, which occupy halide ion lattice sites, together with interstitial silver ions which compensate the additional negative charges; the increased ionic conductivity is due to the drift of these interstitial ions. The primary process in electronic conductivity is the liberation of electrons and positive holes by photons or by charged particles. We assume that the lifetime of the positive hole is less than that of the electron. In silver halide crystals of high purity and perfection, the positive holes are trapped at the external surfaces and at dislocations. The resulting positively charged centre has, on account of Coulomb interaction, a large cross section for the capture of an electron so that the lifetime of a conduction electron is correspondingly short. Unless the positively charged centre dissociates with the loss of a silver ion into an interstitial position before recombination occurs (see Mitchell 1957), the external surfaces and the dislocations furnish recombination centres for positive holes and electrons. This is the reason for the small initial sensitivity of pure crystals of silver halides for the production of photocurrents and current pulses on irradiation.

The air sensitized crystals have different properties. Here, the doubly negatively charged oxide ion has a large cross section for the capture of a positive hole, on account of the Coulomb interaction, whereas the resulting singly charged oxide ion has a very small cross section for the subsequent capture of a conduction electron. The interstitial silver ion which then compensates the negative charge of the conduction electron does not provide a trap for it except, possibly, at extremely low temperatures. After the positive holes have been trapped by doubly charged oxide ions they have to be released by thermal activation or optical excitation from the singly charged oxide ions before they can be trapped at the surface recombination centres. The result of dissolving molecules of silver oxide in crystals of silver halides is therefore to reduce the rate at which positive holes are captured by the surface traps, which act primarily as the recombination centres. The consequence of this is that the lifetime of the electrons in the conduction band is increased in the air sensitized crystals compared with crystals of the pure silver halide. This accounts for their increased photoconductive and photographic sensitivity. The correspondingly increased electron ranges provide an explanation of why experiments of the type introduced by Haynes and Shockley (1948, 1951) may be successfully carried out with air sensitized crystals but fail with crystals of pure silver halides (Evans 1955).

This model for air sensitized crystals of silver halides which introduces two correlated energy levels in the forbidden band—an upper donor level associated with doubly charged oxide ions, and a lower acceptor level associated with singly charged oxide ions—should be compared with the double acceptor model for n-type germanium sensitized with iron, nickel, cobalt or manganese which has been developed by Newman, Tyler and Woodbury (Newman and Tyler 1954, Tyler, Newman and Woodbury 1955 a, b, Tyler and Newman 1955, Newman, Woodbury and Tyler 1956). The close parallelism will be immediately evident. Both models provide examples of the basic mechanism for sensitized photoconductivity which has been outlined by Rose (1956). A further parallel may exist between the scattering of the conduction electrons by the doubly charged oxide ions in the sensitized silver halides (see the experimental results of Allemand and Rossel 1954, and of Brown 1955) and by the doubly charged manganese centres in germanium (Tyler and Woodbury 1956) as deduced from measurements of mobility at low temperatures. This interpretation of the origin of impurity scattering in air sensitized silver halide crystals at low temperatures is consistent with the estimated densities of impurity centres (Allemand and Rossel 1954) and it seems likely that charged impurity scattering will always accompany air sensitization.

The study of the temperature dependence of the electronic component of the electrical conductivity of solid solutions of silver oxide in silver bromide which are in contact with bromine vapour should yield information on the height above the full band of the lower acceptor level. The oxide ions will then be in the singly charged state and the crystal should behave as a p-type semiconductor because of the transference of electrons from the full band to the acceptor levels by thermal activation. From measurements at low temperatures of the wavelength dependence of the photoconductive response of air sensitized crystals of silver halides, it should be possible to determine the depth below the conduction band of the donor levels associated with the doubly charged oxide ions.

The secondary photocurrents observed in air sensitized crystals at low temperatures by Lehfeldt (1935) may also be interpreted with this model. Under illumination, the upper levels in the forbidden band are emptied when the positive holes are trapped by doubly charged oxide ions. The lower levels associated with singly charged oxide ions which then appear can neither accept electrons from the full band at low temperatures nor, on account of the small cross section, capture electrons from the conduction band. In the steady state, a concentration of mobile conduction electrons with a compensating positive charge of immobile interstitial silver ions is therefore built up and comparatively large electronic dark currents can flow through the crystals.

This model thus resolves most of the difficulties which have arisen in the discussion of photoconductivity in the silver halides and of their behaviour as crystal counters. Their high photoconductive sensitivity, which has always been contrasted with the absence of photoconductivity in non-sensitized alkali halides, is due partly to sensitization and partly to intrinsic properties. It is clearly important to establish the intrinsic photoconductive behaviour of the silver halides over the whole range of temperatures; measurements made by Braun and Mitchell (1957) with crystals of high purity silver bromide at temperatures between −183° and −70°C will be published shortly.

The presence of positive hole traps with the properties which have been attributed here to dissolved molecules of silver oxide appears to be a necessary condition for high photochemical sensitivity in silver halide crystals (Mitchell 1957, Mitchell and Mott 1957).

References

Allemand, C., and Rossel, J., 1954, *Helv. Phys. Acta*, **27,** 212, 519.

Braun, E. A., and Mitchell, J. W., 1957, *Phil. Mag.* (to be published).

Brown, F. C., *Phys. Rev.*, **97,** 355; 1957, *J. Phys. Chem. Solids* (in the press), (the author is indebted to Professor F. C. Brown for providing him with a manuscript copy of this paper, " Transient Photoconductivity in AgCl at Room Temperature ").

Brown, F. C., and Waifan, N., 1957, *Phys. Rev.*, **105,** 93.

Clark, P. V. McD., and Mitchell, J. W., 1956, *J. photogr. Sci.*, **4,** 1.

Evans, T., 1955, *Thesis*, University of Bristol.

Evans, T., Hedges, J. M., and Mitchell, J. W., 1955, *J. photogr. Sci.*, **3,** 73.

Haynes, J. R., 1948, *Rev. sci. Instrum.*, **19,** 51.

Haynes, J. R., and Shockley, W., 1948, *Report on Conference on Strength of Solids* (London: Physical Society), p. 151; 1951, *Phys. Rev.*, **82,** 935.

Hecht, K., 1932, *Z. Phys.*, **77,** 235.

Hedges, J. M., and Mitchell, J. W., 1953, *Phil. Mag.*, **44,** 357.

van Heerden, P. J., 1945, *Thesis*, University of Utrecht; 1950, *Physica*, **16,** 505.

Keith, H. D., and Mitchell, J. W., 1953 a, *Sci. Industr. Photogr.* (2), **23A,** 260; 1953 b, *Phil. Mag.*, **44,** 877.

Lehfeldt, W., 1935, *Nachr. Ges. Wiss. Gottingen*, **1,** 171.

Mitchell, J. W., 1957, *Rep. Progr. Phys.* (London: Physical Society), **20,** 433.

Mitchell, J. W., and Mott, N. F., 1957, *Phil. Mag.*, **2,** 1149.

Newman, R., and Tyler, W. W., 1954, *Phys. Rev.*, **96,** 882.

Newman, R., Woodbury, H. H., and Tyler, W. W., 1956, *Phys. Rev.*, **102,** 613.

Rose, A., 1956, *Photoconductivity Conference* (New York: John Wiley), p. 3.

Toy, F. C., and Harrison, G. B., 1930, *Proc. roy. Soc.* A, **127,** 613, 629.

Tyler, W. W., and Newman, R., 1955, *Phys. Rev.*, **98,** 961.

Tyler, W. W., Newman, R., and Woodbury, H. H., 1955 a, *Phys. Rev.*, **97,** 669; 1955 b, *Ibid.*, **98,** 461.

Tyler, W. W., and Woodbury, H. H., 1956, *Phys. Rev.*, **102,** 647.

The Thermal Instability of a Rotating Fluid Sphere Heated Within: II†

By S. Chandrasekhar, F.R.S.
University of Chicago

[Received July 3, 1957]

Summary

It is shown that the characteristic value problem specifying the state of marginal stability of a rotating incompressible fluid sphere heated within, can be reformulated in terms of a variational principle.

§ 1. Introduction

In an earlier paper (Chandrasekhar 1957, this paper will be referred to hereafter as I) the problem of the thermal instability of an incompressible rotating fluid sphere has been considered in case the motions and the associated perturbations have symmetry about the axis of rotation ; and the underlying characteristic value problem was solved for a slightly modified set of boundary conditions. In this paper, it will be shown that the mathematical problem (as in other cases of thermal instability which have been investigated) can be reformulated in terms of a variational principle. This principle will be used in a later paper to solve the basic problem more rigorously than was accomplished in I.

§ 2. The Variational Principle

The basic equations governing the problem are (I, eqns. (6), (16), (17) and (22)) :

$$\kappa \Delta_3 \theta = 2\beta\left(\frac{\partial}{\partial z} - \frac{z}{\varpi}\frac{\partial}{\partial \varpi}\right)\varpi^2 U, \qquad (1)$$

$$\Delta_5^2 U - \frac{2\Omega}{\nu}\frac{\partial V}{\partial z} = \frac{\gamma}{\nu}\left(\frac{\partial}{\partial z} - \frac{z}{\varpi}\frac{\partial}{\partial \varpi}\right)\theta \qquad (2)$$

and

$$\Delta_5 V = -\frac{2\Omega}{\nu}\frac{\partial U}{\partial z}, \qquad (3)$$

where the various symbols have the same meaning as in I. By measuring distance in units of the radius, R, of the configuration and making the transformations

$$\theta \to \left(\frac{2\beta}{\kappa} R^3\right)\theta \text{ and } V \to \left(\frac{2\Omega}{\nu} R\right) V, \qquad (4)$$

---

† Communicated by the Author.

eqns. (1)–(3) can be reduced to the more convenient forms

$$\Delta_3\theta = \frac{1}{r}\frac{\partial}{\partial\mu}[r^2(1-\mu^2)U], \qquad \ldots\ldots \quad (5)$$

$$\Delta_5^2U - T\frac{\partial V}{\partial z} = C\frac{1}{r}\frac{\partial\theta}{\partial\mu} \qquad \ldots\ldots \quad (6)$$

and

$$\Delta_5V = -\frac{\partial U}{\partial z}, \qquad \ldots\ldots\ldots \quad (7)$$

where T and C are the Taylor and Rayleigh numbers, respectively, (cf. I, eqn. (38)).

Multiply eqn. (5) by θ and integrate over the volume of the unit three-dimensional sphere. Both sides of the equation can be reduced by integration by parts and we find :

$$\iint |\operatorname{grad}\theta|^2 r^2\,dr\,d\mu = \iint \frac{1}{r}\frac{\partial\theta}{\partial\mu}\,Ur^4(1-\mu^2)\,dr\,d\mu, \qquad \ldots \quad (8)$$

the integrated parts vanishing on account of the boundary condition on θ (I, § 3.1). It will be observed that on the right-hand side of eqn. (8) the integration is over the unit five-dimensional sphere.

Making use of eqn. (6) we can rewrite eqn. (8) in the form

$$C\iint |\operatorname{grad}\theta|^2 r^2\,dr\,d\mu = \iint U\left(\Delta_5^2U - T\frac{\partial V}{\partial z}\right)\varpi^3\,d\varpi\,dz. \qquad \ldots (9)$$

Considering first the term in U on the right-hand side of this equation, we can reduce it by making use of eqn. (7) and a sequence of integrations by parts. Thus,

$$\begin{aligned}
&-\iint U\frac{\partial V}{\partial z}\varpi^3\,d\varpi\,dz\\
&=\iint V\frac{\partial U}{\partial z}\varpi^3\,d\varpi\,dz\\
&=-\iint V\Delta_5 Vr^4(1-\mu^2)\,dr\,d\mu\\
&=-\iint V\left\{(1-\mu^2)\frac{\partial}{\partial r}\left(r^4\frac{\partial V}{\partial r}\right)+r^2\frac{\partial}{\partial\mu}\left[(1-\mu^2)^2\frac{\partial V}{\partial\mu}\right]\right\}dr\,d\mu\\
&=\iint\left\{\left(\frac{\partial V}{\partial r}\right)^2+\frac{1-\mu^2}{r^2}\left(\frac{\partial V}{\partial\mu}\right)^2\right\}r^4(1-\mu^2)\,dr\,d\mu\,; \qquad \ldots\ldots \quad (10)
\end{aligned}$$

the integrated parts do not make any contributions in view of the conditions that U and either V or $\partial V/\partial r$ vanish on the boundary (cf. I, eqns. (34) and (35)).

Next, letting

$$X = \Delta_5U, \qquad \ldots\ldots\ldots \quad (11)$$

we can transform the remaining integral in eqn. (9) as follows :

$$\begin{aligned}\iint U\Delta_5 X\varpi^3\, d\varpi\, dz &= \iint U\left\{(1-\mu^2)\frac{\partial}{\partial r}\left(r^4\frac{\partial X}{\partial r}\right)+r^2\frac{\partial}{\partial\mu}\left[(1-\mu^2)^2\frac{\partial X}{\partial\mu}\right]\right\} dr\, d\mu\\ &= -\iint\left\{r^4(1-\mu^2)\frac{\partial U}{\partial r}\frac{\partial X}{\partial r}+r^2(1-\mu^2)^2\frac{\partial U}{\partial\mu}\frac{\partial X}{\partial\mu}\right\} dr\, d\mu\\ &= -\int_{-1}^{+1}\left(\frac{\partial U}{\partial r}\right)_{r=1}[X]_{r=1}(1-\mu^2)\, d\mu+\iint X\Delta_5 U r^4(1-\mu^2)\, dr\, d\mu. \qquad (12)\end{aligned}$$

On a rigid boundary $\partial U/\partial r=0$ (I, eqn. (30)) and the 'surface' integral in the last line of eqn. (12) will vanish. On the other hand, on a free boundary (I, eqn. 32))

$$\frac{\partial^2 U}{\partial r^2}+\frac{2}{r}\frac{\partial U}{\partial r}=0. \qquad . \; . \; . \; . \; . \; . \quad (13)$$

Consequently,

$$[X]_{r=1}=[\Delta_5 U]_{r=1}=2\left(\frac{\partial U}{\partial r}\right)_{r=1}. \qquad . \; . \; . \; . \; . \quad (14)$$

Accordingly,

$$\begin{aligned}\iint U\Delta_5^2 U\varpi^3\, d\varpi\, dz &= -2\int_{-1}^{+1}\left(\frac{\partial U}{\partial r}\right)_{r=1}^2(1-\mu^2)\, d\mu\\ &\quad+\iint(\Delta_5 U)^2 r^4(1-\mu^2)\, dr\, d\mu. \qquad . \; . \; . \; . \; . \quad (15)\end{aligned}$$

Finally, combining eqns. (9), (10) and (15), we obtain,

$$\begin{aligned}C\int_0^1\int_{-1}^{+1}|\operatorname{grad}\theta|^2 r^2\, dr\, d\mu &= -2\int_{-1}^{+1}\left(\frac{\partial U}{\partial r}\right)_{r=1}^2(1-\mu^2)\, d\mu\\ &\quad+\int_0^1\int_{-1}^{+1}\left\{(\Delta_5 U)^2+T\left[\left(\frac{\partial V}{\partial r}\right)^2+\frac{1-\mu^2}{r^2}\left(\frac{\partial V}{\partial\mu}\right)^2\right]\right\}r^4(1-\mu^2)\, dr\, d\mu. \quad (16)\end{aligned}$$

This is the required formula which, it can be readily shown, provides the basis for a variational procedure for determining C.

One general result† which can be proved from eqn. (16) is that C is a monotonic increasing function of T.

ACKNOWLEDGMENTS

The research reported in this paper has in part been supported by the Geophysics Research Directorate of the Air Force Cambridge Research Center, Air Research and Development Command, under Contract AF19(604)–2046 with the University of Chicago.

REFERENCE

CHANDRASEKHAR, S., 1957, *Phil. Mag.*, **2**, 845.

---

† I am indebted to Dr. George Backus for this remark.

CORRESPONDENCE

On Spiral Etch Pits in Germanium and Silicon

By S. G. Ellis
RCA Laboratories, Princeton, New Jersey

[Received July 16, 1957]

In an earlier communication (Ellis 1955) I have reported the observation of etch pits with a spiral terrace in germanium crystals. They were there ascribed to the nucleation of the etching by screw dislocations with Burgers vectors of the order 10^{-5} cm. Although screw dislocations of this strength were not inconceivable in the dendritic crystals studied, the observation of similar pits in germanium and silicon crystals grown slowly from the melt casts doubt on the above interpretation. Etch pits of this sort have now been observed in a number of cases (Christian and Jensen 1956, Bardsley and Straughan 1956, Vogel and Lovell 1956), and Lang (1957) has suggested that they are formed when the rate of etching parallel to the surface of the crystal is asymmetric about the point in the surface at which the attack is nucleated.

A simpler explanation is suggested by some recent observations of Bontinck and Amelinckx (1957). By decorating the dislocations in synthetic fluorite crystals they observe that some of the dislocations form helices when a dislocation of mixed character (i.e. a composite dislocation) climbs as vacancies condense on it. If such dislocations exist in germanium and silicon and if the axis of the helix is nearly normal to the surface being etched, then the terraces in the pit will spread from a point which has moved in a circle as the etching proceeds. Figure 2 of Lang's paper then shows how with the limited resolution of the light microscope a spiral terrace appears. This explanation differs from Lang's in supposing that the lateral rate of etching is constant and that the point of nucleation moves in a circle.

If this explanation is correct the lateral distance between terraces is a measure of the diameter of the helix, and the step height between terraces is a measure of its pitch. The pitch, as Bontinck and Amelinckx point out, can be much larger than the Burgers vector of the dislocation.

While these ideas are consistent with the observations of etched crystals such observations cannot give complete confirmation. This would be better done by decoration methods. If the idea is correct it provides further information about the character of the original dislocations, and the extent of vacancy condensation at them.

In conclusion it may be added that spiral etch pits have also been seen on the (100) and (110) surfaces of germanium crystals.

References

Bardsley, W., and Straughan, B. W., 1956, *J. Electron.*, **1**, 561.
Bontinck, W., and Amelinckx, S., 1957, *Phil. Mag.*, **2**, 94.
Christian, S. M., and Jensen, R. V., 1956, *Bull. Amer. Phys. Soc.*, **1**, 140.
Ellis, S. G., 1955, *J. appl. Phys.*, **26**, 1140.
Lang, A. R., 1957, *J. appl. Phys.*, **28**, 497.
Vogel, F. L., Jr., and Clarice Lovell, L., 1956, *J. appl. Phys.*, **27**, 1413.

REVIEWS OF BOOKS

Progress in Cosmic Ray Physics, Vol. III. Edited by J. G. Wilson (North-Holland, Amsterdam.) [Pp. xii+420.] Price 76*s*.

This third report on recent important advances in cosmic ray physics contains valuable articles by K. Greisen on Extensive Air Showers; H. S. Bridge on Charged K-mesons and Hyperons; R. W. Thompson on Neutral K-mesons and Hyperons, and G. Puppi on the Energy Balance of Cosmic Radiation. This volume, published late in 1956, is no more up to date than Spring 1955; strange particle physics grows and changes rapidly, so this delay is unfortunate.

It is intended that future volumes will cover elementary particle theory as well as cosmic ray physics. J. H.

Quantum Mechanics. By H. A. Kramers, English translation by D. ter Haar. (Amsterdam: North-Holland), [Pp. xvi+496]. Price 90*s*.

Dr. ter Haar has made a very satisfactory translation of Kramers' well known monograph on quantum mechanics. The original was completed in 1937; the scope of the work does not go much beyond the quantum theory of atomic systems. J. H.

[*The Editors do not hold themselves responsible for the views expressed by their correspondents.*]

Fig. 5

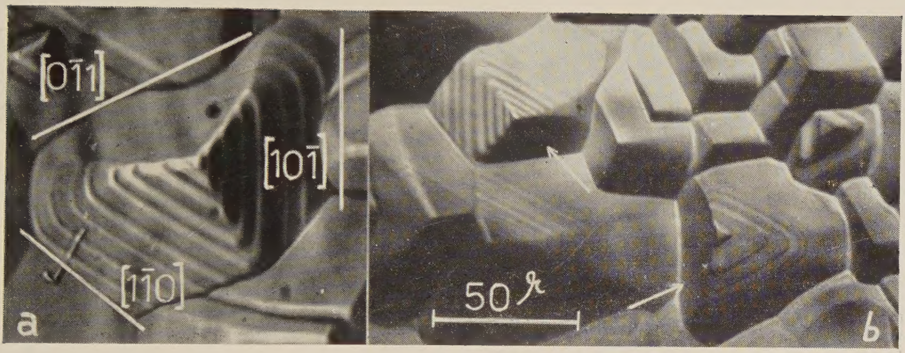

Etch-pits on (111) cleavage faces of CaF_3. (*a*) Observe the bunching of steps in the [$\bar{2}$11] direction. (*b*) Etch-pits having the sector of bunched steps in different [11$\bar{2}$] directions.

Fig. 6

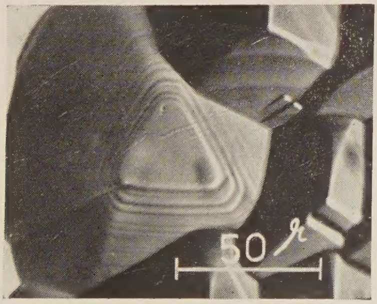

Etch-pit due to a sequence of prismatic loops. Notice the radial discontinuity in a [11$\bar{2}$] direction.